

ANTIOXIDANT EFFECT OF HUMIC SUBSTANCES FROM HUNGARIAN LEONARDITE

ATTILA CSICSOR*^{1,2} AND ETELKA TOMBÁ CZ^{1,3}

¹Doctoral School of Environmental Sciences, University of Szeged, Rerrich Béla tér 1, Szeged, 6720, HUNGARY

²Hymato Products Kft., Kossuth Lajos u. 33, Szentkirályszabadja, 8225, HUNGARY

³Soós Ernő Water Technology Research and Development Center, University of Pannonia, Zrínyi Miklós u. 18, Nagykanizsa, 8800, HUNGARY

Humic substances are natural substances that are continuously formed from the decay of plant residues. These materials have a very diverse range of properties, making them versatile. According to many new studies, these humic substances also exhibit antioxidant propensities. The aim of this paper was to shed light on whether humic substances really have antioxidant properties.

Keywords: humic substances, humic acid, fulvic acid, himatomelanin acid, antioxidant, leonardite

1. Introduction

The majority of the population of Hungary suffers from one of the diseases associated with free radicals, e.g. diseases of civilization, obesity, cardiovascular disease, malignant neoplasms, etc. Although it is well-known that our consumption of vegetables and fruit lags far behind those of the other Member States of the European Union, it has been scientifically proven that essential fresh vitamins and provitamins as well as minerals are fundamental not only for the smooth functioning of the body but also for their antioxidant components. Furthermore, they can play a key role in terms of disease prevention. Berries have become a major player in a number of related research papers as they are also essential in the prevention as well as aftercare of cancer and cardiovascular disease. What other options are available and what other substances may still have high antioxidant contents? Based on the aforementioned points, it is also important and justified to study the antioxidant properties of new compounds such as humic substances and determine which of their components play a crucial role in the development of their antioxidant effect, both qualitatively and quantitatively. The aim of this research is to compare the antioxidant properties of humic acids with already well-known natural antioxidants. Firstly, different humic acid

fractions were prepared. The expected results should help to more accurately interpret the complex behavior of humic acids, thereby helping to expand their range of applications. Therefore, if the results are convincing, this could open up new fields with regard to the application of humic acids in the food and cosmetics industries [1].

2. Humic substances

Humic substances are a group of naturally occurring macromolecules found throughout nature, that is, in soil, air, water, carbon deposits and peat. Chemically ill-defined humic substances are natural organic colloids comprised of decomposition products of plant-derived biomass as the result of a process called humification. Their conversion into stabilized humic material is one of the most complex and least understood biogeochemical processes of the carbon cycle. Most natural humic acids (HA) are found in older peat, lignite and juvenile lignite. In Hungary, the HA content of the so-called leonardite, a famous source of HA, is close to 70% in its natural form. (A near-surface deposit of leonardite is located in Dudar, where this geological formation can be mined).

In the humification process, dead plant matter that enters the soil is broken down by enzymes found in soil bacteria and fungi, so simple compounds like sugar and ammonia are formed from carbohydrates, fats, proteins and lignin, which on the one hand serve as a source of food for the soil microbes but on the other hand as a source in the formation of humic substances. As a result of biotic and abiotic (condensation and polymerization) processes,

Received: 26 August 2021; Revised: 16 September 2021; Accepted: 20 September 2021

*Correspondence: csicsor.attila@gmail.com

the decomposition products form high-molecular-weight humus compounds, the presence of which is characteristic of the soil [2].

On the basis of differences in solubility, humic substances can be divided into several groups such as the main fractions humin, HA, and fulvic acids (FA), as well as the alcohol soluble himatomelanic acids (HY). They are a mixture of similarly behaving, yellow-brown-black, acidic, high-molecular, natural organic substances that are operationally defined. Humic substances themselves contain too many kinds of molecules that can be separated by changing the solubility conditions. Even though these molecules behave similarly, each fraction has different properties and their molecular structure is not uniform [2]. The nomenclature of fractions that can be separated according to their solubility is suggested in the guidelines of the International Humic Substances Society (IHSS):

- **Humin** - a black fraction of humic substances that is insoluble in water at any pH.
- **Humic acids** - the fraction of humic substances that is insoluble in water under acidic conditions (pH < 2) but soluble in water at higher pH values. They can be extracted by various alkaline solutions before being precipitated by a strong acid and are dark brown or black in color.
- **Fulvic acids** - the fraction of humic substances that is soluble in water at all pH values. Fulvic acids are light yellow or yellowish brown in color.
- **Himatomelanic acids** - the fraction of humic substances that is soluble in an alcohol.

3. Antioxidants

The most important physiological role of antioxidants is to neutralize the free radicals that are continuously formed in the Szent-Györgyi-Krebs cycle and counteract the free radicals with different oxidizing forces that enter the body. An antioxidant is a substance that inhibits oxidation, more broadly speaking, retards or hinders oxidation. They are chemically reducing agents, i.e. electron donors. These materials are usually organic compounds but include metals and organometallic complexes. Many different types of antioxidants exist, which usually work together and do not neutralize free radicals on their own. Although our body itself is able to produce some antioxidants, sometimes it is necessary for us to ingest these substances from external sources. Together, these antioxidants already form a very strong line of defence in our body, e.g. vitamin C, Vitamin A, flavonoids, glutathione, resveratrol, unsaturated fatty acids, etc. [3, 4]

4. Methods for measuring the antioxidant capacity

The antioxidant capacity is the combined free radical scavenging effect of all antioxidant compounds in the

system studied. Since the need for its accurate numerical determination is growing, a number of analytical procedures and measurement systems have been developed. Given that methodologies are constantly being modified and refined, nowadays, the number of applied methods exceeds one hundred. In the literature, the majority of studies use several methods to determine the antioxidant capacity [5]. The most common methods of measuring the antioxidant capacity can be divided into two main groups: electron transition-based ones (Ferric iron Reducing Antioxidant Power, Total Polyphenol Content, Copper ion Reducing Antioxidant Capacity, Trolox Equivalent Antioxidant Capacity, and 2,2-Diphenyl-1-picrylhydrazyl (DPPH)) as well as those based on hydrogen atom transfer (Oxygen Radical Absorbance Capacity, total peroxy radical-trapping potential, chemiluminescence-based methods, and photochemiluminescence measurements just to mention the most commonly used methods).

Although these two types of measurements determine the antioxidant capacity, the results obtained do not necessarily have to be correlated with each other, since the reducing power of a sample is not necessarily related to its ability to scavenge for the reaction of test compounds.

Electron transfer reactions involve colour changes, from which the antioxidant capacity can be deduced. The essence of these methods is to create a free radical as the result of a reaction. To this free radical, the antioxidant is added at various dilutions leading to a colour change, which is monitored by a spectrophotometer and then the antioxidant capacity of the test substance is calculated from the results obtained.

Methods involving hydrogen atom transfer are based on the kinetics of the reaction. Tests measure how effective a sample is against a given free radical, namely its free radical scavenging capacity [5].

5. Antioxidant effect of humic substances

The question may arise as to why humic substances would exhibit an antioxidant effect. Humic acids are chemically very complex mixtures of composite molecules, that is, natural polymers formed during the varying degrees of polymerization of basic building blocks. According to their chemical structure, they are polyhydroxy carboxylic acids with quinone and semiquinone groups. In some respects, they are similar to flavonoids and phenols, in which the so-called flavone skeleton is polysubstituted by hydroxy groups. However, they also have a quinoid structure that is known to be responsible for antioxidant properties. These properties of HA have already been demonstrated in a number of scientific publications by both classical analytical methods (redox titrations) and instrumental analytical measurements (Electron Spin Resonance) [6].

The general structure of HA and the formulae of some well-known antioxidants are presented in Fig. 1 From

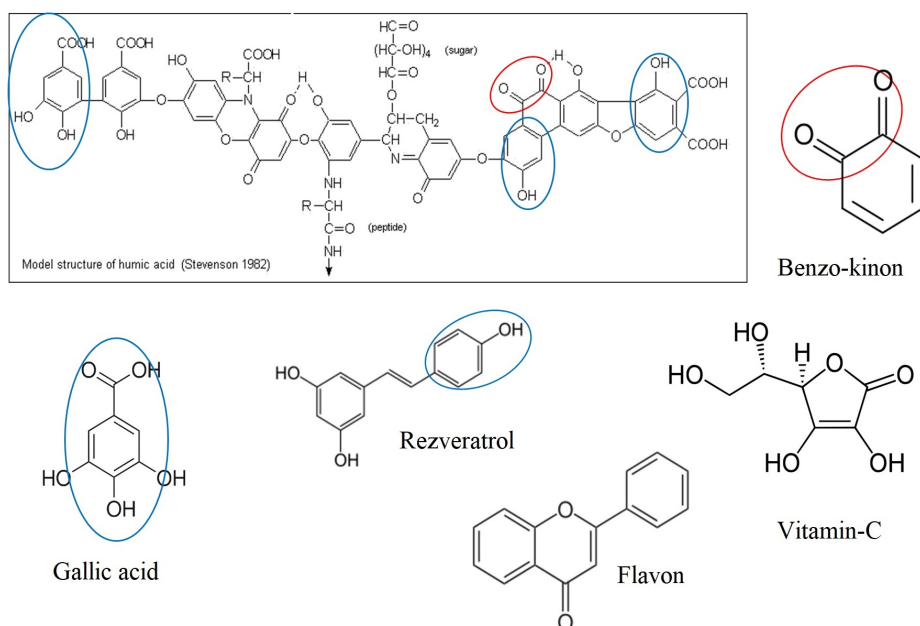


Figure 1: Model structure of HA and identical moieties of known antioxidants [2]

their structure, it is clear that HA are comprised of a number of groups such as already well-known antioxidants, so will exhibit exceptionally high antioxidant capacities [7].

6. Results

6.1 Measurement of total phenolic content

All measurements of total phenolic content were made according to the method developed by Shetty et al. [8]. During these measurements, only high-quality (a.r.) chemicals were used. The fractions of humic substances were extracted by ourselves from samples of leonardite retrieved from Dudar. Rather than indirectly measuring the antioxidant property of the sample, the method measures its total phenolic content, from which its antioxidant capacity can be deduced. The method consisted of diluting 1 ml of the sample in 5 ml of distilled water and 1 ml of 95% ethanol in a test tube before adding 0.5 ml of 50% Folin-Ciocalteu (FC) reagent (half of distilled water in half FC reagents) to each sample. After being stirred for 5 minutes, 1 ml of 5% Na_2CO_3 was added to the reaction mixture and allowed to stand for 1 hour before the absorbance values of the samples were measured at 725 nm. These absorbance values were then converted into μg gallic acid equivalents in order to compare the measured values with each other and with other data from the literature.

Whilst measuring the total phenolic content of the samples, a series of dilutions was made from our samples of known mass, for which the total phenolic content was measured. A series of dilutions had to be produced in order to measure an absorbance value of approximately one for each sample. This was necessary to be able to

compare the samples because the three different fractions yielded one absorbance value at different concentrations once the reaction was complete. Furthermore, since the samples are coloured (brownish - dark brown), the measured absorbance values had to be calibrated in light of the background of the samples. Therefore, the samples were diluted to the concentration present in the reaction volume. After measuring the series of samples, their total phenolic content was calculated from the calibration curve, which can be seen in Fig. 2, and the results obtained are shown in Table 1.

The results show that different initial concentrations of the various samples are required to achieve a similar absorbance. In the humic acid samples, since the majority of the phenol groups are in this fraction, the lowest initial concentration is required to achieve an absorbance of approximately one. Himatomelanic acid has an average number of phenol groups while FA is comprised of the

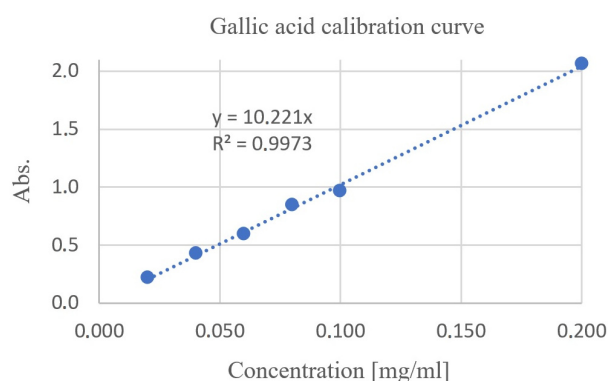


Figure 2: Calibration curve of gallic acid

Table 1: The measured and corrected absorbance of the samples and the gallic acid equivalent (GAE) values

Sample	Corrected concentration [mg/ml]	Abs measured	Abs corrected	GAE [mg/ml] from the calibration curve	GAE [mg/g]
HY	0.59	1.027	0.953	0.103	174.5
FA	1.18	0.999	0.948	0.102	86.8
HA	0.35	1.024	1.024	0.11	310.3
IHSS FA	0.684	-	1	0.107	156.8
IHSS HA	0.212	-	1	0.107	506.1

Table 2: The IC50 readings of the different samples

Name of the sample	Original concentration	IC50 [$\mu\text{g/ml}$]
HY	1.5 mg/ml	200
FA	2 mg/ml	300
HA	3.25 mg/ml	460

fewest. The results suggest that the studied humic fractions are likely to exhibit an antioxidant effect.

6.2 DPPH method

Measurement of the antioxidant capacity based on stable DPPH radical scavenging is one of the first methods. The reaction proceeds as follows: the dark purple radical formed in the reaction mixture loses its colour when it reacts with antioxidants.

This method is widely used because the radical-forming molecule DPPH is commercially available, stable as well as not particularly reactive nor aggressive, which is beneficial in the reactions that take place as taking measurements is simple. On the other hand, a stable radical that is not found in the living organism is used instead of a radical formed during the normal metabolism in the cell. Using this method, it is not possible to estimate how effective the sample is as an antioxidant with regard to biological radicals [8].

During the measurements, 6 ml of a DPPH working solution (0.1 mg/ml) was added to one ml of the sample, vortexed and stored in the dark for 30 minutes until the colour reaction began. After 30 minutes, the absorbances were measured at 517 nm. From the measured values that had previously been corrected, the percentage of inhibition (Inhibition%, Inhib.%) and the value corresponding to 50% inhibition (IC50 value) were calculated. While the measurements were taken, in the same way as when the total phenolic content was measured, a series of dilutions was made from a sample of known concentration. From the measured absorbances, after background correction the percentages of inhibition of the samples were calculated and plotted as a function of the concentration in order to determine the IC50 values of the samples (Fig. 3).

From the data, it can be concluded that the materials prepared and tested exhibit antioxidant properties because they inhibit the decomposition of the DPPH radical.

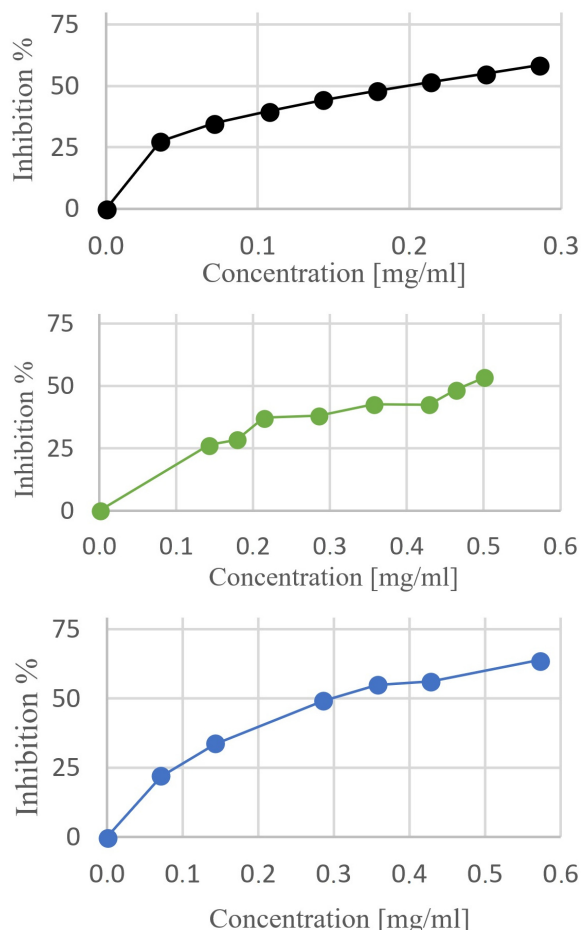


Figure 3: Percentage of inhibition of himatomelanic acid (top), humic acid (middle), and FA (bottom) as functions of the concentration to determine the IC50 values

Their IC50 values (Table 2) are promising and comparable with other data in the literature [9].

7. Conclusions

Although the results revealed that the samples made from domestic raw materials exhibit antioxidant properties, further studies are needed to gain a complete picture of the antioxidant capacity of these substances. Furthermore, in the future, it is our intention to confirm the results collected so far with in-vitro and in-vivo experiments.

REFERENCES

- [1] Balogh, E.; Hegedus, A.; Stefanovits-Banyai, E.: Application of and correlation among antioxidant and antiradical assays for characterizing antioxidant capacity of berries *Sci. Hortic.*, 2010, **125**(3), 332–336 DOI: [10.1016/j.scienta.2010.04.015](https://doi.org/10.1016/j.scienta.2010.04.015)
- [2] Stevenson, F.J.: *Humus Chemistry: Genesis, composition, reactions* (Wiley & Sons, New York, USA) 1994, pp. 188–210 ISBN: 978-0-471-59474-1
- [3] NCCIH: Antioxidants: In depth, retrieved 20 June 2018 <https://www.nccih.nih.gov/health/antioxidants-in-depth>
- [4] Škvára, P.; Kezmanová, J.; Mišřanová, C.; Vojs Staňová, A.: Analysis and identification of polyphenolic compounds in green foods using a combination of HPLC-ESI-IT-TOF-MS/MS *Hung. J. Ind. Chem.*, 2018 **46**(1), 35–38 DOI: <https://doi.org/10.1515/hjic-2018-0008>
- [5] Huang, D.; Ou, B.; Prior, R.L.: The chemistry behind antioxidant capacity assays *J. Agric. Food Chem.*, 2015, **53**(6), 1841–1856 DOI: [10.1021/jf030723c](https://doi.org/10.1021/jf030723c)
- [6] Csicsor, J.; Gerse, J.; Tikos, A.: The biostimulant effect of different humic substance fractions on seed germination, In: *Humic substances in the global environment and implications on human health*, N. Senesi and T. M. Miano (eds.) pp. 557–562; Proc. 6th Intern. Meeting of the Intern. Humic Substances Soc., Monopoli, Bari, Italy, Sept. 20–25, 1994
- [7] Ponomarenko, E.V.; Anderson, D.W.: Importance of charred organic matter in Black Chernozem soils of Saskatchewan *Can. J. Soil Sci.*, 2001, **81**(3), 285–297 DOI: [10.4141/s00-075](https://doi.org/10.4141/s00-075)
- [8] Vattem, D.A.; Shetty, K.: Ellagic acid production and phenolic antioxidant activity in cranberry pomace (*Vaccinium macrocarpon*) mediated by *Lentinus edodes* using a solid-state system *Process Biochem.*, 2003, **39**(3), 367–379 DOI: [10.1016/S0032-9592\(03\)00089-X](https://doi.org/10.1016/S0032-9592(03)00089-X)
- [9] Ruiz-Torralba, A.; Guerra-Hernández, E.J.; García-Villanova, B.: Antioxidant capacity, polyphenol content and contribution to dietary intake of 52 fruits sold in Spain. *CyTA - Journal of Food*, 2018, **16**(1), 1131–1138 DOI: [10.1080/19476337.2018.1517828](https://doi.org/10.1080/19476337.2018.1517828)

A SURVEY OF SARS-COV-2 GENETIC MATERIAL REDUCTION DURING A TRADITIONAL WASTEWATER TREATMENT TECHNOLOGY

ORSOLYA ADAMCSIK^{*1}, RENÁTA GERENCSÉR-BERTA¹, BORBÁLA OLÁHNÉ HORVÁTH¹,
NIKOLETTA KOVÁCS¹, VIOLA SOMOGYI², ENDRE GÁBOR DOMOKOS², GÁBOR KEMENESI³,
ENDRE GÁBOR TÓTH³, FERENC JAKAB³, AND ILDIKÓ GALAMBOS¹

¹Soós Ernő Water Technology Research and Development Center, University of Pannonia, Zrínyi Miklós u. 18, Nagykanizsa, 8800 HUNGARY

²Research Centre for Biochemical, Environmental and Chemical Engineering, University of Pannonia, Egyetem u. 10, Veszprém, 8200 HUNGARY

³National Virology Laboratory, Szentágotthai János Research Centre, University of Pécs, Ifjúság u. 20, Pécs, 7624 HUNGARY

The transmission of Severe Acute Respiratory Syndrome Coronavirus-2 in a community can be monitored by a wastewater-based epidemiological approach due to fecal shedding. Although sewage surveillance has gained a considerable amount of attention over the last 16 months, an indirect issue within the topic is whether traditional wastewater treatment technologies are sufficiently efficient to eliminate the genetic material of SARS-CoV-2. Samples were taken from the Wastewater Treatment Plant in Nagykanizsa before the virus was concentrated, nucleic acid extracted and SARS-CoV-2 detected by RT-qPCR (Quantitative reverse transcription PCR). The influent and primary treated samples tested positive, while after the secondary treatment, all the results were negative. Consequently, the activated sludge process proved to be efficient in terms of the removal of SARS-CoV-2.

Keywords: warning system, COVID-19, wastewater-based epidemiology

1. Introduction

During the transmission of severe acute respiratory syndrome coronavirus 2 (SARS-CoV-2) since the start of the COVID-19 pandemic, wastewater-based epidemiology (WBE) has gained a considerable amount of attention as a surveillance system. Numerous research groups and health authorities are currently engaged in sewage monitoring worldwide. Apart from viruses, various compounds can be monitored, e.g. pharmaceuticals or illicit drugs, to indirectly monitor the behavior or habits of a defined population [1]. Furthermore, the approach allows anonymous, area-based monitoring in a community that is cost-, labor- and time-efficient compared to human nasopharyngeal swab test campaigns [2]. Moreover, fecal shedding can occur earlier than the onset of symptoms [3,4], should any be expressed. While the ratio and role of asymptomatic and mild-symptomatic cases is debatable [5,6], the WBE approach estimates the SARS-CoV-2 RNA concentration of the total community that is inde-

pendent of patients' perception of well-being. Although WBE has its own limitations, sewage monitoring and human test campaigns can also support national and municipal decision-making. Considering the successful detection of SARS-CoV-2 from wastewater and during the consecutive steps of wastewater treatment, a considerable amount of aerosol formation has been observed. Moreover, since droplets are regarded as the most important transmission route of SARS-CoV-2, the working conditions at wastewater treatment plants (WWTP) should be addressed in terms of safety. According to the WHO [7], no special care is required other than the usual safety protocols at such plants since SARS-CoV-2 particles present in untreated and treated wastewater have been proven to be non-infectious. Another side interest within this topic is whether the sewage treatment technology is sufficiently effective to eliminate the SARS-CoV-2 virus particles detected in the influent to ensure the WWTP effluents are SARS-CoV-2-free, even if their infectivity has already been ruled out. The aim of this work is to assess the presence and concentration of SARS-CoV-2 RNA in untreated and treated wastewater samples.

Received: 26 August 2021; Revised: 20 September 2021; Accepted: 20 September 2021

*Correspondence: adamcsik.orsolya@sooswrc.hu

Table 1: SARS-CoV-2 RNA detection from wastewater influent and effluent samples at Nagykanizsa WWTP.

Sample type	Date	Cq value (E-gene)
Influent	30/09/2020	+(35.69)
Influent	14/10/2020	+(33.88)
Influent	09/11/2020	+(32.39)
Influent	10/11/2020	+(33.70)
Influent	11/11/2020	+(34.27)
Influent	18/11/2020	+(36.67)
Influent	25/11/2020	+(37.03±0.11)
Effluent	25/11/2020	–
Influent	02/12/2020	+(33.70±0.50)
Effluent	02/12/2020	–

2. Materials and Methods

Sampling was conducted by Délzalai Víz és Csatornamű Zrt. at Nagykanizsa WWTP during the morning peak time. From May until December 2020, samples of influent and occasionally effluent as well were taken at various sampling frequencies. While in December, on three consecutive days, in addition to influent and effluent sampling points, primary and secondary treated samples were also checked. The pairs of influent and effluent samples were processed in duplicates, while to assess the efficacy of the WWTP, three repetitions were used over three consecutive days. 1 L grab samples were taken and placed in sterile bottles, transported to our laboratory at 4 °C and immediately processed. The virus was concentrated and nucleic acid extracted according to Meleg et al. [8] with minor modifications. Concentrates were stored and transported at –80 °C to the National Virology Laboratory, University of Pécs for specific SARS-COV-2 detection by the quantitative reverse transcription polymerase chain reaction (RT-qPCR) technique, targeting the E and RdRp genes. Modular SARS-CoV-2 E-gene and Modular SARS-CoV-2 RdRp-gene detection kits (Roche, Germany) on the MyGo Pro real-time PCR instrument were employed. Quantification cycle values (Cq values) were used to compare the SARS-CoV-2 RNA concentration of the above-mentioned samples.

3. Results and Discussion

Sewage samples tested negative during the summer months of 2020 (data not shown), which is plausible considering the insignificant number of open cases nationwide [9] and the temperature of the sewage as one of the most important environmental factors [10]. At the end of September, as the second wave progressed, the concentration of SARS-CoV-2 RNA increased above the detection limit of the methods in the influent samples, while all effluent samples tested negative. During the autumn of 2020 - although the first positive result was registered, followed by fluctuating quantification cycles - all the results from influent samples (Table 1) were positive, while

Table 2: SARS-CoV-2 RNA concentration at different stages of wastewater treatment at the Nagykanizsa WWTP (due to the rules of PCR amplification, higher quantification cycle values are linked to lower SARS-CoV-2 RNA concentrations)

Sample type	Date	Cq value (E gene)
Influent	08/12/2020	+(28.89)
	09/12/2020	+(34.06)
	10/12/2020	+(31.04)
Primary treated	08/12/2020	+(40.04)
	09/12/2020	+(35.43)
	10/12/2020	+(37.13)
Secondary treated	08/12/2020	–
	09/12/2020	–
	10/12/2020	–
Effluent	08/12/2020	–
	09/12/2020	–
	10/12/2020	–

their effluent sample pairs all tested negative without exception. From this information alone, it can be concluded that the commonly used, complex wastewater treatment technology itself is sufficiently efficient to decrease the SARS-CoV-2 RNA load from wastewater without any additional steps, e.g. UV light treatment or surplus chemicals. Our results concerning the influent-effluent pairs are in good agreement with earlier findings by Haramoto et al. [11]

By progressing one step further, samples were tested after primary and secondary treatment at the Nagykanizsa WWTP (Table 2). Over three consecutive days - while the influent samples tested positive, although the primary treated wastewater exhibited a slightly lower concentration of SARS-CoV-2 RNA - the results were still positive (manifesting in higher quantification cycles). From this reduction, it can be seen that the majority of the SARS-CoV-2 particles are not attached to the solid particles sedimented in this step. However, the duration of SARS-CoV-2 particles in wastewater is also an important factor [10] that can be partially responsible for the loss in RNA load compared to the raw influent. After the activated sludge process, the estimated duration of SARS-CoV-2 particles was longer than 8 hours and all samples tested negative. This loss of signal is reasonable considering the lengthy nature of the secondary treatment, the microbial activity together with the limited resistance of these viral particles to external agents [12] as well as the extreme sensitivity of the RNA. As in the case of the earlier tested influent-effluent pairs, all treated effluent samples yielded negative results. Over the last year, numerous other research groups have tested various WWTPs with partially different technological setups [11, 13–16] to that employed at Nagykanizsa WWTP. A general consensus has been reached in all these experiments regarding the negative results of all the effluent material flow (treated

effluent water and sludge line). Even though some studies yielded positive results for some of the secondary treated effluents [11, 13] or secondary sludges [16], in these cases all the treated materials exiting the WWTP produced negative results without exception.

4. Conclusion

According to our findings, which are in good agreement with other published research on this topic, the common treatment of wastewater is capable of decreasing the SARS-CoV-2 RNA concentration below the complex detection limit of the multi-step measurement process. WWTPs are capable of minimizing the presence of coronavirus nucleic acid without having to add further steps to the traditional technology. All in all, the SARS-CoV-2 viral particles are particularly stable in aquatic environments, so the treated wastewater discharge and risks related to its reuse have not proved to be considerable.

5. Acknowledgement

Financial support was received from the National Research, Development and Innovation Office (grant no. 2020-2.2.1-ED-2020-00014). The authors would like to express their gratitude to the MOL Group for their cooperation.

REFERENCES

- [1] Lorenzo, M.; Picó, Y.: Wastewater-based epidemiology: current status and future prospects, *Curr. Opin. Environ. Sci. Health*, 2019, **9**, 77–84 DOI: [10.1016/j.coesh.2019.05.007](https://doi.org/10.1016/j.coesh.2019.05.007)
- [2] Bivins, A. et al.: Wastewater-based epidemiology: Global collaborative to maximize contributions in the fight against COVID-19, *Environ. Sci. and Technol.*, 2020, **54**(13), 7754–7757 DOI: [10.1021/acs.est.0c02388](https://doi.org/10.1021/acs.est.0c02388)
- [3] Ahmed, W.; Angel, N.; Edson, J.; Bibby, K.; Bivins, A.; O'Brien, J.W.; Choi, P.M.; Kitajima, M.; Simpson, S.L.; Li, J.; Tschärke, B.; Verhagen, R.; Smith, W.J.; Zaugg, J.; Dierens, L.; Hugenholtz, P.; Thomas, K.V.; Mueller, J.F.: First confirmed detection of SARS-CoV-2 in untreated wastewater in Australia: A proof of concept for the wastewater surveillance of COVID-19 in the community, *Sci. Total Environ.*, 2020, **728**, 138764 DOI: [10.1016/j.scitotenv.2020.138764](https://doi.org/10.1016/j.scitotenv.2020.138764)
- [4] Medema, G.; Heijnen, L.; Elsinga, G.; Italiander, R.; Brouwer, A.: Presence of SARS-Coronavirus2 RNA in sewage and correlation with reported COVID-19 prevalence in the early stage of the epidemic in the Netherlands, *Environ. Sci. Technol. Lett.*, 2020, **7**(7), 511–516. DOI: [10.1021/acs.estlett.0c00357](https://doi.org/10.1021/acs.estlett.0c00357)
- [5] Koh, W.C.; Naing, L.; Chaw, L.; Rosledzana, M.A.; Alikhan, M.F.; Jamaludin, S.A.; Amin, F.; Omar, A.; Shazli, A.; Griffith, M.; Pastore, R.; Wong, J.: What do we know about SARS-CoV-2 transmission? A systematic review and meta-analysis of the secondary attack rate and associated risk factors, *PLOS One*, 2020, **5**(10), e0240205 DOI: [10.1371/journal.pone.0240205](https://doi.org/10.1371/journal.pone.0240205)
- [6] Slifka, M.K.; Gao, L.: Is presymptomatic spread a major contributor to COVID-19 transmission?, *Nat. Med.*, 2020, **26**, 1531–1533 DOI: [10.1038/s41591-020-0869-5](https://doi.org/10.1038/s41591-020-0869-5)
- [7] World Health Organization: Water, sanitation, hygiene, and waste management for SARS-CoV-2, the virus that causes COVID-19: Interim guidance, *WHO statement*, 2020 <https://www.who.int/publications/i/item/WHO-2019-nCoV-IPC-WASH-2020.4>
- [8] Meleg, E.; Bányai, K.; Martella, V.; Jiang, B.; Kocsis, B.; Kisfali, P.; Meleg, B.; Szucs, G.: Detection and quantification of group C rotaviruses in communal sewage, *Appl. Environ. Microbiol.*, 2008, **74**, 3394–3399 DOI: [10.1128/AEM.02895-07](https://doi.org/10.1128/AEM.02895-07)
- [9] John Hopkins Coronavirus Resource Center: COVID-19 Database, *John Hopkins University Database*, 2021 <https://coronavirus.jhu.edu/map.html>
- [10] Hart, O.E.; Halden, R.U.: Computational analysis of SARS-CoV-2/COVID-19 surveillance by wastewater-based epidemiology locally and globally: Feasibility, economy, opportunities and challenges, *Sci. Total Environ.*, 2020, **730**, 138875 DOI: [10.1016/j.scitotenv.2020.138875](https://doi.org/10.1016/j.scitotenv.2020.138875)
- [11] Haramoto, E.; Malla, B.; Kitajima, M.: First environmental surveillance for the presence of SARS-CoV-2 RNA in wastewater and river water in Japan, *Sci. Total Environ.*, 2020, **737**, 140405 DOI: [10.1101/2020.06.04.20122747](https://doi.org/10.1101/2020.06.04.20122747)
- [12] van Doremalen, N.; Bushmaker, T.; Morris, D.H.; Holbrook, M.G.; Gamble, A.; Williamson, B.N.; Tamin, A.; Harcourt, J.L.; Thornburg, N.J.; Gerber, S.I.; Lloyd-Smith, J.O.; de Wit, E.; Munster, V.J.: Aerosol and Surface Stability of SARS-CoV-2 as Compared with SARS-CoV-1, *New Engl. J. Med.*, 2020, **382**, 1564–1567 DOI: [10.1056/NEJMc2004973](https://doi.org/10.1056/NEJMc2004973)
- [13] Randazzo, W.; Truchado, P.; Cuevas-Ferrando, E.; Simón, P.; Allende, A.; Sánchez, G.: SARS-CoV-2 RNA in wastewater anticipated COVID-19 occurrence in a low prevalence area, *Water Res.*, 2020, **181**, 115942 DOI: [10.1016/j.watres.2020.115942](https://doi.org/10.1016/j.watres.2020.115942)
- [14] Arora, S.; Nag, A.; Sethi, J.; Rajvanshi, J.; Saxena, S.; Shrivastava, S.K.; Gupta, A.B.: Sewage surveillance for the presence of SARS-CoV-2 genome as a useful wastewater based epidemiology (WBE) tracking tool in India, *Water Sci. Technol.*, 2020, **82**(12), 2823–2836 DOI: [10.1101/2020.06.18.20135277](https://doi.org/10.1101/2020.06.18.20135277)
- [15] Sherchan, S.P.; Shahin, S.; Ward, L.M.; Tandukar, S.; Aw, T.G.; Schmitz, B.; Ahmed, W.; Kitajima, M.: First detection of SARS-CoV-2 RNA in

- wastewater in North America: A study in Louisiana, USA, *Sci. Total Environ.*, 2020, **743**, 140621 DOI: [10.1016/j.scitotenv.2020.140621](https://doi.org/10.1016/j.scitotenv.2020.140621)
- [16] Balboa, S.; Mauricio-Iglesias, M.; Rodriguez, S.; Martínez-Lamas, L.; Vasallo, F.J.; Regueiro, B.; Lema, J.M.: The Fate of SARS-CoV-2 in WWTPS Points Out the Sludge Line as a Suitable Spot for Monitoring, *Sci. Total Environ.*, 2020, **772**, 145268 DOI: [10.1101/2020.05.25.20112706](https://doi.org/10.1101/2020.05.25.20112706)

PLANT GROWTH-PROMOTING RHIZOBACTERIA – BIOTECHNOLOGICAL TOOLS TO IMPROVE CEREAL YIELDS

GYÖNGYI SZÉKELY ^{*1,2,3} AND CSENGELE BARTA⁴

¹Hungarian Department of Biology and Ecology, Faculty of Biology and Geology, Babeş-Bolyai University, 5-7 Clinicilor St., Cluj-Napoca, 400006 ROMANIA

²Institute for Research-Development-Innovation in Applied Natural Sciences, Babeş-Bolyai University, 30 Fântânele St., Cluj-Napoca, 400294 ROMANIA

³Centre for Systems Biology, Biodiversity and Bioresources (3B), Babeş-Bolyai University, 5-7 Clinicilor St., Cluj-Napoca, 400006 ROMANIA

⁴Department of Biology, Missouri Western State University, 4525 Downs Drive, Agenstein-Remington Halls, St. Joseph, MO 64507, USA

Ensuring food security for the world's growing population is a significant challenge for scientists. Efforts are constantly being made to solve this problem, including the use of expensive molecular engineering techniques, which are not always successful. A cost-effective and environmentally friendly biotechnological alternative would be the use of plant growth-promoting rhizobacteria, demonstrated by numerous studies to play many beneficial roles in improving plant traits, e.g. enhanced yields.

Keywords: plant growth-promoting rhizobacteria (PGPR), yield, environmentally friendly, low-cost

1. Introduction

Cereals like bread wheat (*Triticum aestivum*), maize (*Zea mays*) and rice (*Oryza sativa*) are fundamental and essential grain crops for both human and animal consumption. According to the Statista statistics site, in 2020-2021, maize production exceeded 1.12 billion metric tons, wheat 775.8 million metric tons and rice about 505 million metric tons [1]. Since the world's population is constantly growing, the need to increase cereal production is continuous. However, the increasing occurrence of biotic and abiotic stress factors in the environment constitutes a severe global threat to improving cereal yields [2, 3]. To alleviate the detrimental effects of yield loss, expensive genetic engineering techniques for crop improvement have been developed. The use of plant growth-promoting rhizobacteria (PGPR) could represent a low-cost and environmentally friendly alternative biotechnological option. These kinds of soil bacteria, first described by Kloepper and Schroth in 1978 [4], were isolated from the immediate vicinity of plants, that is, from the rhizosphere. Later, several beneficial effects of PGPR in stimulating plant growth were described [5–7].

Nowadays, the PGPR biotechnology is more and more frequently used in the management of biotic and abiotic stress factors for a wide range of crop species in

order to reduce their damaging effects, which ultimately can cause important yield losses [6, 7]. Understanding the mechanisms at the basis of the PGPR technology in alleviating biotic and abiotic stress-induced damage in crops could be essential to reduce subsequent crop yield losses. Exploiting the positive effects of plant-microbe interactions might provide multiple multi-pronged solutions to the global food crisis, reduce the amount of irrigation provided by fresh water as well as solve environmental stress concerns and maintain soil health.

2. The most common effects of PGPRs on plants

Over the last decade, versatile positive properties of PGPRs have been intensely documented. Dozens of articles highlight the importance of these rhizobacteria in the process of alleviating damage brought about by abiotic stress. A large number of different PGPR species, e.g. *Pseudomonas alcaligenes*, *P. mendocina*, *Bacillus polymyxa*, *B. pumilus* and *Mycobacterium phlei*, have been described to play a positive role in stimulating growth in various plant species as well as in the process of improving their tolerance of high temperatures and the salinity of many crops [6, 7]. Shrivastava and Kumar (2015) indicated that certain PGPR species can produce antioxidants, therefore, can be useful for reducing oxidative stress-induced damage to plants [6]. In-

*Correspondence: gyongyi.szekely@ubbcluj.ro

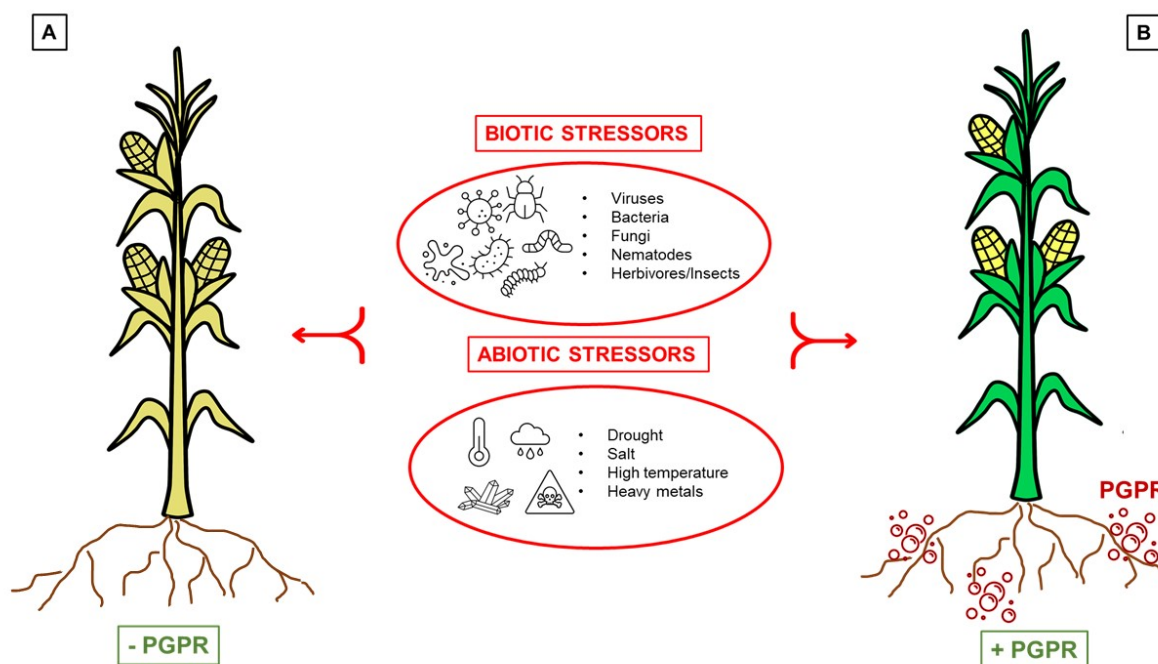


Figure 1: The impact of biotic and abiotic stress on crop resistance in the absence (panel A) and presence (panel B) of PGPR.

oculation with PGPRs improved seed germination and seedling growth, increased the concentrations of chlorophylls, antioxidant enzymes, proline, malondialdehyde and flavonoids as well as reduced the Na^+ content in different crops [8, 9]. Recently, a couple of authors documented a set of plant growth-promoting traits, namely the ability to solubilize phosphate as well as produce indole-3-acetic acid (IAA) and 1-aminocyclopropane-1-carboxylic acid (ACC) deaminase of different PGPR species [7, 10, 11]. Furthermore, several physiological traits such as leaf chlorophyll content, stomatal conductance, leaf relative water content and membrane leakage adversely affected by cold stress were mitigated by PGPR [12].

In addition, certain PGPR species are important factors in relieving not only abiotic but also biotic stress-induced damage. Plants are commonly attacked by aphids and fungi, which cause substantial yield losses in crops and especially affect the production of cereal grains globally [3, 13, 14]. Naem et al. (2018) showed the positive effect of *Bacillus* spp. and *Pseudomonas* spp. in terms of enhancing the productivity of wheat attacked by aphid populations [3]. Fungi represented by the genus *Fusarium* infest cereals worldwide, moreover, *F. graminearum* is responsible for cereal head blight and maize ear rot in North and South America, Europe as well as Asia [14, 15]. To reduce the considerable amount of destruction caused by *F. graminearum*, several authors propose the use of an effective, economical and environmentally friendly biotechnological tool. They demonstrate that different PGPR species have antagonistic effects on *F. graminearum* and possess the ability to promote wheat

growth under adverse biotic and abiotic stress conditions as well [16, 17]. Fig. 1 illustrates the impact of biotic and abiotic stress on crop resistance in the absence and presence of PGPR.

Finally, PGPR species can also function as important components of biofertilizers and biopesticides since they can improve the nutrient content and quality of soil through the mechanisms of nitrogen fixation and phosphate solubilization. As biopesticides, these rhizobacteria protect the plants as a result of their ability to synthesize antibiotics [18, 19]. Efforts to implement such environmentally friendly technologies are increasing annually and could be part of the solution to the ever-increasing demand for food to feed the growing global population.

3. PGPR mediates increases in cereal-crop yields

Biotic and abiotic stress factors usually cause a series of negative effects on crop yield, quantity and quality. Under adverse environmental conditions and exposed to multifarious pathogen attacks from viruses, bacteria, fungi, insects, etc., plants respond defensively, implying changes in several physiological and nutritional parameters, hormonal imbalances and important yield losses [7, 10, 18]. Globally, wheat, maize and rice are essential staple foods for billions of people. Annually, these cereals are grown on hundreds of millions of hectares of land and are consumed by several billion people in hundreds of countries. As a result of population growth, production must continuously be enhanced. Predictions state that by the year 2050, consumers will need 60% more wheat compared to the present production rate [20]. This must be

Table 1: Beneficial effects of some PGPR species on wheat, maize and rice yields

PGPR species	Effect on yield	Cereal species	Reference
<i>Azospirillum</i> sp.	Enhanced grain yield;	wheat	[12]
<i>Bacillus</i> sp.	Enhanced straw yield;		
<i>Bacillus megaterium</i>	Increased uptake of macro nutrients (N, P, K, Ca, Mg and S);		
<i>Paenibacillus polymyxa</i>			
<i>Raoultella terrigena</i>	Increased uptake of micro nutrients (Fe, Mn, Zn and Cu).		
<i>Bacillus</i> sp.	Enhanced grain yield;	wheat	[3]
<i>Pseudomonas</i> spp.	Enhanced straw yield; Enhanced number of grains per spike; Enhanced number of productive tillers.		
<i>Alcaligenes faecalis</i>	Enhanced grain yield;	wheat	[21]
<i>Bacillus aryabhatai</i>	Enhanced plant growth-promoting traits (shoot and root lengths, fresh and dry weights).		
<i>Pseudomonas corrugata</i>			
<i>Pseudomonas arsenicoxydans</i>			
<i>Pseudomonas brassicacearum</i>			
<i>Pseudomonas azotoformans</i>			
<i>Bacillus pumilus</i>	Enhanced grain yield;	maize	[22]
<i>Bacillus safensis</i>	Phosphate solubilization (except for <i>L. sphaericus</i>);		
<i>Lysinibacillus sphaericus</i>	Nitrogen fixation.		
<i>Paenibacillus alvei</i>			
<i>Cupriavidus necator</i>	Enhanced aerial biomass;	maize	[23]
<i>Pseudomonas fluorescens</i>	Increase in N and P use efficiencies.		
<i>Azospirillum brasilense</i>	Enhanced grain yield;	rice	[24]
<i>Azotobacter chroococcum</i>	Enhanced IAA production;		
<i>Pseudomonas aeruginosa</i>	Enhanced phosphate solubilization.		
<i>Pseudomonas fluorescens</i>			
<i>Pseudomonas putida</i>			
<i>Bacillus</i> sp.	Enhanced grain yield;	rice	[26]
<i>Bacillus thuringiensis</i>	Enhanced root and shoot biomasses;		
<i>Pseudomonas mosselii</i>	Enhanced production of IAA, siderophores and ACC deaminase as well as the ability to solubilize phosphate.		

achieved without expanding the area of arable land and by using eco-friendly and low-cost biotechnological strategies. One of these strategies is the use of PGPR to enhance crop productivity. Table 1 presents the impact and efficacy of different PGPR species in enhancing wheat, maize and rice yields [3, 12, 21–25].

4. Conclusions

The use of plant growth-promoting rhizobacteria to improve cereal yields represents a prosperous, environmentally friendly and economical strategy. PGPR are useful tools to reduce the effects of biotic and abiotic stress on plants, therefore, could contribute towards optimal plant growth and development as well as enhance their yields. Finally, PGPR could represent a resource to ease the emerging global food crisis.

REFERENCES

- [1] Worldwide production of grain in 2021/22, by type <https://www.statista.com/statistics/263977/world-grain-production-by-type/> retrieved 27 October 2021
- [2] Afzal, A.; Bano, A.: *Rhizobium* and phosphate solubilizing bacteria improve the yield and phosphorus uptake in wheat (*Triticum aestivum*), *Int. J. Agric. Biol.* 2008, **10**(1), 85–88
- [3] Naeem, M.; Aslam, Z.; Khaliq, A.; Ahmed, J. N.; Nawaz, A.; Hussain, M.: Plant growth promoting rhizobacteria reduce aphid population and enhance the productivity of bread wheat, *Braz. J. Microbiol.* 2018, **49**(1) 9–14 DOI: 10.1016/j.bjm.2017.10.005
- [4] Kloepper, J. W.; Schroth, M. N.: Plant growth promoting rhizobacteria on radishes, Proceedings of the 4th International Conference on Plant Pathogenic Bacteria. Angers, France: Station de Pathologie végétale et Phytobactériologie, INRA. 1978, **2** 879–882
- [5] Aziz, Z. F. A.; Saud, H. M.; Rahim, K. A.; Ahmed, O. H.: Variable responses on early development of shallot (*Allium ascalonicum*) and mustard (*Brassica juncea*) plants to *Bacillus cereus* inoculation, *Malays. J. Microbiol.* 2012, **8**(1) 47–50 DOI: 10.21161/mjm.33711
- [6] Shrivastava, P.; Kumar, R.: Soil salinity: A serious environmental issue and plant growth promoting bacteria as one of the tools for its alleviation, *Saudi J. Biol. Sci.* 2015, **22**(2) 123–131 DOI: 10.1016/j.sjbs.2014.12.001

- [7] Etesami, H.; Beattie, G. A.: Mining halophytes for plant growth-promoting halotolerant bacteria to enhance the salinity tolerance of non-halophytic crops, *Front. Microbiol.* 2018, **9**, 148 DOI: 10.3389/fmicb.2018.00148
- [8] Qin, S.; Feng, W. W.; Zhang, Y. J.; Wang, T. T.; Xiong, Y. W.; Xing, K.: Diversity of bacterial microbiota of coastal halophyte *Limonium sinense* and amelioration of salinity stress damage by symbiotic plant growth-promoting *Actinobacterium glutamicibacter* halophytocola KLBMP 5180, *Appl. Environ. Microbiol.* 2018, **84**(19), e01533-18 DOI: 10.1128/AEM.01533-18
- [9] Akhtar, S. S.; Amby, D. B.; Hegelund, J. N.; Fimognari, L.; Großkinsky, D. K.; Westergaard, J. C.; Müller, R.; Moelbak, L.; Liu, F.; Roitsch, T.: *Bacillus licheniformis* FMCH001 increases water use efficiency via growth stimulation in both normal and drought conditions, *Front. Plant. Sci.* 2020, **7**, 297 DOI: 10.3389/fpls.2020.00297
- [10] Ferreira, M. J.; Cunha, A.; Figueiredo, S.; Faustino, P.; Patinha, C.; Silva, H.; Sierra-Garcia, I. N.: The root microbiome of *Salicornia ramosissima* as a seedbank for plant-growth promoting halotolerant bacteria, *Appl. Sci.* 2021, **11**(5), 2233 DOI: 10.3390/app11052233
- [11] Saleem, S.; Iqbal, A.; Ahmed, F.; Ahmad, M.: Phytobeneficial and salt stress mitigating efficacy of IAA producing salt tolerant strains in *Gossypium hirsutum*, *Saudi J. Biol. Sci.* 2021, **28**(9), 5317–5324 DOI: 10.1016/j.sjbs.2021.05.056
- [12] Turan, M.; Gulluce, M.; Çakmakçı, R.; Oztas, T.; Tahin, F.; Gilkes, R.; Prakongkep, N.: The effect of PGPR strain on wheat yield and quality parameters. Conference paper: Proceedings of the 19th World Congress of Soil Science: Soil solutions for a changing world, Australia, 2010, **15**, 140–143
- [13] Goswami, R. S.; Kistler, H. C.: Heading for disaster: *Fusarium graminearum* on cereal crops, *Mol. Plant. Pathol.* 2004, **5**(6), 515–525 DOI: 10.1111/j.1364-3703.2004.00252.x
- [14] Mielniczuk, E.; Skwaryło-Bednarsz, B.: *Fusarium* head blight, mycotoxins and strategies for their reduction, *Agronomy* 2020, **10**(4), 509 DOI: 10.3390/agronomy10040509
- [15] Hietaniemi, V.; Rämö, S.; Yli-Mattila, T.; Jestoi, M.; Peltonen, S.; Kartio, M.; Sieviläinen, E.; Koivisto, T.; Parikka, P.: Updated survey of *Fusarium* species and toxins in Finnish cereal grains, *Food Add. Contam. Part. A.* 2016, **33**(5), 831–848 DOI: 10.1080/19440049.2016.1162112
- [16] Abdulkareem, M.; Aboud, H.; Saood, H.; Shibly, M.: Antagonistic activity of some plant growth rhizobacteria to *Fusarium graminearum*, *Int. J. Phytopathol.* 2014, **3**(1), 49–54 DOI: 10.33687/phytopath.003.01.0660
- [17] Singh, R. P.; Jha, P. N.: The PGPR *Stenotrophomonas maltophilia* SBP-9 augments resistance against biotic and abiotic stress in wheat plants, *Front. Microbiol.* 2017, **8**, 1945 DOI: 10.3389/fmicb.2017.01945
- [18] Sindhu, S. S.; Sharma, R.: Amelioration of biotic stress by application of rhizobacteria for agriculture sustainability. In: Sayyed, R. (Eds.) Plant growth promoting rhizobacteria for sustainable stress management. Microorganisms for sustainability; Springer, 2019, 13 DOI: 10.1007/978-981-13-6986-5_5
- [19] Riaz, U.; Murtaza, G.; Anum, W.; Samreen, T.; Sarfraz, M.; Nazir, M. Z.: Plant growth-promoting rhizobacteria (PGPR) as biofertilizers and biopesticides. In: Hakeem, K. R.; Dar, G. H.; Mehmood, M. A.; Bhat, R. A. (Eds.) Microbiota and Biofertilizers; Springer. 2021, 181–196 DOI: 10.1007/978-3-030-48771-3_11
- [20] Wheat in the world <https://wheat.org> retrieved 27 October 2021
- [21] Sheirdil, R. A.; Hayat, R.; Zhang, X. X.; Abbasi, N. A.; Ali, S.; Ahmed, M.; Khattak, J. Z. K.; Ahmad, S.: Exploring potential soil bacteria for sustainable wheat (*Triticum aestivum* L.) production, *Sustainability* 2019, **11**(12), 3361 DOI: 10.3390/su11123361
- [22] Breedts, G.; Labuschagne, N.; Coutinho, T. A.: Seed treatment with selected plant growth-promoting rhizobacteria increases maize yield in the field, *Ann. Appl. Biol.* 2017, **171**(2), 229–236 DOI: 10.1111/aab.12366
- [23] Pereira, S. I. A.; Abreu, D.; Moreira, H.; Vega, A.; Castro, P. M. L.: Plant growth-promoting rhizobacteria (PGPR) improve the growth and nutrient use efficiency in maize (*Zea mays* L.) under water deficit conditions, *Heliyon* 2020, **6**(10), e05106 DOI: 10.1016/j.heliyon.2020.e05106
- [24] Lavakush, L.; Yadav, J.; Verma, J. P.; Jaiswal, D. K.; Kumar, A.: Evaluation of PGPR and different concentration of phosphorus level on plant growth, yield and nutrient content of rice (*Oryza sativa*), *Ecol. Eng.* 2014, **62**, 123–128 DOI: 10.1016/j.ecoleng.2013.10.013
- [25] Kóczán-Manninger, K.; Badak-Kerti, K.: Investigations into flour mixes of *Triticum Monococcum* and *Triticum Spelta*, *Hung. J. Ind. Chem.* 2018, **46**(2), 63–66 DOI: 10.1515/hjic-2018-0020
- [26] Aw, X.; Li, Z.; Li, W. C.; Ye, Z. H.: The effect of plant growth-promoting rhizobacteria (PGPR) on arsenic accumulation and the growth of rice plants (*Oryza sativa* L.), *Chemosphere* 2020, **242**, 125136 DOI: 10.1016/j.chemosphere.2019.125136

MEMBRANE UNIT FOR INTEGRATED GAS SEPARATION – MEMBRANE BIOREACTOR (GS-MBR) SYSTEM

ZBYNĚK PIENKA *¹, JAKUB PETER¹, AND ROBERT VÁLEK²

¹Institute of Macromolecular Chemistry CAS, Heyrovského nám. 2, 162 06 Prague 6, CZECH REPUBLIC

²MemBrain s.r.o., Pod Vinicí 87, 471 27 Stráž pod Ralskem, CZECH REPUBLIC

One of the research directions of renewable energy sources is the production of biohydrogen from the dark fermentation of organic matter. During this fermentation process, since hydrogen is produced along with a complex mixture of other gases and vapors, hydrogen gas requires further purification. One relatively easy solution to this problem might be the utilization of gas separation membrane modules given their low energy consumption, simple operation and ease of upscaling. In this work, hollow fiber (HF) membranes based on polyetherimide (PEI) were developed and tested. HF membranes were spun from a polymer solution of PEI using the wet phase inversion process into a water bath using a pilot-scale spinning device. Gas transport measurements showed that membranes exhibited permeances of between 9.3 and 19.2 GPU with CO₂/H₂ selectivities within the range of 3.3 – 5.6. Morphology studies showed regular shapes resembling hollow fibers with outer diameters within the range of 250–320 microns, depending on various parameters of the spinning process. The best performing membranes were selected and a morphological analysis carried out. Selected fibers were incorporated into two types of membrane modules. One type was a laboratory-scale membrane mini-module used for preliminary tests, while the other membrane module was designed for the treatment of larger amounts of biohydrogen. Two types of laboratory-scale membrane separation units were constructed. For laboratory use, the low-pressure unit proved more accurate regulation to match the fermenters performance with the separation unit in comparison with the high-pressure one.

Keywords: polymer membranes, gas separation, hollow fibers, membrane module

1. Introduction

The motivation of this research is the need to reduce the ecological footprint of society by developing green technologies enabling carbon sequestration, sustainable production of valuable chemicals and environmentally-friendly energy production. This task is to be completed by the development of a novel, circular-loop gas separation membrane bioreactor system.

Microalgae grown in a photobioreactor capture refused-CO₂ from the fermentative reactor, which simply ferments these microalgae. During the process, a mixture of hydrogen and CO₂ is produced. The hydrogen can be separated and utilized for energy production. In addition, some valuable chemicals are produced. The newly developed system is known as a Gas Separation Membrane Bioreactor (GS-MBR) [1].

A key component of the GS-MBR is a membrane unit, which forms technological solutions for the separation of

H₂ and CO₂ from the fermentation product. The basic elements in the membrane unit are membrane modules that utilize hollow fiber (HF) membranes.

2. Experimental

2.1 Materials

PEI (ULTEM™ 1000 Resin grade) was purchased from SABIC. The chemical structure of a repeated unit of ULTEM™ 1000 Resin and the details regarding its preparation have previously been presented [2].

2.2 Development of HF membranes

Hollow fiber membranes were prepared with the strategic cooperation of the company MemBrain s.r.o. located in the Czech Republic. The procedure was described in our previous paper [2]. The spinline used for fabrication of the membranes is shown in Fig. 1.

2.3 Development of HF membrane modules

The HC1 HF membrane mini-module was prepared by fixing 10 – 20 fibers into the Swagelok tube fitting using

Received: 17 December 2021; Revised: 3 January 2022; Accepted: 4 January 2022

*Correspondence: pientka@imc.cas.cz

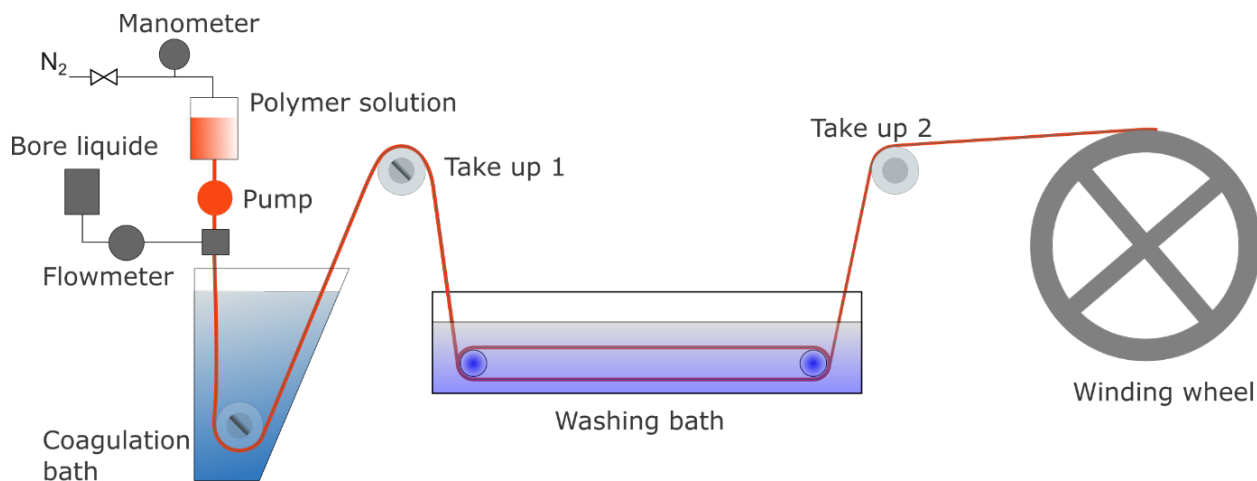


Figure 1: The spinline used for the fabrication of HF membranes

3M of the epoxy resin DP100. The same resin was used to create the dead end of the fibers. The whole assembly was inserted into the 12-mm-wide tube using the corresponding Swagelok tube fittings as presented in Fig. 2. The module was equipped with 6-mm-wide connectors.

P2-type HF membrane modules were constructed in a similar manner to those reported in [2], that is, from an arranged bundle of 250 A5-7 fibers (membrane area: 844 cm²) inserted into a PVC pipe. A schematic diagram of the P2-type HF membrane module and a photograph of it are presented in Fig. 3.



Figure 2: HC1 HF membrane mini-module

2.4 Determining the gas transport properties of the HF membrane

Laboratory modules containing 10 – 20 fibers of about 20 cm in length were prepared. One end of the fibers was sealed by an epoxy resin. The outer surface of the fibers was exposed to a mixture of gases which permeate into their hollow centers. Gas permeation experiments were carried out using a mixture of CO₂ and H₂ (1 : 1 volume ratio) at 2.0 and 4.2 bars (Δp was 1.0 and 3.2 bars, respectively) to determine the separation properties of the asymmetric PEI HF membrane. Its composition, pressures and flow rates were managed by the Poseidon

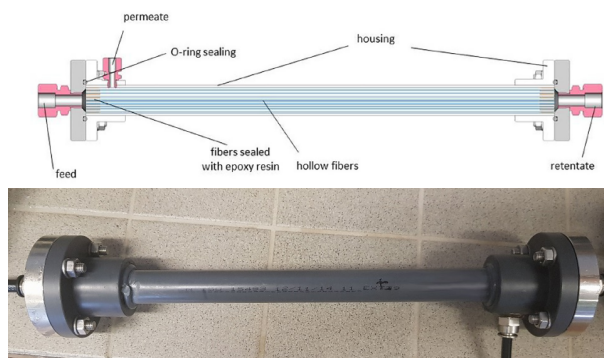


Figure 3: Schematic diagram of a cross-section of the P2-type HF membrane module

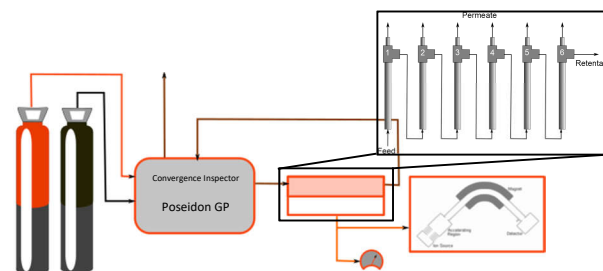


Figure 4: Testing of gas transport properties of prepared HF membranes

Table 1: Process parameters with regard to the production of asymmetric PEI membranes

Sample	Polymer dope dose ml/min	Bore liquid dose ml/min	Towing speed m/min	Air gap cm	OD μm	ID μm
A5-1	4.2	2.1	12	2	417	248
A5-2	4.2	2.1	9.7	5	405	234
A5-3	4.2	2.6	12	5	410	265
A5-7	6	2.6	12	2	420	239
B3-1	0.75	0.625	12	2.5	289	186
B3-2	0.75	0.625	15	6	270	190
B3-3	0.75	0.45	12	6	290	185
B3-7	0.9	0.45	12	2.5	320	171

Convergence Inspector Gas Permeation (Convergence Industry B.V.). The permeate flow rate was measured by a bubble flowmeter and the composition of the permeate stream analyzed by a Prima BT Bench Top mass spectrometer (Thermo Fisher Scientific). Six laboratory modules were tested in series, where the retentate from the first module was used as a feed for the second module and so on (Fig. 4). Although this setting minimizes gas consumption and saves time, the correct mass balance on each module should be calculated. More information with regard to this can be found in [3].

The permeance P_i for CO_2 and H_2 as well as the CO_2/H_2 mixed gas selectivity $\alpha_{i/j}^*$ were evaluated from measured data. The permeance P_i is defined as the volumetric flow rate per unit driving force per unit area:

$$P_i = \frac{Q_P \cdot y_i}{(p_P \cdot x_i - p_P \cdot y_i) \cdot A} \quad (1)$$

where Q_P denotes the flow rate of the permeate, y_i stands for the mole fraction of gas i in the permeate, p represents the absolute pressure in the feed or permeate and A is the membrane area.

2.5 Development of the membrane separation unit

The membrane apparatus was built using fittings from SUPERLOK; tubing 6 mm in diameter and Parker 201LG solenoid valves manufactured by Parker, 250 kPa BD Sensors pressure sensors and a BP300-1-S back pressure regulator by Pressure Tech; a KK15 A 035/62 compressor by Dürr Technik: oil-free, max. performance = 25 l/min, 8 bar, max. pressure = 12 bar; a Rocker 410 oil-free vacuum pump; a control unit based on an Arduino Uno microcomputer and software developed by the authors.

3. Results and discussion

3.1 Preparation of HF membranes

The preparation of HF membranes was carried out using 4 spinnerets simultaneously, resulting in a higher towing speed (15 m/min) which corresponds to the production of 3600 m of HF membrane per hour. There were two series

(denoted as A5 and B3) of fibers prepared using various spinning process parameters. The significant difference between the A5 and B3 series are the dimensions of the nozzles. For the A5 series, the outer outlet diameter (OD) of the larger nozzle was used (0.512 mm), whereas for the B3 series, the outer OD of the nozzle was 0.330 mm. The process parameters with regard to the production of the asymmetric PEI membranes are listed in Table 1. As can be seen, all the membranes with a dosing of polymer dope of 0.75 ml/min apparently had a smaller outer outlet diameter (OD) than the fibers with a flow rate of polymer dope of 0.9 ml/min. It can also be observed that at higher towing speeds, the ODs of HF membranes were lower (with the exception of membranes B3-6).

3.2 Characterization of gas transport across HF membranes

Each sample of membrane was measured in three membrane modules by simultaneously connecting six modules to a Poseidon Group system (i.e. two samples of membrane were tested simultaneously). The average values were recorded and presented in Table 2. The results showed that all the membranes exhibited permeances within the range of 9.3–19.2 GPU and H_2/CO_2 selectivities within the range of 3.3–5.6. It is well known that gas separation in polymers can be described by a solution-diffusion model [4] which states that the permeability coefficient is the product of the diffusion and solubility co-

Table 2: Gas transport properties of the prepared HF membranes for the H_2/CO_2 mixture measured at a pressure of 8 bars.

Sample	CO_2 permeance (GPU)	H_2/CO_2 selectivity
A5-1	11.5	4.4
A5-2	10.3	4
A5-3	17.5	5.3
A5-7	19.2	5.6
B3-1	9.5	4.4
B3-2	9.3	4
B3-3	10.3	5.3
B3-7	20.3	4.5

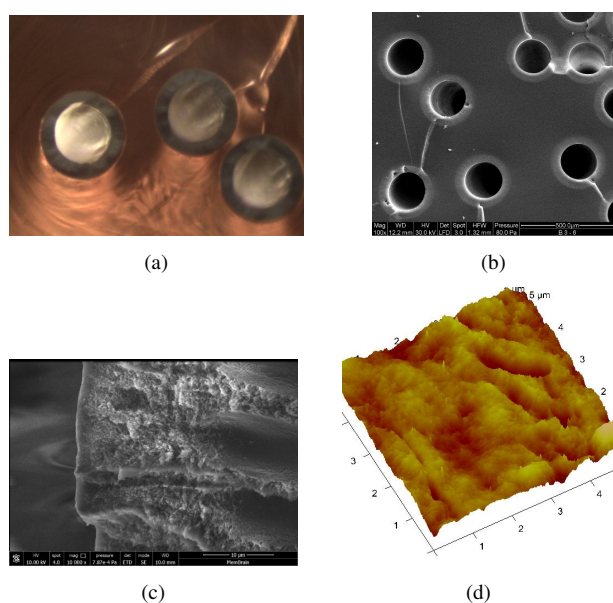


Figure 5: Optical microscopy image (a); SEM micrographs (b-c) and AFM micrograph (d) of the cross-section and surface of the prepared HF membranes.

efficient. In our case, H_2 permeates faster than CO_2 and since the diffusion coefficient of H_2 is significantly larger than that of CO_2 [5], it can be concluded that the separation is based on differences in diffusivities. This is typical for glassy polymers, including the PEI applied in this paper.

The best membrane from the A5 series was used to fabricate the P2 membrane module containing 250 fibers. From the whole B3 series, the two best membranes, namely B3-3 and B3-7, were selected to be incorporated into the membrane mini-modules.

3.3 Morphology of HF membranes

The resulting hollow fiber membranes (Fig. 5) had a regular round shape with a sponge-like structure containing typical relatively small finger-like pores ($<30 \mu m$). As determined using an optical microscope, the outer and inner diameters of the hollow fibers were $313 \pm 9 \mu m$ and $290 \pm 5 \mu m$, respectively. The separation layer was on the outer surface for all the fibers. Atomic Force Microscopy (AFM) of the surfaces of the fibers revealed a relatively smooth surface consisting of a protective coating of PDMS with no defects.

3.4 Hollow fiber membrane modules

HC1 mini-modules

Once the best membranes from the B3 series had been chosen (B3-3 and B3-6), the requirements of the project coordinator with regard to modules for membrane bioreactors were established. According to the requirements, three HC1 modules were manufactured with assistance

from MemBrain s.r.o. Their single gas transport properties were measured and are summarized in Table 3. The first two modules (HC1_1 and HC1_2) contained the same B3-7 HF membrane, the only difference between them was the number of fibers they consisted of and thus their membrane areas. HC1_1 consisted of 10 fibers with a corresponding membrane area of 19.7 cm^2 , while HC1_2 consisted of 20 fibers with a corresponding membrane area of 39.3 cm^2 . Hydrogen permeation flow rates were 28.2 (for HC1_1) and 53.0 ml/min (for HC1_2) at a feed pressure of 4.2 bars (abs) and achieving ideal H_2/CO_2 selectivities of 4.4 and 3.7, respectively. The permeate was released at atmospheric pressure. The slightly lower selectivity of the second module can be attributed to the variation in the membrane properties, minuscule leakage within the module or a combination of both.

The HC2 mini-module consisted of 23 fibers of B3-3 membrane, corresponding to a membrane area of 41.9 cm^2 . As can be seen in Table 3, the permeate fluxes of the membrane modules were more than two times lower and only yielded negligibly higher selectivities. The modules were handed over to a Korean participant in the aforementioned project for further testing on real biogas.

The same modules were also tested for the H_2/CO_2 mixture to demonstrate their ability to concentrate the hydrogen. From Table 4, it can be seen that the modules were able to concentrate hydrogen from an initial percent concentration of 57 % to 88 % in the case of the HC1_1 module at a membrane stage cut of 96 % and from 57 % to 77 % in the case of the HC2 module at a membrane stage cut of 88 %. The membrane stage cut is defined as the ratio of the permeate flow rate to the feed flow rate. Generally, by increasing the membrane stage cut, the concentration of the more permeating penetrant is also higher. On the other hand, the hydrogen recovery is lower because most of the hydrogen from the feed is transferred into the low-concentration permeate.

P2-type module

Thicker HF membranes with an average OD of $420 \mu m$ were incorporated into a quarter-scale membrane module. From the number of fibers the module consisted of, that is, 250, and their active length, namely 25.6 cm, the total membrane area of the module was calculated to be 844 cm^2 . The membrane module was tested against the gas transport properties of various single gases. The measured values are presented in Table 5. According to the measurements, the permeances more than doubled compared to the same membrane measured in a small-scale laboratory module. Furthermore, different values of H_2/CO_2 selectivities were calculated, the selectivity dropped from 5.6 to almost 3.0 to be exact. This perhaps indicates the presence of some microdefect on one of the fibers or a minuscule leakage between the feed and permeate. Nevertheless, the separation performance was sufficient to demonstrate the concept of biohydrogen purifi-

Table 3: Characterization of HC1 and HC2 mini-modules - gas transport properties were measured for single gases at pressure differentials of 1.0 and 3.2 bars as well as at a temperature of 25 °C

Gas	Number of fibers	Fiber diameter (cm)	Fiber length (cm)	Δp (bar)	Permeate flow rate (ml/min)	Membrane area (cm ²)	Permeance (GPU)	H ₂ /CO ₂ selectivity
Module HC1_1								
CO ₂	10	0.0313	20	1	1.96	19.7	22.1	4.41
	10	0.0313	20	3.2	6.45	19.7	22.8	4.37
H ₂	10	0.0313	20	1	8.65	19.7	97.7	
	10	0.0313	20	3.2	28.2	19.7	99.6	
Module HC1_2								
CO ₂	20	0.0313	20	1	3.92	39.3	22.1	4.46
	20	0.0313	20	3.2	14.3	39.3	25.2	3.71
H ₂	20	0.0313	20	1	17.5	39.3	98.9	
	20	0.0313	20	3.2	53	39.3	93.6	
Module HC2								
CO ₂	23	0.029	20	1	1.65	41.9	8.7	4.5
	23	0.029	20	3.2	5.54	41.9	9.2	4.3
H ₂	23	0.029	20	1	7.43	41.9	39.4	
	23	0.029	20	3.2	23.8	41.9	39.4	

Table 4: Gas transport properties of the HC1 and HC2 membrane mini-modules for the CO₂/H₂ mixture measured at a feed pressure of 3.6 bars (abs)

Module	Parameter	Composition [%]			
		Feed	Retentate	Permeate	
HC1_1	H ₂ Permeance (GPU)	–	57	54	88
	CO ₂ Permeance (GPU)	–	43	46	12
	Membrane stage cut	0.96	–	–	–
	CO ₂ /H ₂ Selectivity	4.2	–	–	–
HC1_2	H ₂ Permeance (GPU)	–	41	40	63
	CO ₂ Permeance (GPU)	–	59	60	37
	Membrane stage cut	0.94	–	–	–
	CO ₂ /H ₂ Selectivity	4.3	–	–	–
HC2	H ₂ Permeance (GPU)	–	57	38	77
	CO ₂ Permeance (GPU)	–	43	62	23
	Membrane stage cut	0.88	–	–	–
	CO ₂ /H ₂ Selectivity	5.7	–	–	–

cation.

timization of the fermentation system and the integration of the gas separation unit into the GS-MBR.

3.5 Development of the membrane gas separation unit

Using the membrane modules, this project included the construction of a membrane gas separation unit, the op-

Table 5: Gas separation properties of the P2 membrane module measured for single gases at 25 °C (number of fibers = 250, average OD = 420 microns, membrane area = 844 cm²)

Gas	Δp (bar)	Permeate flow rate (ml/min)	Permeance (GPU)	H ₂ /CO ₂ selectivity
CO ₂	2	356	46.2	2.92
	5.6	949	44	2.99
H ₂	1.2	625	135.3	–
	2	1012	131.5	–
O ₂	0.65	28	11.2	–
	1.1	46	10.9	–

High-pressure membrane unit utilizing a laboratory air compressor

The model membrane unit consisted of a P2 HF membrane module, a laboratory air compressor, three pressure sensors, a pressure regulator valve, two solenoid valves, a back pressure regulator, fittings and an Arduino control unit. A schematic diagram and photograph of the unit are presented in Fig. 6. Both bioreactors were simulated by pressure vessels with inlets. The control unit senses the pressures in both pressure vessels (bioreactors) and at the feed of the membrane module. To achieve a high degree of efficiency, it is necessary to match the fermentation performance of both bioreactors to the performance of the membrane gas separation unit.

An attempt was made to control the compressor using pulses, namely the compressor was switched on when the fermented amount of biogas in the main bioreactor reached the specified limit. Since the power of the compressor considerably exceeded the performance of both fermenters and the membrane unit, it was necessary to control the flow of the compressed gas mixture into the membrane module by means of a back pressure regulator, which transferred the excess amount of compressed gas into the bypass. In order to maintain the pressure in the loop at close to atmospheric pressure, an expansion vessel was connected to it.

The compressor was controlled by pulses once again – an Arduino microcontroller opened the solenoid valves when the amount of biogas in the main bioreactor exceeded the set limit. The regulating valve in the retentate stream of the membrane module regulates its stage cut. When the pressure in the main bioreactor decreased under the set limit, the Arduino microcontroller closed the solenoid valves. This type of control guaranteed that the feed pressure in the membrane module was sufficiently high to maintain the required separation efficiency. The pressure was kept by back-pressure regulator. The flow rate of the gas mixture that was simultaneously fed into the membrane module varied from 0 to 3 l/min, which is

given by the pulse width or duty cycle.

It should be noted that the mixture of hydrogen and carbon dioxide is reactive under certain conditions [6]. It probably cannot be ruled out that the pressures and temperatures in the compressor together with the presence of metal alloys will not trigger any undesired hydrogenation. The compressor must therefore be an internal ATEX version. The problem can be managed as shown in [7], where the same gas mixture was pressurized up to 380 bars.

Low-pressure membrane unit utilizing a vacuum pump

The second model membrane unit generates the driving force at the membrane by the suction force supplied by a vacuum pump. The unit again consists of the P2 HF membrane module, a laboratory vacuum pump, two pressure sensors, two solenoid valves, a peristaltic pump, fittings and an Arduino microcontroller. A schematic diagram and photograph of the unit is presented in Fig. 7. When the pressure of the biogas in the main bioreactor exceeded the set limit, the Arduino microcontroller opened both solenoid valves and started the peristaltic pump. The flow rate produced by this pump regulated the membrane stage cut. The permeate flux was considerably lower as the pressure differential was smaller than in the first unit. However, regulation in laboratory-scale experiments more accurately matched the performance of the fermenter with that of the gas separation unit. The amount of gas mixture fed into the membrane module can vary from 0 to 0.5 l/min, which is given by the pulse width or duty cycle as presented in the first set-up.

4. Conclusion

A series of 8 batches of HF membranes was prepared. Each batch had different spinning process parameters. The morphology and gas transport properties were characterized to select the 2 best HF membranes which were incorporated into 2 types of membrane modules. The first module was designed for laboratory tests and had a small membrane area and low permeate flow rate. The other module consisting of 250 hollow fibers was constructed for larger flow rates and scale. All membrane modules were tested for single- as well as mixed-gas transport properties and exhibited good levels of performance.

The design and development of a membrane separation unit is a very complex task. Firstly, membranes in the form of hollow fibers based on PEI were prepared. Then modules from each batch were built and characterized according to gas transport. The most efficient module achieved a separation factor for H₂/CO₂ in excess of 5. Three modules of this type were fabricated as well as tested using a model mixture and may hopefully be appropriate for real-life gas separation [8], which is going to be carried out by our partners.

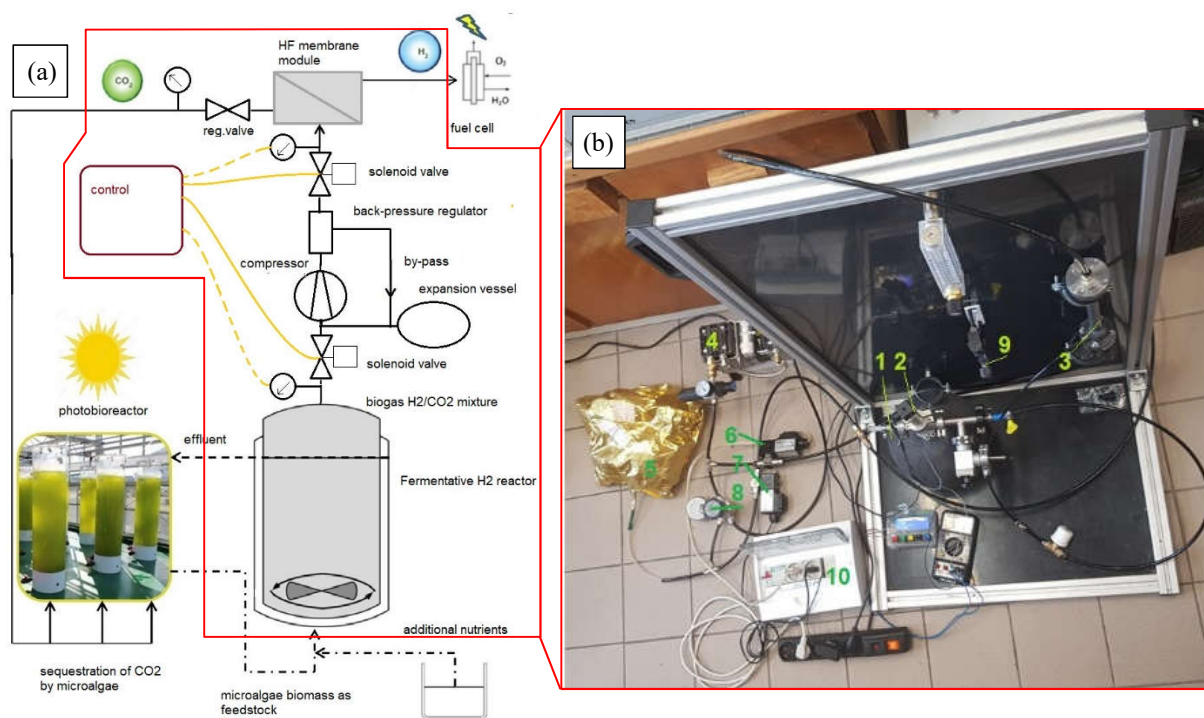


Figure 6: Schematic diagram (a) and photograph (b) of the high-pressure membrane unit for the integrated GS-MBR system: 1 - pressure vessel, 2 - pressure sensor, 3 - P2 membrane module, 4 - laboratory air compressor, 5 - expansion vessel, 6-7 - two solenoid valves, 8 - back pressure regulator, 9 - regulating valve with a flow meter, 10 - Arduino microcontroller.

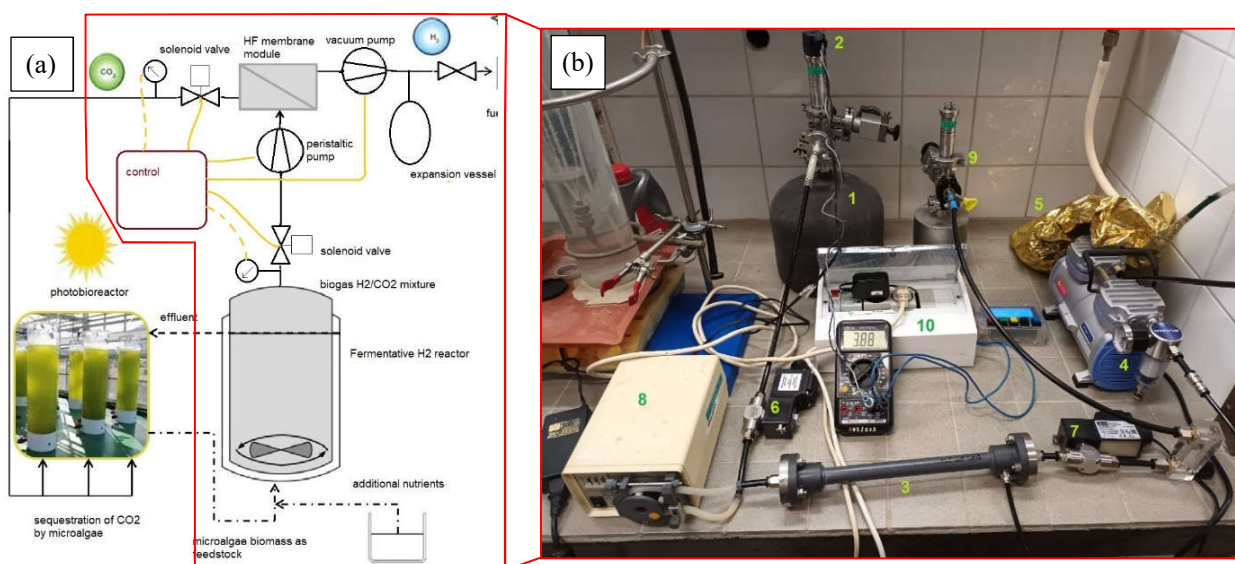


Figure 7: Schematic diagram (a) and photograph (b) of the low-pressure laboratory-scale membrane unit: 1 - pressure vessel, 2 - pressure sensor, 3 - P2 membrane module, 4 - laboratory vacuum pump, 5 - expansion vessel, 6-7 - two solenoid valves, 8 - peristaltic pump, 9 - pressure vessel – retentate recipient, 10 - Arduino control unit.

Two types of laboratory membrane separation units were constructed using the larger P2 HF membrane module. The high-pressure unit utilizes a compressor to pressurize the gas mixture into the feed of the module, while the low-pressure unit utilizes a vacuum pump to maintain a low pressure in the permeate of the membrane module. To ensure the separation efficiency remains high, pulse regulation was utilized. For laboratory use the low-pressure unit proved more accurate regulation to match the fermenters performance with the separation unit.

Acknowledgement

This part of the international cooperation was supported by project 8F17005 and contract no. MSMT-20364/2017-3/5 provided by the Czech Ministry of Education, Youth and Sports. Thanks to all participants of the common Korea – Visegrad Countries project i-AlgMemB for cooperation.

REFERENCES

- [1] Bakonyi, P.; Kumar, G.; Bélafi-Bakó, K.; Kim, S.-H.; Koter, S.; Kujawski, W.; Nemestóthy, N.; Peter, J.; Pientka, Z.: A review of the innovative gas separation membrane bioreactor with mechanisms for integrated production and purification of biohydrogen, *Bioresour. Technol.*, 2018, **270**, 643–655 DOI: [10.1016/j.biortech.2018.09.020](https://doi.org/10.1016/j.biortech.2018.09.020)
- [2] Bakonyi, P.; Peter, J.; Nemestóthy, N.; Malý, D.; Kumar, G.; Koter, S.; Kim, S.-H.; Kujawski, W.; Bélafi-Bakó, K.; Pientka, Z.: Feasibility study of polyetherimide membrane for enrichment of carbon dioxide from synthetic biohydrogen mixture and subsequent utilization scenario using microalgae, *Int. J. Energy Res.*, 2021, **45**, 8327–8334 DOI: [10.1002/er.5732](https://doi.org/10.1002/er.5732)
- [3] Válek, R.; Malý, D.; Peter, J.; Gruart, M.: Effect of the preparation conditions on the properties of polyetherimide hollow fibre membranes for gas separation, *Desalin. Water Treat.*, 2017, **75**, 300–304 DOI: [10.5004/dwt.2017.20747](https://doi.org/10.5004/dwt.2017.20747)
- [4] Wijmans, J. G.; Baker, R. W.: The solution-diffusion model: a review, *J. Membr. Sci.*, 1995, **107**(1–2), 1–21 DOI: [10.1016/0376-7388\(95\)00102-1](https://doi.org/10.1016/0376-7388(95)00102-1)
- [5] Freeman, B.; Yampolskii, Y.; Pinnau, I. (eds.): Materials science of membranes for gas and vapor separation (John Wiley & Sons, Ltd, Chichester, UK) 2006. DOI: [10.1002/047002903X](https://doi.org/10.1002/047002903X)
- [6] Zeng, L.; Wang, Z.; Wang, Y.; Wang, J.; Guo, Y.; Hu, H.; He, X.; Wang, C.; Lin, W.: Photoactivation of Cu centers in Metal-Organic Frameworks for selective CO₂ conversion to ethanol, *J. Am. Chem. Soc.* 2020, **142**, 75–79 DOI: [10.1021/JACS.9B11443](https://doi.org/10.1021/JACS.9B11443)
- [7] Härtel, G.; Püschel, T.: Permselectivity of a PA6 membrane for the separation of a compressed CO₂/H₂ gas mixture at elevated pressures, *J. Membr. Sci.* 1999, **162**, 1–8 DOI: [10.1016/S0376-7388\(99\)00066-6](https://doi.org/10.1016/S0376-7388(99)00066-6)
- [8] Rózsenberszki, T.; Koók, L.; Bakonyi, P.; Nemestóthy, N.; Bélafi-Bakó, K.: Comparative study on anaerobic degradation processes of pressed liquid fraction of organic solid waste, *Hung. J. Ind.Chem.*, 2021, **49**(1), 31–35 DOI: [10.33927/hjic-2021-05](https://doi.org/10.33927/hjic-2021-05)

PRODUCTION OF CHIRAL (S)-2-PHENYL-1-PROPANOL BY ENANTIOSELECTIVE BIOCATALYSTS

PIROSKA LAJTAI-SZABÓ^{*1}, TÍMEA BRIGITTA BAGÓ¹, AND NÁNDOR NEMESTÓTHY¹

¹Research Group on Bioengineering, Membrane Technology and Energetics, University of Pannonia, Egyetem u. 10, Veszprém, 8200, HUNGARY

Enantioselective production of (S)-2-phenyl-1-propanol is important as in order to be applied in industry, a high degree of optical purity is required. Besides organocatalysts and metal complexes, biocatalysts can be used for its synthesis in their isolated form or as whole-cell biocatalysts, both of which have various advantages and disadvantages. In this research, *Saccharomyces cerevisiae*, as a whole-cell biocatalyst, and recombinant horse-liver alcohol dehydrogenase (ADH), as an isolated enzyme, were investigated in terms of their activity, kinetics and enantioselectivity. In the case of yeast, the rate of cofactor regeneration was twice that of substrate conversion, moreover, the biocatalyst *Saccharomyces cerevisiae* can be characterised by substrate-limited kinetics and low enantioselectivity. In contrast, the isolated enzyme recombinant horse-liver ADH exhibited biphasic kinetics and cofactor regeneration was the rate-limiting step. The outstanding enantioselectivity of recombinant horse-liver ADH renders it a promising catalyst for the purpose of this synthesis.

Keywords: alcohol dehydrogenase, whole-cell biocatalyst, *Saccharomyces cerevisiae*

1. Introduction

2-phenyl-1-propanol is a fragrance ingredient that produces the Lila-hyacinth odour commonly used in cosmetics, fine fragrances and household cleaners [1]. Besides, it is the basis of some non-steroidal anti-inflammatory drugs and the precursor of other fragrances [2]. These fields of use require a high degree of optical purity since the enantiomers of the compound, by and large, bring about different biological effects [3].

Asymmetric syntheses are preferentially obtained using enzymes, given the capability of most to catalyse organic reactions with high enantioselectivity under mild conditions [4, 5]. Besides isolated enzymes, whole cells are also being applied more and more often as biocatalysts, given the disparate attributes of both. Whole-cell biocatalysts ensure the optimal environment for the enzyme, thereby providing a quite stable system. Furthermore, they contain cofactors and are able to bring about cofactor regeneration without the necessary addition of any other compounds [6]. However, the presence of a variety of enzymes may lead to side reactions. Also, isozymes with different enantiomeric preferences may lower the overall enantiomeric excess into

the bargain [7]. Unlike whole-cell biocatalysts, isolated enzymes improve the level of control over the process in the absence of side reactions, thereby enhancing its reproducibility. In addition, inhibition is less likely to occur because of the greater degree of tolerance concerning the concentrations of both the substrate and product. On the other hand, the provision of a cofactor and its regenerating system significantly increases costs. In order to choose the optimal catalyst for a given synthesis, a detailed comparison of their advantages and disadvantages, e.g. attainable yield, productivity, product purity, required downstream processes and costs, should be made [8].

In this research, two types of alcohol dehydrogenases (ADH) were investigated with regard to the conversion of racemic 2-phenylpropionaldehyde to (S)-2-phenyl-1-propanol. For the catalysis, the cofactor nicotinamide adenine dinucleotide (NADH) is required by the enzyme which has to be regenerated in order to ensure continuous product formation. Ethanol was applied as an auxiliary substrate for the regeneration which was catalysed by the ADH. The reaction schemes are presented in Fig. 1. Because of the low solubility of the substrate and the product in aqueous media, a two-phase system was applied.

Saccharomyces cerevisiae was applied in dried form (instant baker's dry yeast) as a whole-cell biocatalyst. Over recent decades, both wild and genetically modified strains of yeast have been gaining more and more attention as biocatalysts in the production of fine chemicals [7]. Although (S)-alcohol is generally the predominant

Received: 11 March 2022; Revised: 21 March 2022; Accepted: 21 March 2022

*Correspondence: lajtai-szabo.piroska@mk.uni-pannon.hu

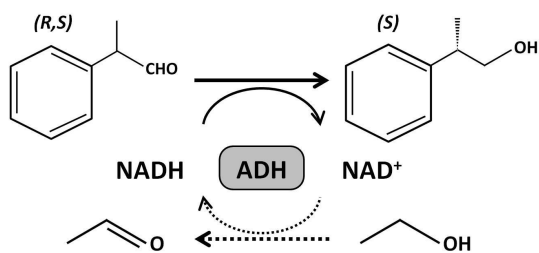


Figure 1: Reaction scheme

enantiomer in the reduction of racemic carboxylic acid compounds by applying yeast [6], this is dependent on the given substrate [9]. Our second catalyst was recombinant horse-liver ADH expressed in *E. coli*. Isolated recombinant horse-liver ADH is frequently applied for asymmetric syntheses [10–12], moreover, its variant expressed in bacteria can be a cheaper and more accessible alternative.

The aim of this research was to characterise the aforementioned biocatalyst in terms of activity, kinetics and enantioselectivity, thereby enabling their critical comparison. In addition, mass transfer through the organic-water interphase was also investigated in order to characterise the relationship between the rates of each step.

2. Experimental Methods

2.1 Applied chemicals

All chemicals were commercially available and used without further purification. Diisopropyl ether (puriss), ethyl alcohol (a.r.), dodecane (a.r.), trifluoroacetic anhydride (98%), racemic 2-phenylpropionaldehyde (98%) and *S*-(2)-phenyl-1-propanol (97%) were purchased from Sigma-Aldrich. Recombinant horse-liver alcohol dehydrogenase (expressed in *E. coli*) as well as lyophilised powder (1.5 U/mg) and β -nicotinamide adenine dinucleotide (sodium salt, 98%) were obtained from Sigma-Aldrich and Thermo Fisher Scientific, respectively. K_2HPO_4 , KH_2PO_4 and Na_2CO_3 were purchased from VWR, while instant baker's dry yeast was purchased from a local store.

2.2 Activity measurements

A spectrophotometric method was used to determine the catalytic activity characteristic of cofactor regeneration. Given that the maximum adsorption of NADH is at 340 nm while that of NAD⁺ is negligible at this wavelength, conversion of the cofactor can be followed by the change in the wavelength of adsorption. In the case of isolated ADH, 10 μ L of enzyme solution (10 mg/mL), 600 μ L of NAD⁺ solution (4 mg/mL) and 1240 μ L of buffer solution were mixed in a quartz cuvette. The reaction was initiated by the addition of 150 μ L cc. of ethyl alcohol and the change in absorbance was measured at 340 nm by a Shimadzu UV-1800 ultraviolet-visible spectrophotometer. In the case of the whole-cell biocatalyst, 10 μ L

of an instant yeast suspension (10 mg/mL) was applied instead of an enzyme solution. The catalytic activity was calculated based on the following equation:

$$VA = \frac{\frac{dA}{dt} V_{\text{cuvette}}}{\epsilon d V_{\text{enzyme}}} h \quad (1)$$

where VA denotes the volume activity [U/cm³], $\frac{dA}{dt}$ represents the gradient of the line (by plotting absorbance vs. time), V_{cuvette} stands for the volume of the mixture [cm³], ϵ refers to the molar extinction coefficient of NADH at 340 nm [6.22 cm²/ μ mol], d is the width of the cuvette [1 cm], V_{enzyme} denotes the volume of the enzyme solution [cm³] and h represents dilution.

The catalytic activity characteristic of the conversion of 2-phenylpropionaldehyde cannot be measured by a spectrophotometer since the reaction mixture consists of two phases. Therefore, the catalytic activity characteristic of the whole process (substrate conversion, cofactor regeneration and mass transfer through the organic-water interface) was calculated from the results gained by measuring the kinetics, as described in Sec. 2.4.

2.3 Mass-transfer rate

Since experimental conditions applied by conversion measurements are unsuitable for determining the mass-transfer rate through organic-water interface, a simplified system was applied for this purpose [13]. 13.4 mg of 2-phenylpropionaldehyde and 18.5 mg of dodecane, which served as an internal standard for gas chromatography (GC) analysis, were dissolved in 10 mL of diisopropyl ether. A Schott glass bottle was filled with 6 L of distilled water and the organic solution carefully poured onto the surface of the water phase. During the following 27 hours, samples were taken from the organic phase and analysed by GC. (The parameters of chromatographic analysis were the same as described in Sec. 2.4).

The ratio of aldehyde to dodecane was plotted as a function of time and a kinetic model was fitted to the measured data in accordance with the following equation:

$$J = d(c_0 - ac_w) \quad (2)$$

where J denotes mass transfer through the interface [mol/(min cm²)], d represents the mass transfer coefficient [cm/min], c_0 stands for the initial substrate concentration in the organic phase [mol/cm³], c_w refers to the substrate concentration in the water phase [mol/cm³] and a is the ratio of the activity coefficients. The difference between the measured and calculated data was minimized by the Excel Solver plug-in. Although the water phase was gently mixed by a magnetic stirrer, the water–organic interface was stationary. Therefore, its surface can be regarded as a constant. The mass transfer rate can be calculated by dividing the mass transfer (J) by the interfacial area.

Table 1: Heating program

Ramp rate [°C/min]	Temperature [°C]	Hold time [min]
	70	25
1	110	0
20	180	2

2.4 Kinetics

In all the experiments, 7 cm³ of organic solvent and 7 cm³ of phosphate buffer (75 mM, pH 8.0) were used. The molar ratio of 2-phenylpropionaldehyde to ethyl alcohol was set at 3.7, based on data from the literature [14]. In the case of isolated ADH, 60 μL of NADH solution (7.5 mg/mL, freshly made with a buffer solution) was added to the reaction media. (The optimal amount of cofactor was determined during preliminary measurements, however, this data is not shown.) In the case of instant baker's dry yeast, since the cell contained a sufficient amount of cofactor, no further addition of NADH was necessary. The reactions were initiated by adding the catalyst – 300 mg of instant baker's dry yeast or 500 μL of enzyme solution (10 mg/mL, freshly made with a buffer solution). The reaction mixtures were shaken in a thermostatic incubator (IKA KS 4000 i control) at 200 rpm and 30 °C. To investigate the product formation, samples were taken from the organic phase and analysed by an HP 5890 gas chromatograph (140 °C isothermal). The GC was equipped with a DB-FFAP column (1 μm × 30 m × 0.53 mm, Agilent Technologies) and a flame ionisation detector.

2.5 Enantioselectivity

While measuring the enantioselectivity, the content of the reaction mixture and operational parameters were the same as described in Sec. 2.3. Before GC analysis, preliminary derivatization was required. 1 mL of trifluoroacetic anhydride and 1 mL of diisopropyl ether were added to 500 μL of the sample while heating the mixture under reflux at 70 °C for 30 mins. Once the reaction mixture had been cooled to room temperature, it was neutralized with 4 mL of Na₂CO₃ (20%) and a sample from the organic phase analysed by a Shimadzu GC-2014 gas chromatograph equipped with a LIPODEX E capillary column (0.2 μm × 25 m × 0.25 mm, Macherey-Nagel) and a flame ionisation detector.

Table 1 contains the parameters of the applied heating program. The peaks were deconvoluted by OriginPro software to fit the Gaussian curves. To identify the peaks of the enantiomers, derivatization and analysis was performed using pure S-(2)-phenyl-1-propanol. The retention time of the derivative of the product was 52.5 mins.

3. Results and Evaluation

3.1 Kinetics

By plotting the amount of product as a function of time, a line can be fitted to the initial linear phase of the graph and its gradient is the initial rate of reaction as a result of the given substrate concentration. A kinetic curve results from repeating the method with different initial substrate concentrations, yielding information about the dependence of the reaction rate on it.

In the case of whole-cell biocatalysts, the product formation can be described by the single-substrate Michaelis-Menten model as the amount of cofactor can be considered to be constant due to its fast regeneration (see Sec. 2.3).

In the region of lower substrate concentrations, first-order kinetics was observed as expected (Fig. 2). However, at 0.267 M, the curve peaked followed by a relatively steady decrease instead of phase saturation. As a result, it can be concluded that higher amounts of substrate limit enzymatic conversion, therefore, 0.267 M is the optimal initial concentration to maximise the reaction rate.

In contrast to yeast cells, by applying recombinant ADH, the reaction rate of cofactor regeneration may limit product formation (see Section 3.2), therefore, cannot be neglected. Since two reactions involved multiple substrates catalysed simultaneously by the same enzyme, the kinetics did not follow the Michaelis-Menten model. Alternatively, a biphasic model was applied which divides the curve into two phases: at low substrate concentrations, the enzyme's affinity is relatively high while the turnover number is low. On the contrary, a low affinity and high turnover number is characteristic of the region of high substrate concentration (Fig. 3).

Biphasic kinetics can be modelled by the following equation [15]:

$$V = \frac{V_{\max 1} [S] + CL_{\text{int}} [S]^2}{K_{M1} + [S]} \quad (3)$$

where $V_{\max 1}$ as well as K_{M1} describe the first high affinity–low–turnover phase and CL_{int} – equal to the ratio $V_{\max 2} : K_{M2}$ – denotes the second low–affinity–high–turnover phase.

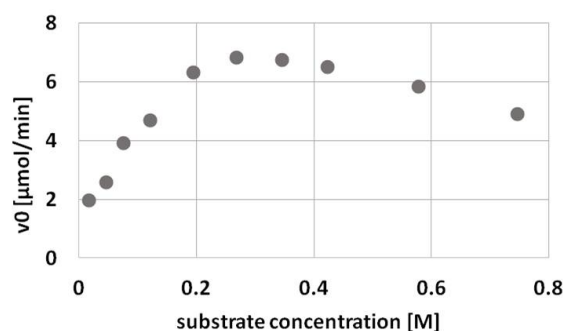


Figure 2: Kinetics of the whole-cell biocatalyst

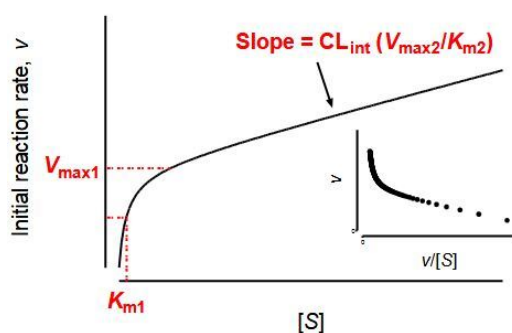


Figure 3: Biphase enzyme kinetics [15]

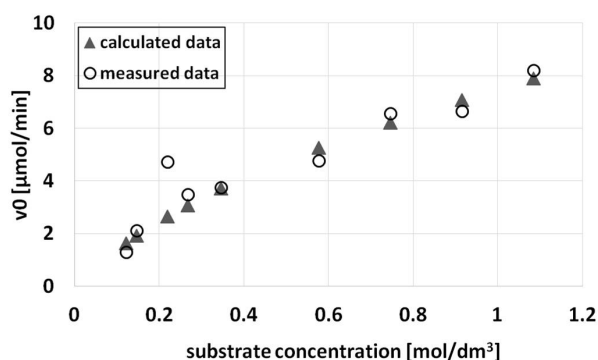


Figure 4: Kinetics of the isolated enzyme

Apart from one exception (at 0.22 M), since model data calculated using Eq. 3 fitted well to the measured data (Fig. 4), biphasic kinetics is presumably a suitable model to describe the kinetics of an isolated enzyme. Having been minimized by the Excel Solver plug-in, the model parameters were the following:

$$V_{\max 1} = 7.523;$$

$$CL_{\text{int}} = 3.458;$$

$$K_{M1} = 0.464.$$

According to Manevski [15], biphasic kinetics may imply the presence of multiple substrate binding sites. However, the applied methods were unsuitable for further investigating the underlying mechanisms of the reactions taking place.

3.2 Activity

The activity of the catalysts was measured during both cofactor regeneration and the process as a whole (Table 2). One Unit (U) stands for the amount of catalyst necessary to produce 1 μmol of product in 1 minute under the measurement parameters. (Substrate conversion could not be investigated separately as previously mentioned in Sec. 2.2). Although normally the catalytic activity should be measured in the saturation phase of the kinetics, none of the kinetic curves enabled this. Therefore, measurements were made at a substrate concentration of 0.27 M, which is the substrate concentration at which the kinetic

Table 2: Activity of the catalysts

	yeast cell [U/mg]	recombinant ADH [U/mg]
cofactor regeneration	0.19	0.05
complete reaction (0.27 M)	0.02	0.7
complete reaction (1.08 M)	–	1.64

curve of the yeast-cell catalyst is at its maximum. In the case of the isolated enzyme, the activity was measured at the same concentration as that of yeast in order to compare the two catalysts. This was also determined at the highest measured point of the kinetic curve, namely at 1.08 M.

Based on the results, cofactor regeneration is one scale faster when applying a whole-cell biocatalyst instead of an isolated enzyme. Although the same enzyme catalyses both substrate conversion and cofactor regeneration when isolated ADH is used, yeast cells contain several enzymes that are capable of participating in regeneration reactions which can occur more rapidly as a result.

On the other hand, the overall reaction rate using the same substrate concentration was 35 times higher when recombinant ADH was used and further increases in substrate concentration resulted in even higher reaction rates.

3.3 Mass transfer through the organic–water interface

In order to determine the rate-limiting step of the whole process, the mass transfer rate through an organic–water interface was investigated. Owing to simplifications of the measurement and the imprecise nature of model fitting, the calculated mass transfer rate may be somewhat inaccurate. Nevertheless, the goal was to estimate its order of magnitude rather than determining its precise value.

Based on the kinetic model fitted to the measured data (Fig. 5), the mass transfer rate was calculated to be $1.33 \cdot 10^{-5}$ mol/min. By comparing this value with the

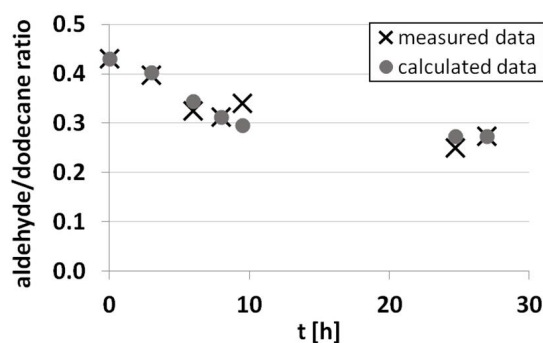


Figure 5: Mass transfer process

Table 3: Enantiomeric excess (ee) and degree of conversion from studies on the production of (*S*)-2-phenyl-1-propanol

Catalyst	Solvent	Substrate conc.	Product, degree of conversion	ee (<i>S</i>)	Ref.
horse-liver ADH	0.24 U/mL	buffer, isopropyl ether (63 % v/v)	41 mM, 25 % (2 h) 82 mM, 50 % (24 h)	91 % 88 %	[14]
horse-liver ADH	0.01 mg/mL	buffer pH= 7.5, CH ₃ CN (10 % v/v)	0.5 mM	0.36 mM, 72 % (5 h)	78 % [12]
recombinant horse-liver ADH, exp. in <i>E. coli</i>	0.5 U/mL	buffer pH= 8.0, diisopropyl ether (1:1 v/v)	267 mM	45 mM, 17 % (1 h)	100 % this work
CtXR D51A mutant <i>E. coli</i> , whole-cell	4 g _{CDW} /L 40 g _{CDW} /L	buffer pH= 7.5	100 mM	41 mM, 41 % (2 h) 70 mM, 70 % (2 h)	95 % 45 % [2]
<i>S. cerevisiae</i> , whole-cell	43 g _{CDW} /L	buffer pH= 8.0, diisopropyl ether (1:1 v/v)	267 mM 345 mM	74 mM, 28 % (1 h) 55 mM, 16 % (1 h)	24 % 36 % this work

reaction rates of both catalysts, it could be established that the mass transfer rate is two or three times faster than those of product formation or cofactor regeneration. Therefore, the rate-limiting step of the whole process is cofactor regeneration and substrate conversion when an isolated enzyme and whole-cell biocatalyst is applied, respectively.

3.4 Enantioselectivity

The enantioselectivity of the whole-cell biocatalyst was measured at three different initial substrate concentrations: at the maximum of the kinetic curve (0.267 M) as well as at two higher values (0.345 M and 0.746 M) to examine whether increasing the substrate concentration is beneficial as far as achieving optical purity is concerned. The enantiomeric ratio was calculated from the ratio of the peak areas at 0.5, 1.0 and 1.5 hours (Fig. 6).

Changes in the enantiomeric ratio as the reaction progressed were insignificant, moreover, the difference in the reaction time between 0.345 M and 0.746 M was negligible. At 0.267 M, the final result was 0.62, while the best result, that is, 0.68, was achieved at 0.746 M. As a result,

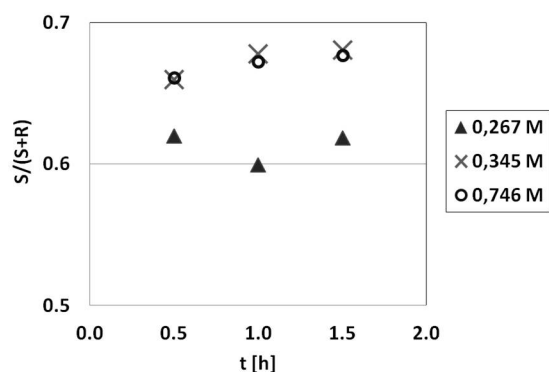


Figure 6: The enantioselectivity of the whole-cell biocatalyst

it could be established that to achieve an optimal reaction rate and enantioselectivity, different initial substrate concentrations are required.

In the case of the isolated enzyme, the enantioselectivity was measured at the same substrate concentrations as when the whole-cell biocatalyst was applied. However, since only one peak corresponding to the (*S*)-enantiomer of the derivative was detected, further analysis was unnecessary and the enantioselectivity regarded as 100%.

As in terms of consumption optical purity is a key concern, the results of this work were compared with some data from the literature (Table 3). In the case of whole-cell biocatalysts, the results of Rapp et al. [16] are more favourable than ours. However, since both studies suggest that the maximum degree of conversion and enantiomeric excess cannot be achieved simultaneously, a compromise must be made. In the case of the isolated enzyme, the degree of conversion in this study is promising if the reaction time is also taken into account. As for the enantiomeric excess, our result is clearly outstanding, therefore, recombinant horse-liver ADH provides a satisfactory alternative for catalysing the production of (*S*)-2-phenyl-1-propanol.

4. Conclusion

In this work, the conversion of racemic 2-phenylpropionaldehyde into (*S*)-2-phenyl-1-propanol was investigated by applying a whole-cell biocatalyst (*Saccharomyces cerevisiae*) and an isolated enzyme (recombinant horse-liver ADH expressed in *E. coli*). Significant differences were observed between the catalysts in terms of all the considered parameters. Firstly, the whole-cell biocatalyst exhibited substrate-limited kinetics, while the isolated enzyme could be described by biphasic kinetics. The yeast cell contained a sufficient amount of cofactor for the reaction, moreover, its regeneration was twice as fast as in the case of the isolated

enzyme. Therefore, the whole-cell biocatalyst is more beneficial from this point of view. On the other hand, the enzymatic activity of the whole process was at least 35 times higher when recombinant horse-liver ADH was applied and could be further enhanced by increasing the initial substrate concentration. Most importantly, the isolated enzyme catalysed the conversion with 100 % enantioselectivity, which is also clearly outstanding compared to data from the literature. In conclusion, although recombinant horse-liver ADH is more expensive, it is definitely a more efficient catalyst than yeast as a whole-cell biocatalyst. Therefore, recombinant horse-liver ADH is a promising biocatalyst with regard to the synthesis of (S)-2-phenyl-1-propanol.

Acknowledgement

This research was supported by the Ministry for Innovation and Technology; the National Research, Development and Innovation Office and the New National Excellence Programme.

This study was financed by the National Laboratory for Climate Change (Hungary) project number NKFIH-471-3/2021.

REFERENCES

- [1] Scognamiglio, J.; Jones, L.; Letizia, C. S.; Api, A. M.: Fragrance material review on β -methylphenethyl alcohol, *Food Chem. Toxicol.*, 2012, **50**(2), 199–203 DOI: [10.1016/j.fct.2011.10.023](https://doi.org/10.1016/j.fct.2011.10.023)
- [2] Rapp, C.; Pival-Marko, S.; Tassano, E.; Nidetzky, B.; Kratzer, R.: Reductive enzymatic dynamic kinetic resolution affording 115 g/L (S)-2-phenylpropanol, *BMC Biotechnol.*, 2021, **21**, 1–13, DOI: [10.1186/s12896-021-00715-5](https://doi.org/10.1186/s12896-021-00715-5)
- [3] Klebe, G.: Optical activity and biological effect, in: Klebe, G. (Ed.): Drug design: Methodology, concepts, and mode-of-action, pp. 89–110 (Springer Berlin Heidelberg; Berlin, Heidelberg, Germany) 2013 DOI: [10.1007/978-3-642-17907-5_5](https://doi.org/10.1007/978-3-642-17907-5_5)
- [4] Lajtai-Szabó, P.; Nemestóthy, N.; Gubicza, L.: The role of water activity in terms of enzyme activity and enantioselectivity during enzymatic esterification in non-conventional media, *Hung. J. Ind. Chem.*, 2020, **48**(2), 9–12 DOI: [10.33927/hjic-2020-22](https://doi.org/10.33927/hjic-2020-22)
- [5] Reetz, M. T.: Controlling the enantioselectivity of enzymes by directed evolution: Practical and theoretical ramifications, *Proc. Natl. Acad. Sci.*, 2004, **101**(16), 5716–5722 DOI: [10.1073/pnas.0306866101](https://doi.org/10.1073/pnas.0306866101)
- [6] Silva, J.; Alarcón, J.; Aguila, S. A.; Alderete, J. B.: Bioreduction of some common carbonylic compounds mediated by yeasts, *Z. Naturforsch., C*, 2010, **65**(1-2), 1–9 DOI: [10.1515/znc-2010-1-201](https://doi.org/10.1515/znc-2010-1-201)
- [7] Pscheidt, B.; Glieder, A.: Yeast cell factories for fine chemical and API production, *Microb. Cell Fact.*, 2008, **7**(1), 25 DOI: [10.1186/1475-2859-7-25](https://doi.org/10.1186/1475-2859-7-25)
- [8] Schallmey, A.; Domínguez de María, P.; Bracco, P.: Biocatalytic asymmetric oxidations in stereoselective synthesis, in: Andrushko V.; Andrushko, N. (Eds.): Stereoselective synthesis of drugs and natural products, pp. 1089–1114 (John Wiley & Sons, Inc., Hoboken, USA) 2013 DOI: [10.1002/9781118596784.ssd036](https://doi.org/10.1002/9781118596784.ssd036)
- [9] Hu, Q.; Xu, Y.; Nie, Y.: Highly enantioselective reduction of 2-hydroxy-1-phenylethanone to enantiopure (R)-phenyl-1,2-ethanediol using *Saccharomyces cerevisiae* of remarkable reaction stability, *Bioresour. Technol.*, 2010, **101**(22), 8502–8508 DOI: [10.1016/j.biortech.2010.06.044](https://doi.org/10.1016/j.biortech.2010.06.044)
- [10] Díaz-Rodríguez, A.; Iglesias-Fernández, J.; Rovira, C.; Gotor-Fernández, V.: Enantioselective preparation of δ -valerolactones with horse liver alcohol dehydrogenase, *Chem. Cat. Chem.*, 2014, **6**(4), 977–980 DOI: [10.1002/cctc.201300640](https://doi.org/10.1002/cctc.201300640)
- [11] Kim, K.; Plapp, B. V.: Inversion of substrate stereoselectivity of horse liver alcohol dehydrogenase by substitutions of Ser-48 and Phe-93, *Chem. Biol. Interact.*, 2017, **276**, 77–87 DOI: [10.1016/j.cbi.2016.12.016](https://doi.org/10.1016/j.cbi.2016.12.016)
- [12] Giacomini, D.; Galletti, P.; Quintavalla, A.; Gucciardo, G.; Paradisi, F.: Highly efficient asymmetric reduction of arylpropionic aldehydes by Horse Liver Alcohol Dehydrogenase through dynamic kinetic resolution, *Chem. Commun.*, 2007, **39**, 4038–4040 DOI: [10.1039/b712290j](https://doi.org/10.1039/b712290j)
- [13] Hidekazu, D.; Yuri, N. Toyokichi, K.: Mass transfer of acetylacetone, ethylene glycol mono-n-butyl ether and ethylene glycol monophenyl ether across water-carbon tetrachloride and water-chloroform interfaces, *Anal. Chim. Acta*, 1990, **237**, 237–240 DOI: [10.1016/S0003-2670\(00\)83923-9](https://doi.org/10.1016/S0003-2670(00)83923-9)
- [14] Kelemen-Horváth, I.; Nemestóthy, N.; Bélafi-Bakó, K.; Gubicza, L.: Stereoselective reduction of 2-phenylpropionaldehyde by alcohol dehydrogenase with cofactor regeneration, *Chem. Pap.*, 2002, **56**, 52–56 URL
- [15] Manevski, N.: Activity and enzyme kinetics of human UDP-glucuronosyltransferases: Studies of psilocin glucuronidation and the effects of albumin on the enzyme kinetic mechanism, Academic dissertation, University of Helsinki, 2013 URL
- [16] Rapp, C.; Pival-Marko, S.; Tassano, E.; Nidetzky, B.; Kratzer, R.: Reductive enzymatic dynamic kinetic resolution affording 115 g/L (S)-2-phenylpropanol, *BMC Biotechnol.*, 2021, **21**, 58 DOI: [10.1186/s12896-021-00715-5](https://doi.org/10.1186/s12896-021-00715-5)

PRODUCTION AND CHARACTERIZATION OF SAND-PLASTIC COMPOSITE FLOOR TILES

ALEXANDER ASANJA JOCK^{*1}, MESSIAH LUKE AKPAN¹, AND FRANCIS ASOKOGENE OLUWADAYO²

¹Department of Chemical and Petroleum Engineering, University of Uyo, Uyo, NIGERIA

²Department of Chemical Engineering Technology, Auchi Polytechnic, Auchi, Edo, NIGERIA

The amount of plastic waste generated in developing nations like Nigeria is increasing day by day, which is non-biodegradable and causes environmental pollution. Among the plastics used, low-density polyethylene is abundant. These plastics can be removed from the environment and recycled into useful products. In this study, low-density polyethylene plastic waste was utilized in the manufacture of floor tiles to curb its generation. The tiles were produced by mixing fine sand with molten plastic waste in different proportions. The physical and mechanical properties of the floor tiles such as water absorption, density, tensile and compressive tests, modulus of elasticity as well as impact strength and friction tests were investigated. The water absorption ranged from 0.02 – 0.38 % (m/m), while the density varied between 998.5 and 1289 kg/m³. The tensile strength and modulus of elasticity fell within the range of 0.050 to 0.232 MPa and 0.924 to 2.806 MPa, respectively. This result proved the applicability of recycled plastic waste in the formulation of floor tiles.

Keywords: plastic waste, floor tiles, low-density polyethylene, pollution, properties

1. Introduction

Plastic waste is now a global problem and one that must be addressed in order to solve worldwide problems concerning resources and energy. Plastics are a generic group of synthetic or natural materials consisting of high-molecular-weight chains composed predominantly if not entirely of carbon. They are classified into two categories, namely thermoplastics and thermosetting plastics, moreover, are found in different forms, e.g. as bags, furniture, cups, basins, drinking and food containers, etc. [1].

The increasing consumption of plastic products in various fields generates a significant amount of waste products, equating to more than 12% of municipal solid waste. Since plastics are non-biodegradable, that is, cannot easily reenter the natural carbon cycle, the life cycle of plastic materials ends at solid waste disposal facilities and in water bodies. However, the full extent of plastic pollution goes far beyond macroplastic litter. Microplastics can contain additives, which have the potential to leach into the surrounding environment, resulting in toxicity to organisms, including carcinogenesis and disruption of the endocrine system in humans [2].

There are several methods for disposing of municipal and industrial plastic waste such as landfill, incineration,

true material recycling and chemical recovery. Treating plastic waste suitably is crucial to waste management and important in terms of energetic, environmental, economic and political viewpoints. Some plastics can safely be recycled, while others cannot so litter the environment [3].

A large and increasing amount of household plastic waste is being produced. The composition of waste varies from country to country, since it is affected by socioeconomic characteristics, consumption patterns and waste management programmes. Nevertheless, generally speaking, the proportion of plastics concerning the composition of waste is high. The largest component of plastic waste is polyethylene, followed by polypropylene, polyethylene terephthalate and polystyrene [4].

Polyethylene is the most common plastic and can be classified into several different categories based mainly on its density and branching. Important grades of polyethylene are high-density polyethylene (HDPE), linear low-density polyethylene (LLDPE) and low-density polyethylene (LDPE). Plastic is recycled worldwide since it reduces environmental impacts associated with the improper disposal of plastic waste. Therefore, this study focused on the production of floor tiles by mixing sand and plastic waste in different proportions. The characterization of the tiles will provide some insight into the suitability of applying sand-plastic composites in building constructions.

Received: 23 January 2022; Revised: 7 February 2022; Accepted: 9 February 2022

*Correspondence: alsanja@gmail.com



(a) Shredded LDPE



(b) Fine sand

Figure 1: Formulation samples

2. Materials and Methods

2.1 Sample collection and preparation

The plastic waste was collected from the University of Uyo Water Company landfill site in Uyo, South-South Nigeria. The LDPE plastic waste was washed with water to remove dust and other impurities. The washed sample was sun dried for 48 h and shredded into smaller pieces (Fig. 1a). A clay-free sample of fine sand (Fig. 1b) was obtained from Ifiayoung stream in Uyo, sun dried for 24 h, then oven dried at 105 °C for 4 h before being sieved through a 125 µm mesh.

2.2 Formulation and Production of Floor Tiles

35 g of plastic waste was continuously introduced into a fabricated melting pot made of stainless steel and heated to a temperature of 160 °C, whilst being stirred continuously to ensure homogeneous melting. 105 g of fine sand was then added to the melted plastic waste before being well mixed. The mixture was transferred into a stainless-steel mould with the dimensions of 10.0 × 10.0 × 1.5 cm coated with a lubricating oil to facilitate demoulding. The mixture in the mould was compressed by applying

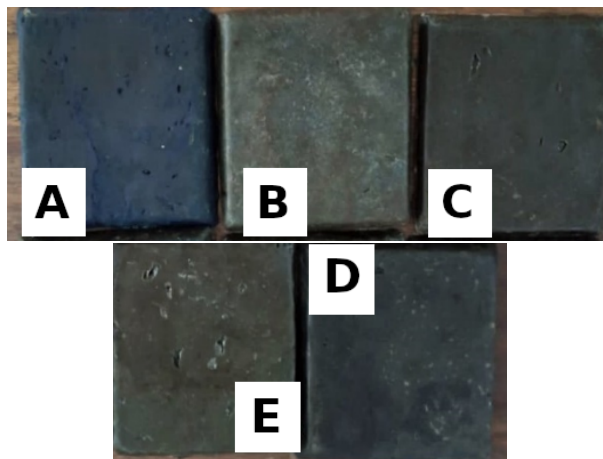


Figure 2: Samples of Floor Tiles

a force before being cooled in a water bath for 5 mins. The resulting tile was then removed from the mould. The production process was repeated by varying the proportions of plastic waste and fine sand. The samples of tiles produced using different formulations are shown in Fig. 2.

2.3 Characterization of Floor Tiles

Water absorption

Water absorption tests were carried out in accordance with the ASTM-C373 standard test method. Each sample was oven dried at 110 °C to constant weight (W_o) before being immersed in distilled water at room temperature (25 °C) for 24 h. The samples were removed from the distilled water, cleaned with a cotton fabric and weighed (W_t). The amount of water absorbed (W_a) by each sample was calculated using

$$\%W_a = \frac{(W_t - W_o)}{W_o} \times 100 \quad (1)$$

Density

The density of each sample was calculated using

$$\text{Density} = \frac{\text{mass of sample}}{\text{sample volume}} \quad (2)$$

Impact strength

Impact strength was measured using a JBS-300N model Charpy impact testing machine and determined according to the ASTM D6110-18 standard test method. A standard sample was prepared with the dimensions 1 × 8 cm while maintaining the original thickness before being placed on the plate of the impact testing machine, wherein the jack handle was carefully released to allow the load to strike the sample of the ceiling board. The energy of the impact was recorded and the impact strength calculated by

$$\text{Impact Strength} = \frac{\text{Absorbed Energy}}{\text{Cross-sectional Area}} \quad (3)$$

Tensile strength

This was determined using the Mohan Brothers Tensile testing machine CAP, 500KGF ISO9001 model. The samples were prepared for this test according to the ASTM C1185 standard test method (Type II). Each sample was carefully placed in the tensile testing machine and clamped at both ends. The machine was turned on and the load at which each sample fractured recorded. The tensile strength was calculated by

$$\text{Tensile Strength} = \frac{\text{Maximum Load}}{\text{Original Cross-sectional Area}} \quad (4)$$

Young’s Modulus of Elasticity

Young’s Modulus of Elasticity (*Y*) is a measure of stress per unit strain and was calculated using

$$Y = \frac{\text{stress}}{\text{strain}} \quad (5)$$

Friction Test

A friction test was conducted using the Cussons friction test device graduated from 0 – 90° and was performed based on the ASTM D1037-94 standard test method. The sample was placed on an inclined plane of the piece of equipment and the angle at which the specimen slid freely down the surface was recorded. The coefficient of friction was calculated by:

$$\text{Coefficient of Friction} = \tan \theta \quad (6)$$

where θ denotes the angle of repose.

Compressive Strength

A compressive strength test was carried out using a universal testing machine and performed based on the ASTM D790 standard test method. The specimens with dimensions of 20 by 20 mm were prepared and tested on a support span of 130 mm in length as per the standard test method. The load at which each sample was compressed as a result of the force applied on it by the machine was recorded. The compressive strength was calculated using

$$\text{Compressive Strength} = \frac{\text{Maximum Load}}{\text{Cross-sectional Area}} \quad (7)$$

Table 1: Composition and Physical Properties of Floor Tiles

Sample	Composition (%(m/m))		Water Absorption (%(m/m))	Density (kg/m ³)
	LDPE	Fine Sand		
A	25	75	0.38	1289.6
B	35	65	0.04	1269.5
C	50	50	0.02	1168.2
D	65	35	0.24	1015.6
E	75	25	0.3	998.5

3. Results and Discussion

3.1 Physical Properties of Floor Tiles

The physical properties of floor tiles are presented in [Table 1](#). Water absorption is the ability of a bisque tile to absorb water or moisture. The calculated water absorption of the floor tiles was between 0.02 and 0.38%(m/m). The lowest water absorption (0.02%(m/m)) was obtained in Batch C with a composition of 50%(m/m) LDPE and 50%(m/m) fine sand. The amount of water absorbed closely resembled that of ceramic tiles of 0.03%(m/m). Generally, tiles with a high level of water absorption have a low resistance to chloride and sulphate as well as to water penetration [5].

The density of the tiles ranged from 998.5 kg/m³ to 1289.6 kg/m³ as is shown in [Table 1](#). The lowest density, calculated in Batch E, was due to the large quantity of LDPE in the formulation. The density decreased as the proportion of LDPE increased. A rise in the density resulted in an increase in the compressive strength and a decrease in water absorption by the tile [6].

3.2 Mechanical properties of the formulated tiles

The mechanical properties of the batches are shown in [Table 2](#). The tensile strength of the floor tiles was between 0.050 and 0.232 MPa. The tensile strength of a material is a measure of the force required to pull a material to the point where it breaks. Batches A and E exhibited the lowest and highest tensile strengths, respectively, possibly due to the amount of LDPE used as a binding agent in their formulations.

The Young’s modulus of elasticity with regard to the batches of tiles ranged from 0.924 to 2.810 MPa as depicted in [Table 2](#). The Young’s modulus of elasticity is a measure of the stiffness of an elastic material and it is an important parameter in evaluating the deformation of materials subjected to a working load. The lowest Young’s modulus of elasticity that was calculated in Batch A may result in a lower stiffness compared to that of Batch E that yielded the highest.

The compressive strength of the tiles presented in [Table 2](#) was between 91.7 and 133.0 MPa. Batches D and B

Table 2: Mechanical properties of Floor Tiles

Sample	Tensile strength (MPa)	Young's modulus of elasticity (MPa)	Compressive strength (MPa)	Impact strength (kJ/m ²)	Coefficient of friction
A	0.05	0.924	116.7	1912	0.6
B	0.067	0.975	91.7	1883	0.53
C	0.083	2.666	118	1955	0.51
D	0.082	2.653	133	2346	0.58
E	0.232	2.806	115	1933	0.58

exhibited the highest and lowest compressive strengths, that is, 133.0 MPa and 91.7 MPa, respectively. This implies that the impact strength of Batch D to compressive loading will be greater than that of Batch B.

Impact strength is the resistance of a material to fracture by being hit, expressed in terms of the amount of energy absorbed before the fracture. The impact strength of the batches ranged from 819.05 to 1720 KJ/m². Since Batches D and B exhibited the highest and lowest impact strengths, respectively, Batch B will easily be fractured.

Table 2 shows that the coefficient of friction of the floor tiles is between 0.51 and 0.60. However, given that these values are similar, all the floor tiles responded similarly to sliding freely over the same surface. The coefficient of friction depends on the surface finish of the floor tiles and the values obtained are in good agreement with the acceptable value of 0.5 outlined by the ASTM standard test method [7].

4. Conclusion

Floor tiles were successfully developed from plastic waste and fine sand. Although the physical and mechanical properties of Batch D yielded the best results, this recycled plastic waste can be used to produce some industrial products like floor tiles which are resistant to highly corrosive environments like offshore platforms.

Competing interests

The authors declare that there are no competing interests.

REFERENCES

- [1] Osarumwense, O.J.; Salokun, O.; Okundaye, O.A.: Utilization of low-density polyethylene (LDPE) plastic wastes in the production of paving tiles, *J. Mater. Environ. Sci.*, 2020, **11**(12), 2052–2060 <https://www.jmaterenvironsci.com>
- [2] Bishop, G.; Styles, D.; Lens, N.L.P.: Recycling of European plastic is a pathway for plastic debris in the ocean *Environ. Int.*, 2020, **142**, 105893 DOI: [10.1016/j.envint.2020.105893](https://doi.org/10.1016/j.envint.2020.105893)
- [3] Puttaraj, M.H.; Basavaraj, P.; Gagan, M.S.; Shivu, S.; Manjunath, S.H.: Reuse of plastics waste for the production of floor tiles, *J. Seybold Report*, 2020, **15**(8), 1633–1639
- [4] Alla, M.M.G.; Ahmed, A.I.; Abdalla, B.K.: Conversion of plastic waste to liquid fuel, *Int. J. Tech. Res. Appl.*, 2014, **2**(3), 29–31 <https://www.ijtra.com>
- [5] Namarak, C.; Bumrungsri, C.; Tangchirapat, W.; Jaturapitakkul, C.: Development of concrete paving blocks prepared from waste materials without portland cement, *Mater. Sci.*, 2018, **24**(1), 92–99 DOI: [10.5755/j01.ms.24.1.17566](https://doi.org/10.5755/j01.ms.24.1.17566)
- [6] Yalley, P.P.; Kwan, A.: Use of waste and low energy materials in building block construction. *Int. Refereed J. Eng. Technol.*, 2013, **2**(1), 1–5 <https://www.irjes.com>
- [7] American Society for Testing and Materials (ASTM C1028) (2008) Standard test method for coefficient of friction for manufactured tiles.

UNRAVELING THE NOVEL BACTERIAL ASSISTED BIODEGRADATION PATHWAY OF MORPHOLINE

RUPAK KUMAR^{*1}, SUMAN KAPUR², AND SRINIVASA RAO VULICHI^{2,3}

¹Central Drugs Standard Control Organization, New Delhi, India

²Birla Institute of Technology and Science – Pilani, Hyderabad Campus, Hyderabad, India

³SVU College of Pharmaceutical Sciences, Sri Venkateswara University, Tirupati, India

Most xenobiotics are biodegradable, persistent or recalcitrant in nature. Morpholine, a typical xenobiotic, was initially regarded as recalcitrant, however, later proved to be biodegradable by bacterial species like *Mycobacterium* and *Pseudomonas* in particular. However, establishing the metabolic pathways involved for the successful biodegradation of morpholine is challenging because of its extreme level of water solubility that affects various analytical procedures. In addition, to date, no suitable analytical methods have been reported to directly estimate morpholine and its degradable products or intermediates. Nevertheless, methods, especially optical density, gas chromatography and mass spectrophotometric analysis, could indirectly estimate the degradation product(s) of morpholine formed as a result of its biotransformation. In the present study, the degradation pathway of morpholine was ascertained by selected bacterial isolates by measuring their capacity to degrade morpholine. Based on this analysis of culture filtrates, it was determined that the novel isolate is the genus *Halobacillus blutaparonensis* which follows the diglycolic acid route from the metabolic degradation pathway of morpholine to induce one of two branches of the morpholine biodegradation pathway. In the presence of concentration of morpholine, out of two branches of morpholine degradation one branch is induced, while the other branch is inhibited. Whatever the branches with regard to the degradation pathway of morpholine exhibited by bacteria are, ammonia is the final end product of degradation which might be biochemically utilized by the isolate.

Keywords: morpholine, xenobiotic, recalcitrant, glycolic acid route, ammonia

1. Introduction

Environmental pollution has become a global problem. Due to the indiscriminate and frequent release of xenobiotics as a result of different anthropogenic activities, each and every day our environment becomes increasingly devastated by the pollutants. Morpholine (1-Oxa-4-azacyclohexane) is one such heterocyclic xenobiotic organic chemical with different versatile applications in various processes in the rubber, paper, iron, textile, personal care, pharmaceutical and agricultural industries amongst others. As a consequence of its vast operational usage, a significant amount of this chemical is released into the environment through the differential process of discharging at both micro- and macro-concentrations. Therefore, it is necessary to mention that anthropogenic environmental pollutants, even at low concentrations, often produce deleterious effects on organisms, which are

difficult to predict because measurable effects are expressed only after prolonged exposure.

In the environment, the majority of exposure to morpholine originates from water and leads to the formation of the carcinogen N-nitrosomorpholine (NMOR) by the process of natural nitrosation [1] (Fig. 1). Furthermore, it is pertinent to mention that this process of nitrosation may occur in biological systems when directly consumed, ingested, inhaled and applied to the skin. In addition, NMOR is known as a mediator of various debilitating cancers associated with organs like the digestive tract, respiratory tract, kidneys and liver, which is eventually biomagnified through different trophic levels of biota by its application or the intake of polluted water leading to this carcinogen entering the food chain. In

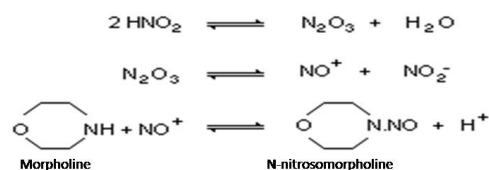


Figure 1: Formation of NMOR

Received: 1 March 2022; Revised: 20 April 2022; Accepted: 26 April 2022

*Correspondence: rupakraman@gmail.com

this regard, it would be best to provide a solution for its efficient discharge or effective removal by different physical and chemical processes. Recently, photocatalysis using catalysts irradiated by ultraviolet or visible light has been applied for the mineralization of toxic organic dyes in water and carbon dioxide [2, 3]. However, a cost-effective, environmentally-friendly biological tool powered by microbes has been widely used as an ancient core concept for the purpose of conserving the natural environment and resources to curb the negative impacts on biotic components. Therefore, a sustainable solution driven by microbes must be explored to elucidate the degradation pathway and measure how potent microbes are for the purposes of decontaminating a wide range of pollutants and their mitigation.

In general, most pollutants are organic and may be biodegradable (transformed by biological mechanisms which might lead to mineralization), persistent (fail to undergo bioremediation in the environment or under a specific set of experimental conditions) or recalcitrant (inherently resistant to biodegradation) in nature. Biogenic or naturally occurring compounds are biodegradable while man-made (anthropogenic) compounds may be biodegradable, persistent or recalcitrant. In terms of xenobiotics that are man-made, the microbial communities present in the environment may not have evolved suitable mechanisms for their degradation. Many possible mechanisms exist which differ from one xenobiotic to another. One common mechanism is the binding of enzymes analogous to their natural substrates which contain xenobiotic functional groups, assuming these do not greatly alter or change the active site which catalyzes a reaction with the xenobiotic. The success of this enzymatic reaction (as a biodegradation mechanism) also depends on other factors such as the ability of the xenobiotic as an inducer or inhibitor and the nature of the product/intermediate formed. Specific to morpholine, the metabolic degradation pathway has been very difficult to establish because of the aforementioned technical limitation.

1.1 Sustainable remediation of morpholine and its degradation pathway

Although morpholine was previously thought to be recalcitrant, several microbes have proven to metabolically degrade it. The majority of studies showed that the species *Mycobacterium* and *Pseudomonas* are the two potential bacterial isolates that utilize morpholine as their sole source of carbon and nitrogen, thereby undergoing degradation [4–7]. A few studies have been carried out to understand the biodegradation of morpholine and its regulation [8–10]. Later a hypothetical pathway was proposed for the complete mineralization of morpholine that could proceed via 2-(2-aminoethoxy)acetate to produce its diglycolate salt and/or ethanolamine [5, 11, 12]. These two different routes of degradation are called the ethanolamine/monoethanolamine pathway (Pathway 1)

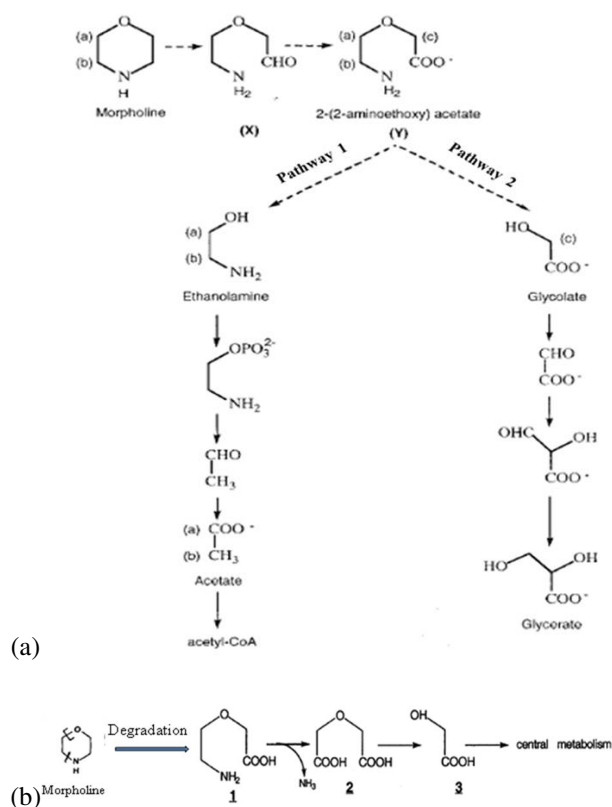


Figure 2: (a) Hypothetical pathway of morpholine degradation where X = 2-(2-aminoethoxy)acetaldehyde, Y = 2-(2-aminoethoxy)acetate and a, b, c indicate the position of carbon atoms in the ring. (b) Postulation of the morpholine degradation pathway after $^1\text{H-NMR}$ and ion spectroscopic analyses where 1 = 2-(2-aminoethoxy)acetate, 2 = diglycolic acid and 3 = glycolic acid.

and diglycolic acid/glycolate pathway (Pathway 2), respectively (Fig. 2a). The illustrated degradation pathway might start with the cleavage of the C-N bond, leading to the formation of an intermediary amino acid which is followed by deamination and oxidation of this amino acid to form a diacid [11, 12].

The degradation of morpholine via the ethanolamine or glycolate pathways has been described in the presence of *Mycobacterium chelonae* and *M. aurum MO1* [8, 9] (Fig. 2a). The degradation of morpholine is likely to begin with the breakage of a bond between a heteroatom and an adjacent carbon atom by the enzyme *morpholine monoxygenase*, which is responsible for the ring cleavage. *Morpholine monoxygenase* is an important enzyme in the degradation of morpholine as it catalyzes the biotransformation of morpholine to form 2-(2-aminoethoxy)acetic acid and contains a catalytic subunit of cytochrome P₄₅₀ [1, 10]. Morpholine could serve as a substrate for flavin-containing monoxygenases or cytochromes P450 which is associated with oxygen consumption [13]. Further inhibitory effects of metyrapone on the degradation of the *Mycobacterium* strain RP1 have been attributed to the involvement of cytochromes P450

in the biodegradation of morpholine [5]. Depending on the concentration of morpholine in the culture medium, one pathway could be expressed while the other might be inhibited [11]. Recently, a new approach was applied in which the culture filtrate was analyzed by $^1\text{H-NMR}$ spectroscopy and ion spectroscopy to identify the metabolic intermediates of morpholine degradation by *M. aurum* MOI [11, 12] (Fig. 2). Although many different species of *Mycobacterium* have been shown to degrade morpholine via this shared group of degradation reactions, little information is known about the enzymes involved (Fig. 2b). Furthermore, the byproducts of the microbial processes can be indicative of a successful bioremediation process. Consequently, since only hypothetical pathways have been proposed, limited interpretations of various experimental designs can be made to establish the degradation pathway that follows the route of degradation pathway that follows the route of Pathway 1 and /or Pathway 2 via the shared formation of 2-(2-aminoethoxy)acetate.

2. Materials and methods

2.1 Environmental samples

The sample used in the present degradation study was collected from natural sources (soil) in and around Durgapur Steel Plant, West Bengal, India. The site is located in Durgapur at a latitude of $51^{\circ}50'43.8''$ north and a longitude of $8^{\circ}16'35.8''$ west in the state of West Bengal, India. Soil samples consisted of blackish fine-to-medium sub-angular gravel in the upper surface, including fine sand and a high content of iron flecks. Samples were collected in a clean, sterile plastic container before being transferred to the laboratory and stored at room temperature until used for further analysis.

2.2 Chemicals and reagents

All chemicals and reagents were of analytical grade and used as received without any further purification. Even though Milli-Q water (Elix Essential 3 Water Purification System with a conductance of 0.12 Siemens) was used to prepare an aqueous solution of reagents, autoclaved double distilled water was used because of the microbial cultures.

2.3 Screening, characterization and sequence accession of the morpholine-degrading isolate

For the initial isolation and cultivation of bacteria, ten-fold serial diluted samples were spread onto nutrient agar plates, which were prepared according to the manufacturer's instructions. The specific colonies obtained were subcultured further to isolate the pure bacterial strain. The selected pure bacterial isolate was identified based on morphological, biochemical and molecular characterization. Morphological characterization was achieved by

visually observing colonies in terms of their appearance, shape, color, arrangement, optical nature, margin, texture and elevation. However, the biochemical tests were performed as per standard methods [14]. Furthermore, the pure colony was then identified by 16S rRNA gene sequence analysis.

In order to verify the phylogenetic affiliation of the selected isolate, a single colony was collected for the purpose of DNA isolation (InstaGeneTM Matrix Genomic DNA isolation kit (Bio-Rad Catalog # 732-6030) as per the kit instructions and procedures) and subjected to Polymeric Chain Reaction (PCR) analysis using primers targeting two 16S rRNA genes [27F (5'-AGAGTTTGATCMTGGCTCAG-3') and 1492R (5'-TACGGYTACCTTGTTACGACTT-3'-)]. A PCR reaction (20 μL) was performed containing 8 μL of Taq DNA Polymerase Master Mix, 1 μL of both 10 μM stock 27F/1492R primers, 9 μL of double distilled water and 1 μL of a DNA template. The PCR (MJ Research PTC-200 Peltier Thermal Cycler; Bio-Rad PTC-200) reaction was conducted using specified conditions from the literature [15]. DNA was denatured at 94°C for 5 mins, followed by 35 cycles of amplification, each consisting of the following components: 94°C for 45 secs (denaturation), 55°C for 60 secs (annealing), 72°C for 60 secs, (extension) followed by 72°C for 10 mins (final extension).

The PCR product was sequenced by Yaazh Xenomics, Chennai, Tamil Nadu, India. The 16S rRNA gene was sequenced using the National Center for Biotechnology Information's Basic Local Alignment Search Tool (BLAST). The phylogenetic analysis of the sequence using the closely related sequence of BLAST results was performed by multiple sequence alignment. The program MUSCLE 3.7 was used for multiple sequence alignments [16]. The resulting aligned sequences were filtered using the program Gblocks 0.91b, which eliminates poorly aligned positions and divergent regions, that is, removes alignment noise [17]. Finally, the program PhyML 3.0 aLRT was used for phylogenetic analysis and HKY85 as a substitution model.

The nucleotide sequence of the isolated bacterium was included in NCBI's GenBank and assigned an accession number consisting of 2 letters and 6 numbers [18].

2.4 Cultivation and acclimatization of the isolate: Microbial adaptation against morpholine

Bacterial inocula were prepared by aseptically transferring the selected identified pure colonies to 10 mL of an enriched media called Knapp Buffer. Alternatively, a mineral salt solution (MSS) comprised of 100 mg of KH_2PO_4 , 100 mg of K_2HPO_4 , 4 mg of $\text{MgSO}_4 \cdot 7\text{H}_2\text{O}$ and 0.2 mg of FeCl_3 was used as previously described by the author supplemented with 0.1% v/v morpholine as previously described by the author [19]. Cultures were incubated at 37°C as well as 150 rpm for 1–2 weeks and

Table 1: GC parameters for the estimation of the monoethanolamine concentration

Parameters	Specificity
Column and its configuration	Rtx-35 30 mm × 0.32 mm × 1 μm
Oven/Column temperature	Initial temp.: 60 °C Hold: 1 min Ramp rate: 30 °C/min Final temp.: 240 °C maintained for 3 mins Linear velocity: 37.6 cm/sec (for nitrogen)
Injection port	Temp.: 200 °C Split Ratio: 30:1 Injection Volume: 1 μL
Carrier gases (mobile phase)	Column gas flow rate: 2 mL/min Purge gas flow rate: 1 mL/min Hydrogen gas flow rate: 40 mL/min Zero air flow rate: 400 mL/min Nitrogen gas flow rate: 15 mL/min
Stationary phase	60% Dimethylpolysiloxane and 35% Diphenyl polysiloxane
Detector	Flame ionization detector at 300 °C
Analysis time	10 mins
Software	GC Solution
Workstation	Windows 8

their absorbance at 600 nm was taken regularly as a measure of growth. Based on their growth, when an optical density of 0.5 was reached (data not shown), the culture was diluted to 1 : 100 before being further spread onto MSS-agar plates (treated with 2% agar + 0.1% morpholine) to confirm the acclimatization of the isolate against morpholine stress. Furthermore, the growing culture was centrifuged at 6500 rpm for 10 mins and the pellet was re-suspended in the MSS medium while gradually increasing the concentration of morpholine to 0.2% which was referred to as a seeded acclimatized bacterial inoculum. For each increased acclimatization study, the tested bacteria were grown in an MSS broth supplemented with an increased concentration of morpholine and a respective MSS-agar plate with the same concentration of morpholine to confirm the said acclimatization.

The acclimatized inoculum was later grown in the presence of an intermediate degradation product of morpholine to explore whether this particular isolate follows Pathway 1 or 2. This was further validated by performing in-vitro chemical and analytical assay(s) with the availability of intermediate product of morpholine degradation in the culture filtrate. Lastly, estimation of the ammoniacal nitrogen (measure of the amount of ammonia) in the culture filtrate revealed the complete degradation of morpholine by this isolate following the concerned pathway.

2.5 Growth on different hypothetical degradation intermediate compounds

The growth of the isolate on various substrates (degradation intermediate compounds) was investigated by adding the corresponding compounds (0.15%) to the MSS. The pH of the media was adjusted to 7 and growth carried

out at 37°C as well as 150 rpm for 48 hours. At regular time intervals, the absorbance was measured in terms of optical density to establish whether these degradation products might have been formed to facilitate the growth of the isolated bacteria.

2.6 Chemical tests of intermediate(s) in the degradation pathway

Chemical tests on degradation products, mainly monoethanolamine (primary amine) and morpholine (secondary amine), were carried out by the standard Simon test - 1 (Rimini test) and Simon test - 2 (modified Rimini test) on the culture filtrate to determine the presence of primary and secondary amines [20]. The amine undergoes a nucleophilic addition reaction with nitroprusside ions in the presence of acetaldehyde or a ketone to yield the characteristic color of primary amines (blue) or secondary amines (violet).

2.7 Gas Chromatography (GC) studies of degradation intermediate(s)

A GC system (Shimadzu GC-2010) equipped with a standard oven for temperature ramping, split condition, injection ports, a flame ionization detector and a Rtx-35 amine column (30 mm × 0.32 mm × 1 μm film thickness) in the presence of nitrogen as a carrier gas by the direct injection method was used for the analysis of monoethanolamine (MEA). The analytical parameters for the analysis of MEA are summarized in Table 1, as per the method (by modifying the column and its parameters) reported in the literature [21].

Table 2: MS operating parameters for intermediate(s)

Parameter	Specificity
Ionization	electrospray ionization Needle voltage = 4.5 kV
Interface temperature	350 °C
Temperature of heating block	200 °C
Sheath/Drying gas flow rate	15 L/min
Nebulizer gas flow rate	1.5 L/min
Acquisition time	2 mins
Acquisition mode	Positive/Negative Scan m/z 50 – 200 Scan speed = 52 units/sec Sampling acquisition time = 1.56 Hz (640 msec)
Detector	Electron multiplier
Software	Lab Solutions
Workstation	Windows 7

A standard solution of 0.125 to 0.5% v/v MEA (corresponding to ppm and prepared in methanol) was injected along with the processed culture supernatant (1:10, filtrate volume of 1 and 9 volumes of methanol), as per the method described above. GC of the test samples was run against blank media using positive controls to quantify or estimate the presence of MEA in the culture filtrate by analyzing the Area Under the Curve (AUC) calculated by the machine.

2.8 Mass spectrometry studies of degradation intermediate(s)

The mass spectrometry (MS) system of an integrated Liquid Chromatography-Mass Spectrometry instrument (Shimadzu LCMS-2020) equipped with an inlet interface, ion source, mass analyzer and detector was used to analyze the degradation products of morpholine. The analytical parameters for ascertain the morpholine degradation products are summarized in Table 2.

The sample for injection was prepared without using a solvent, as per the method reported in the literature [12]. The culture sample (5 mL) was centrifuged at 10,000 rpm for 10 mins before the supernatant was filtered through a nylon filter with a pore size of 0.22 µm (Axiva Sicheem Biotech, India) to remove any bacterial cells. 1 mL of neat filtrate was injected directly into the MS instrument.

2.9 Estimation of the ammonia concentration

The presence of ammonia in the culture supernatant was estimated by the standard Nessler's method [22], which involves coupling of ammonium to the Nessler's reagent

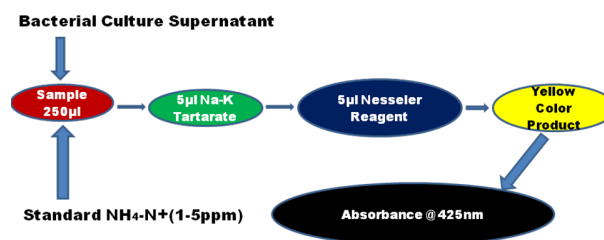


Figure 3: Estimation of the ammoniacal nitrogen concentration by Nessler's method

to produce a yellow color under strongly alkaline conditions (Fig. 3). The resulting yellow color was formed in proportion to the ammonium (NH_4^+) concentration and was measured at a wavelength of 405 nm using an Elisa reader (ELx50/8MS BioTek India) against a reagent blank. The ammonia level in terms of ammoniacal nitrogen was expressed in mg/L (ppm). A standard solution of 10 ppm of $\text{NH}_4^+ -\text{N}$ was prepared by dissolving 4.773 mg of ammonium chloride in 125 ml of double-distilled water and further diluted to make solutions of 1 – 5 ppm $\text{NH}_4^+ -\text{N}$. A calibration curve was plotted and is presented in the results section.

3. Results and discussion

3.1 Morphological, biochemical and molecular identification

Morphologically, the isolate was found to be white in color with a dull opaque appearance, rod-shaped, have a smooth texture and grow as a convex elevation colony. Standard staining reported it to be a Gram-negative bacterium with high motility which also showed signs of growth on a selective medium, namely HiCrome UTI Agar M1353.

The primary sequence of the 16S rRNA from the present bacterial isolate was determined. The program PhyML 3.0 aLRT for phylogenetic analysis and HKY85 as a substitution model on the 16S rRNA gene sequences determined the phylogenetic position of said isolate to be a species closely related to the genus *Halobacillus blutaparonensis* with a sequence representative of *E. coli* (Fig. 4).

Nucleotide sequence accession was assigned by GenBank, NCBI and an accession number of KC345029 was

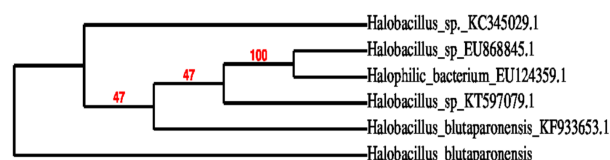


Figure 4: Molecular phylogeny of the 16S rRNA gene sequence and sequences from identified bacteria in the database. The sequence of *E. coli* served as the outgroup for rooting the tree.

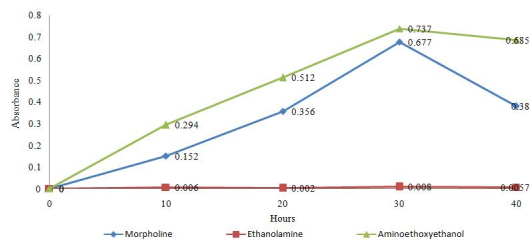


Figure 5: Growth of the isolate in the presence of intermediates of morpholine degradation

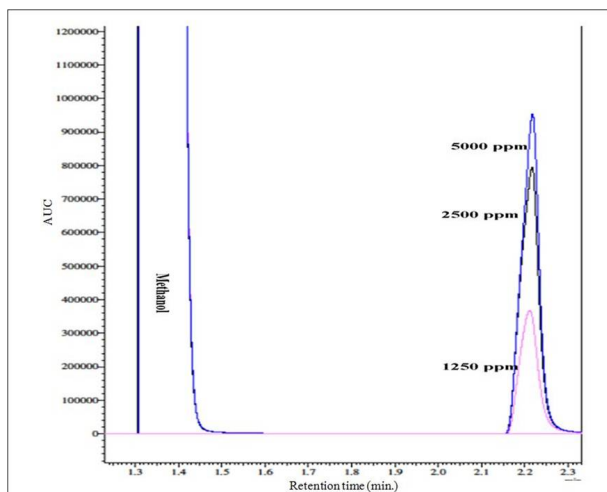


Figure 6: GC (Rtx-35)- flame ionization detector chromatogram of MEA

assigned to this bacterial isolate of genus *Halobacillus blutaparonensis*.

3.2 Growth on intermediates

The isolate grew in the presence of morpholine and the intermediate, namely aminoethoxy ethanol (reduced product of aminoethoxy acetate) by consuming it as a source of carbon and nitrogen. However, no growth was recorded in the presence of ethanolamine in the culture media shown in Fig. 5. The count of bacterial cells was adjusted to 1×10^8 cells/mL (1 unit of absorbance = 5×10^8 cells) by varying the incubation periods up to 48 hours.

3.3 Chemical assay of intermediate(s)

Based on Simon tests - 1 and 2 [20], the presence of MEA and morpholine in the culture filtrate is shown in Table 3.

3.4 GC studies of MEA in the culture supernatant

GC of the culture supernatant was run at different concentrations (ppm) of a standard MEA solution. Table 4 and Fig. 6 indicate a retention time of MEA equal to 2.2

mins which was absent in the diluted culture supernatant. GC analysis revealed that no MEA was present in the culture supernatant suggesting that bacteria might prefer the diglycolic route (Pathway 2) of morpholine degradation which was later confirmed by MS analysis.

3.5 MS studies of the culture filtrate

MS was run directly with a neat culture filtrate. Each sample was analyzed separately in both the positive and negative ion modes (Table 5 and Fig. 7).

It was observed that the m/z peak of the neat culture filtrate (Fig. 7) indicates the presence of 2-(2-aminoethoxy)acetate ($C_4H_9NO_3$, molecular weight = 119.119 and m/z = 120 as $[M+H]^+$) and an anion of diglycolic acid ($C_4H_6O_5$, molecular weight = 134.09 and m/z = 133 as $[M-H]^-$) which supports the fact that this particular isolate prefers the degradation pathway of diglycolic acid (Pathway 2), similar to a strain of *mycobacterium* reported earlier by conducting electrospray ionization mass spectrometry on the culture filtrate [12].

Further MS analysis supports the GC findings that MEA is not present in the culture filtrate because it might have an inhibitory effect on the bacteria. Therefore, the said bacterial isolate prefers the diglycolic acid route of the metabolic pathway given the fact that in the presence of morpholine, one of the two branches of morpholine biodegradation was induced while the other was inhibited. The illustrated degradation pathway might start with the cleavage of C-N bond, leading to the formation of an intermediary amino acid followed by deamination and oxidation of this amino acid to form a diacid as is shown in Fig. 2b.

3.6 Ammonia release: As the end product of morpholine degradation

Morpholine can be degraded by bacteria which releases ammonia. Whichever degradation pathway of morpholine is followed, ammonia is produced as an end product.

The concentration of ammoniacal nitrogen produced by the isolate was calculated (Table 6 and Fig. 8) by the regression equation of a standard curve ($y = 0.137x$ with $r^2 = 0.98$) and found to be present at a concentration of 5.2 ppm based on Nessler's quantification. The initial morpholine concentration in the culture supernatant (before degradation) was reported to be 2000 ppm. The molar ratio with regard to the conversion of morpholine into ammonia was found to be 1 : 0.014. Furthermore, it was shown that the final pH of the media throughout the experiment did not change, supporting the fact that a low concentration of ammonia was released as an end product of morpholine degradation.

Table 3: Simon tests for the presence of the primary amine MEA and secondary amine morpholine in the culture supernatant

Sample	Test	Feature	Remark	Result
Morpholine	Simon 1	Characteristic blue color of the secondary amine		Morpholine positive
MEA	Simon 2	Characteristic violet color of the primary amine		MEA positive
Culture media	Simon 1	No characteristic blue color		Morpholine negative
	Simon 2	No characteristic violet color		MEA negative
Culture Supernatant (Filtrate)	Simon 1	No characteristic blue color		Morpholine negative
	Simon 2	No characteristic violet color		MEA negative

Table 4: GC analysis of the diluted culture filtrate

Vial	Retention time (mins)	AUC	Interpretation (Compound)
Methanol	1.331	378534920.9	Methanol
5000 ppm MEA	1.333	366649701.7	Methanol
	2.218	2748948.5	MEA
2500 ppm MEA	1.331	374551161.2	Methanol
	2.216	2397300.9	MEA
1250 ppm MEA	1.331	378803557.4	Methanol
	2.211	1149593.1	MEA
Culture Supernatant (1:10)	1.334	310947764.4	Methanol
	2.331	92353.6	No/Negligible MEA

Table 5: Expected intermediate according to the MS analysis of the culture filtrate.

Sample	m/z Positive mode	m/z Negative mode	Remark
Neat Culture filtrate	120		[M+H] ⁺ 2,2 Aminoethoxy acetate
		133	[M-H] ⁻ Anion of diglycolic acid

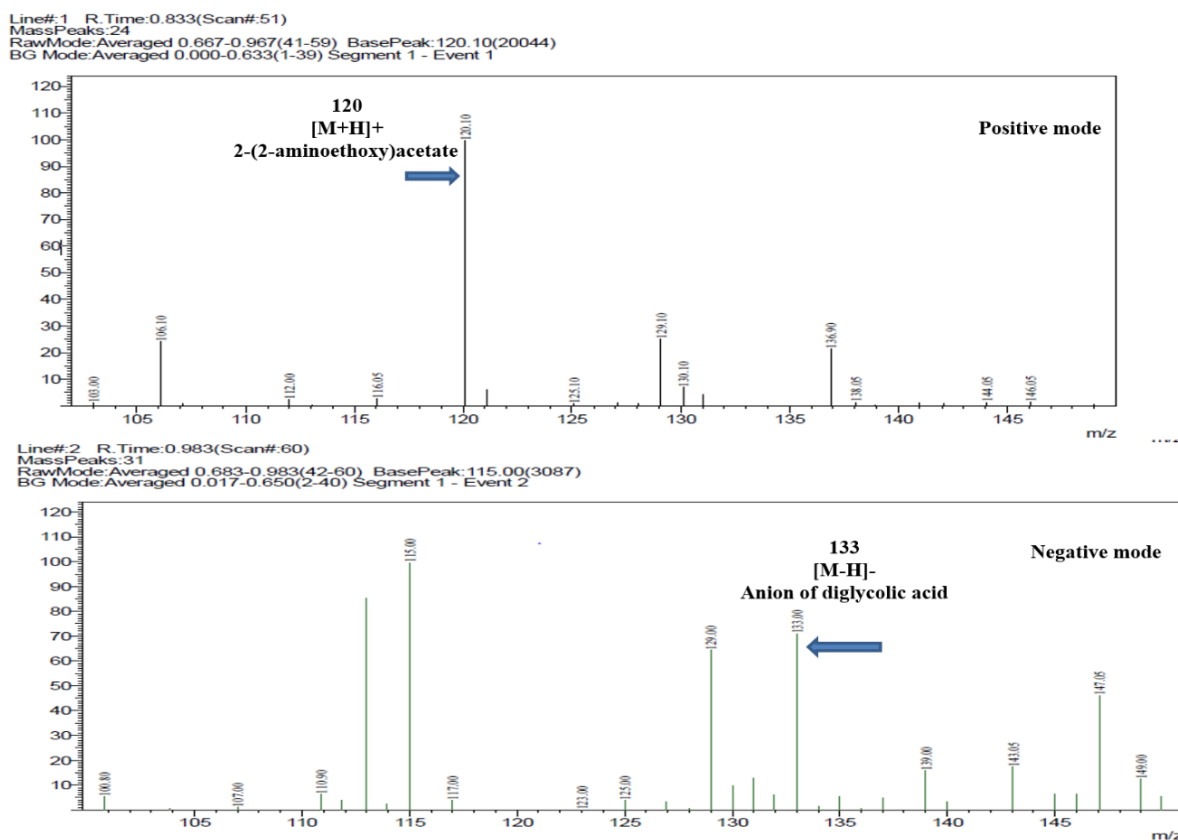


Figure 7: Electrospray ionization - MS spectra recorded under positive and negative ionization of the neat culture filtrate.

Table 6: Estimation of ammoniacal nitrogen concentration by Nessler's reagent

Well	10 ppm Stock NH ₄ -N+ (μL)	Milli-Q water (μL)	Culture media (μL)	50% Na-K Tartrate (μL)	Nessler's reagent (μL)	Net absorbance at 405 nm
1 ppm	25	225	—	5	5	0.091
2 ppm	50	200	—	5	5	0.284
3 ppm	75	175	—	5	5	0.353
4 ppm	100	150	—	5	5	0.552
5 ppm	125	125	—	5	5	0.725
Culture supernatant	250	—	—	5	5	0.725

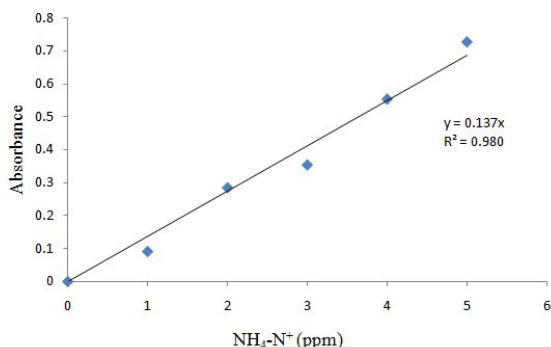


Figure 8: Standard curve of ammoniacal nitrogen concentration by Nessler's reagent

4. Discussion

Based on the results summarized, it has been reported that the isolate prefers to undergo the diglycolic acid route of degradation instead of the ethanolamine pathway, which might be an inhibitory effect on bacterial growth. The illustrated degradation pathway starts with cleavage of the C-N bond, leading to the formation of an intermediary amino acid which is followed by deamination and oxidation to form the diacid (Fig. 9). This diacid, namely diglycolate, later participates in intermediate metabolism and is converted indirectly into TCA by the Krebs cycle, which is beyond the scope of the present article.

Moreover, the presence of degradation intermediate compounds in culture filtrate also favors this finding with the conclusion that the diglycolic acid route of biodegradation might be a common degradation mechanism, which is also shown by other strains of bacteria, proceeding via 2-(2-aminoethoxy)acetate. The said investigation to reveal the degradation pathway of morpholine is supported by similar findings published by other authors [5, 10–12].

Furthermore, whatever the degradation pathway exhibited by the bacterial isolate, the end product, that is, ammonia, will be biochemically produced and used. Our studies confirm the presence of ammonia as an end product in a molar conversion ratio of morpholine to ammonia of 1 : 0.014. Due to the low concentration of ammonia produced, the pH of the culture medium did not change throughout the experiment. However, a higher molar ra-

tio of morpholine to ammonia brought about an inhibitory effect on the growth of bacteria by increasing the pH of the medium and making it more alkaline. The molar ratio of morpholine to ammonia was found to be different for different strains of bacteria as viz., namely 1 : 0.5 for *Mycobacterium sp. HE5* [6], 1 : 0.89 for *Mycobacterium sp.* [7] and 1 : 0.82 for *Mycobacterium sp. MO1* [9].

5. Conclusions

The large scale industrial applications of morpholine and its known carcinogenic effect thus have an environmental interest for its biodegradation and exploring the degradative pathway so that unrevertable damage to the natural environment and biota can be minimized. Along with the *Mycobacterium* and *Pseudomonas sp.* another potential isolate namely *Halobacillus blutaparonensis* has been investigated for its ability to removal of morpholine by adopting the diglycolate degradation pathway. Hence, sustainable remediation practice by utilizing effective microbes should be applied to bring the environmental cleanup or facilitate the existing system of effluent treatment mechanism incorporation with biological approaches to minimize the impact of xenobiotic pollutants in the anthropocentric epoch.

Conflicts of interest

The authors confirm no conflicts of interest with regard to the results derived from this study on the sustainable remediation of morpholine and its micro-scale degradation pathway.

REFERENCES

- [1] Sielaff, B.; Andreesen, J. R.; Schröder, T. A.: Cytochrome P450 and a ferredoxin isolated from *Mycobacterium sp.* strain HE5 after growth on Morpholine. *Appl. Microbiol. Biotechnol.*, 2001, **56**(3-4), 458–464 DOI: 10.1007/s002530100634
- [2] Dhiwahaar, A. T.; Maruthamuthu, S.; Marnadu, R.; Sundararajan, M.; Manthrammel, M. A.; Shkir, M.; Sakthivel, P.; Reddy, V. R. M.: Improved photocatalytic degradation of rhodamine B under visible light and magnetic properties using microwave

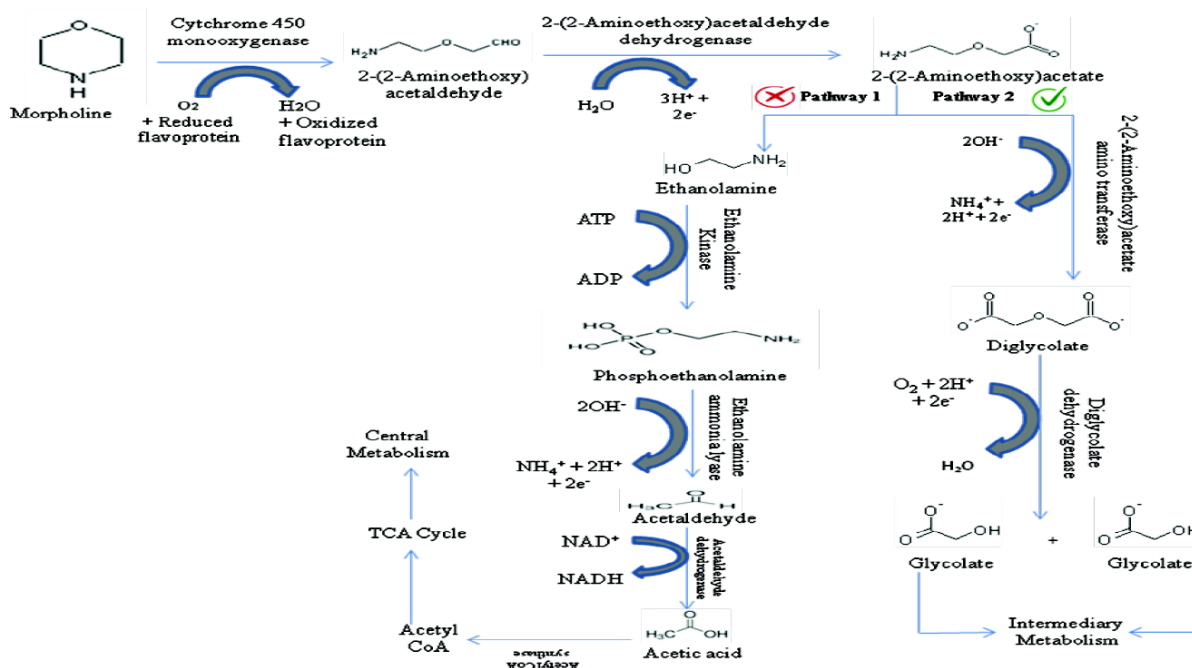


Figure 9: The complete illustration of a possible degradation pathway of morpholine. The isolate, namely *Halobacillus blutaparonensis*, prefers Pathway 2 for the successful removal of morpholine. Abbreviations used - TCA: Tricarboxylic acid; ATP: Adenosine triphosphate; ADP: Adenosine diphosphate; H^+ : Hydrogen atom; e^- : Free electron; O_2 : Oxygen molecule; NH_4^+ : Ammonium ion

- combustion grown Ni doped copper ferrite spinel nanoparticles. *Solid State Sci.*, 2021, **113**, 106542 DOI: 10.1016/j.solidstatedciences.2021.106542
- [3] Khan, A.; Valicsek, Z.; Horváth, O.: Photocatalytic Degradation of Rhodamine B in Heterogeneous and Homogeneous Systems. *Hung. J. Ind. Chem.*, 2021, **49**(1), 9–16 DOI: 10.33927/hjic-2021-02
- [4] Chandrasekaran, S.; Lalithakumari, D.: Plasmid-assisted morpholine degradation by *Pseudomonas fluorescens* CAS 102. *World J. Microbiol. Biotechnol.*, 1997, **14**, 7–10 DOI: 10.1023/A:1008855912907
- [5] Poupin, P.; Truffaut, N.; Combourieu, B.; Besse, P.; Sancelme, M.; Veschambre, H.; Delort, A. M.: Degradation of Morpholine by an environmental Mycobacterium strain involves a Cytochrome P-450. *Appl. Environ. Microbiol.*, 1998, **64**(1), 159-165 DOI: 10.1128/AEM.64.1.159-165.1998
- [6] Schröder, T.; Schuffenhauer, G.; Sielaff, B.; Andreesen, J. R.: High morpholine degradation rates and formation of cytochrome P450 during growth on different cyclic amines by newly isolated Mycobacterium sp. Strain HE5. *Microbiology*, 2000, **146**(5), 1091–1098 DOI: 10.1099/00221287-146-5-1091
- [7] Magda, M.; Aly: Degradation of morpholine by Mycobacterium sp. isolated from contaminated wastewater collected from Egypt. *Afr. J. Biotechnol.*, 2011, **10**(42), 8351–8358 DOI: 10.5897/AJB11.308
- [8] Swain, A.; Waterhouse, K. V.; Venables, W. A.; Calley, A. G.; Lowe, S. E.: Biochemical studies of morpholine catabolism by an environmental mycobacterium. *Appl. Microbiol. Biotechnol.*, 1991, **35**(1), 110–114 DOI: 10.1007/BF00180646
- [9] Mazure, N.; Truffaut, N.: Degradation of morpholine by Mycobacterium aurum MO1. *Can. J. Microbiol.*, 1994, **40**(9), 761–765 DOI: 10.1139/m94-120
- [10] Shaikh, A. R.; Sahnoun, R.; Broclawik, E.; Koyama, M.; Tsuboi, H.; Hatakeyama, N.; Endou, A.; Takaba, H.; Kubo, M.; Carpio, C.; Miyamoto, A.: Quantum chemical studies for oxidation of morpholine by Cytochrome P450. *J. Inorg. Biochem.*, 2009, **103**(1), 20–27 DOI: 10.1016/j.jinorgbio.2008.08.013
- [11] Combourieu, B.; Besse, P.; Sancelme, M.; Veschambre, H.; Delort, A. M.; Poupin, P.; Truffaut, N.: Morpholine degradation pathway of Mycobacterium aurum MO1: direct evidence of intermediates by in situ 1H nuclear magnetic resonance. *Appl. Environ. Microbiol.*, 1998, **64**(1), 153–158 DOI: 10.1128/AEM.64.1.153-158.1998
- [12] Combourieu, B.; Besse, P.; Sancelme, M.; Godin, J.-P.; Monteil, A.; Veschambre, H.; Delort, A.-M.: Common Degradative Pathways of Morpholine, Thiomorpholine, and Piperidine by Mycobacterium aurum MO1: Evidence from 1H -Nuclear Magnetic Resonance and Ion Spray Mass Spectrometry Performed Directly on the Incubation Medium. *Appl. Environ. Microbiol.*, 2000, **66**(8), 3187–3193 DOI: 10.1128/aem.66.8.3187-3193.2000

- [13] Knapp, J. S.; Emtiazin, G.; Yusoff, S.; Heron, S. T.: The utilization of morpholine as a sole nitrogen source by Gram-negative bacteria. *Lett. Appl. Microbiol.*, 1996, **23**(5), 334–338 DOI: [10.1111/j.1472-765X.1996.tb00202.x](https://doi.org/10.1111/j.1472-765X.1996.tb00202.x)
- [14] Buchanan, R. E.; Gibbons, N. R.: *Bergey's Manual of Determinative Bacteriology*, 8th ed., (Williams and Wilkins, Baltimore, USA) 1974 ISBN: 978-0-6830-1117-3
- [15] Unissa, R.; Sudhakar, M.; Reddy, A. S. K.: Screening of marine bacterial cultures for extracellular production of l-argininedeiminases. *World J. Pharm. Res.*, 2015, **4**(6), 1194–1204 <https://www.wjpr.net>
- [16] Edgar, R. C.: MUSCLE: multiple sequence alignment with high accuracy and high throughput. *Nucleic Acids Res.*, 2004, **32**(5), 1792–1797 DOI: [10.1093/nar/gkh340](https://doi.org/10.1093/nar/gkh340)
- [17] Talavera, G.; Castresana, J.: Improvement of phylogenies after removing divergent and ambiguously aligned blocks from protein sequence alignments. *Syst. Biol.*, 2007, **56**(4), 564–577 DOI: [10.1080/10635150701472164](https://doi.org/10.1080/10635150701472164)
- [18] NCBI accession number tool; <https://www.ncbi.nlm.nih.gov/genbank>
- [19] Kumar, R.; Manga, P.; Gupta, S.; Kapur, S.: Biological approaches for treating industrial effluents containing morpholine. *Industrial and Environmental Biotechnology*, edited by Krishna Pramanik and Jayant Kumar Patra, Studium Press India Pvt Ltd - New Delhi, 2014, 255–264 ISBN: 9789380012674
- [20] United Nations Office on Drugs and Crime, Scientific and Technical Notes SCITEC/20, December 2005 <https://www.unodc.org>
- [21] Gerster, F. M.; Hopf, N. B.; Huynh, C. K.; Plateel, G.; Charrière, N.; Vernez, D.: A simple gas chromatography method for the analysis of monoethanolamine in air. *J. Sep. Sci.*, 2012, **35**(17), 2249–2255 DOI: [10.1002/jssc.201200196](https://doi.org/10.1002/jssc.201200196)
- [22] Crosby, N. T.: Determination of ammonia by the Nessler method in waters containing hydrazine. *Analyst*, 1986, **93**(1107), 406–408 DOI: [10.1039/AN9689300406](https://doi.org/10.1039/AN9689300406)

ENZYME REACTION ENGINEERING AS A TOOL TO INVESTIGATE THE POTENTIAL APPLICATION OF ENZYME REACTION SYSTEMS

NEVENA MILČIĆ¹, IVANA ČEVID¹, MEHMET MERVAN ÇAKAR¹, MARTINA SUDAR¹, AND ZVJEZDANA FINDRIK BLAŽEVIĆ^{*1}

¹Faculty of Chemical Engineering and Technology, University of Zagreb, Marulićev trg 19, Zagreb, HR-10000, CROATIA

It is widely recognized and accepted that although biocatalysis is an exquisite tool to synthesize natural and unnatural compounds under mild process conditions, much can be done to better understand these processes as well as detect resulting bottlenecks and help to resolve them. This is the precise purpose of enzyme reaction engineering, a scientific discipline that focuses on investigating enzyme reactions with the goal of facilitating their implementation on an industrial scale. Even though reaction schemes of enzyme reactions often seem simple, in practice, the interdependence of different variables is unknown, very complex and may prevent further applications. Therefore, in this work, important aspects of the implementation of enzyme reactions are discussed using simple and complex examples, along with principles of mathematical modelling that provide explanations for why some reactions do not proceed as planned.

Keywords: enzyme kinetics, modelling, reaction optimisation

1. Setting up the reaction conditions for an enzyme reaction

In each reaction system, first a proper buffer must be selected and the pH dependence of the enzyme activity determined in order to identify the optimal working conditions [1]. Although the impact of temperature on enzyme activity is also important, it should be remembered that the temperature at which the enzyme exhibits the highest level of activity is not necessarily that at which the enzyme stability is optimal. At higher temperatures, the enzyme activity is often increased but at the cost of progressive and irreversible denaturation due to poor thermal stability [2, 3]. When multiple enzymes are present in the reaction system and are supposed to operate in the same reactor, as is the case in cascade reactions, the optimal conditions can seldom be chosen for all of them. Usually, a compromise must be reached whereby the selection of the reaction conditions depends on the enzyme activity required to catalyse the reaction [4, 5]. After selecting the buffer, temperature and pH for the studied reaction system, it must be analysed in detail, starting from the reaction scheme. Even though the reaction scheme usually clearly depicts the reaction, it should be noted that

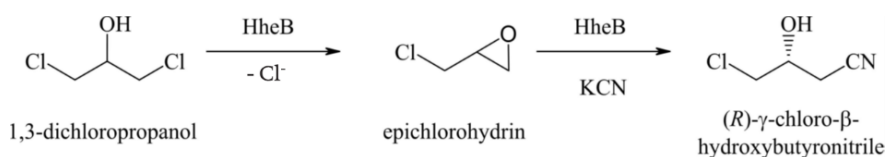
issues beyond the reaction scheme of the enzymatic reaction need to be discussed and analysed.

In many cases, unwanted but insignificant side reactions may take place that sometimes also have a detrimental effect on the outcome of the reaction. Although this may not be so important on the laboratory scale as far as screening for enzyme activities is concerned, given that the concentrations applied on that scale fall within the range of a few mM, it must be noted that the rate of chemical reactions increases as the concentration of reactants increases, e.g. first- and second-order reactions. Therefore, further analyses to determine the effect of increasing the scale of the reaction by hundreds of mM are required. The same applies to the chemical stability of compounds present in the reactor. In this case, engineering methodology is priceless for the purpose of exploring the possibility of slowly feeding the reactive compound into the reactor. Alternatively, if an intermediate is reactive, the reaction rate in the reactor may be tuned to ensure its concentration is always minimal. For example, in the case of epoxides that are substrates of halohydrin dehalogenases [6], it is known that their stability is poor [7, 8]. As a result, in these reactions, a prochiral substrate is often used to start the reaction [9, 10]. The same is true in this case whereby an epoxide intermediate is formed in situ and immediately spent in the subsequent reaction with the same or a different enzyme such as the one presented in [Scheme 1](#).

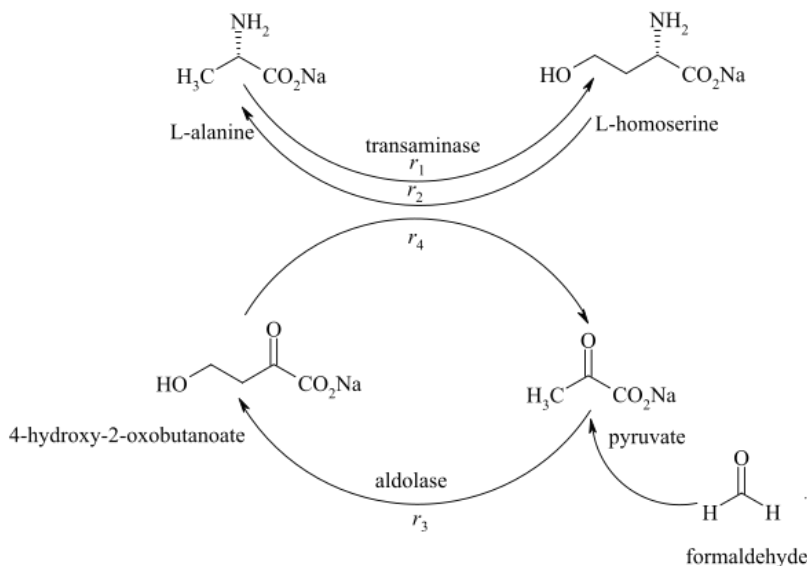
Additionally, since both epoxides and their corre-

Received: 4 April 2022; Revised: 10 April 2022; Accepted: 11 April 2022

*Correspondence: zfindrik@fkit.hr



Scheme 1: Synthesis of (*R*)- γ -chloro- β -hydroxybutyronitrile from an achiral substrate



Scheme 2: Synthesis of L-homoserine in a cascade reaction

sponding nucleophiles can inhibit the catalytic activity of an enzyme [11], the selection of their concentrations in the reactor is crucial in facilitating a successful reaction [12]. Clearly, these are very complex reaction systems and the suitable set up of a reactor as well as reaction conditions determined by the model-aided approach can be vital [13].

Multi-step reactions cannot always be performed simultaneously in one pot due to complex relationships between the process variables [14, 18]. In a study of an innovative reaction scheme for the preparation of the atorvastatin side-chain precursor, it was found that the two reaction steps consisting of aldol addition and the oxidation of the corresponding product amino lactol could not be performed simultaneously [14]. This was mostly due to the fact that acetaldehyde as the substrate in the first reaction step interferes with the oxidoreduction and coenzyme regeneration by acting as a substrate for the oxidoreductase or as an inhibitor as well as deactivator of both oxidoreductase and NADH oxidase. It is important to determine if all the reaction steps are compatible with each other before deciding how to develop the reaction. Although this might suggest a significant amount of experimental work, this can be considerably reduced by evaluating the enzyme kinetics [13, 19, 20].

Forming the reaction model enables a vast variable space to be explored in silico. Apart from that, combining the kinetic model with mass balances in different reactors enables different types of reactors to be explored

in each system. This was found to be crucial with regard to improving the process metrics in the synthesis of L-homoserine [21], a system governed by the unfavourable equilibrium of the transaminase-catalysed reaction and aided by the pyruvate recycling system catalysed by aldolase (Scheme 2).

The application of model-based optimization techniques led to a doubling of the product concentration (up to 80 gL^{-1}) and an 18% increase in the volumetric productivity (up to $3.2 \text{ gL}^{-1}\text{h}^{-1}$) in comparison with a previously published work [22]. In this system, it was crucial that both reactions were carried out simultaneously to improve the position of the equilibrium. Formaldehyde was gradually added to the system by using a pump due to its reactivity and inhibiting effect on enzyme activity. Additionally, pyruvate and L-alanine were added sequentially once the pyruvate had been consumed in several doses, which, according to calculations, was found to work in silico experiments (Fig. 1 A-B) and subsequently proved experimentally (Fig. 1 C-D).

2. Side reactions and their effect on the reaction scheme.

When studying a complex reaction system, possible side reactions must be taken into account. These can be caused by the instability of reactants, products or intermediates; by chemical reactions between the compounds present in the reaction mixture; as well as by the side reactions

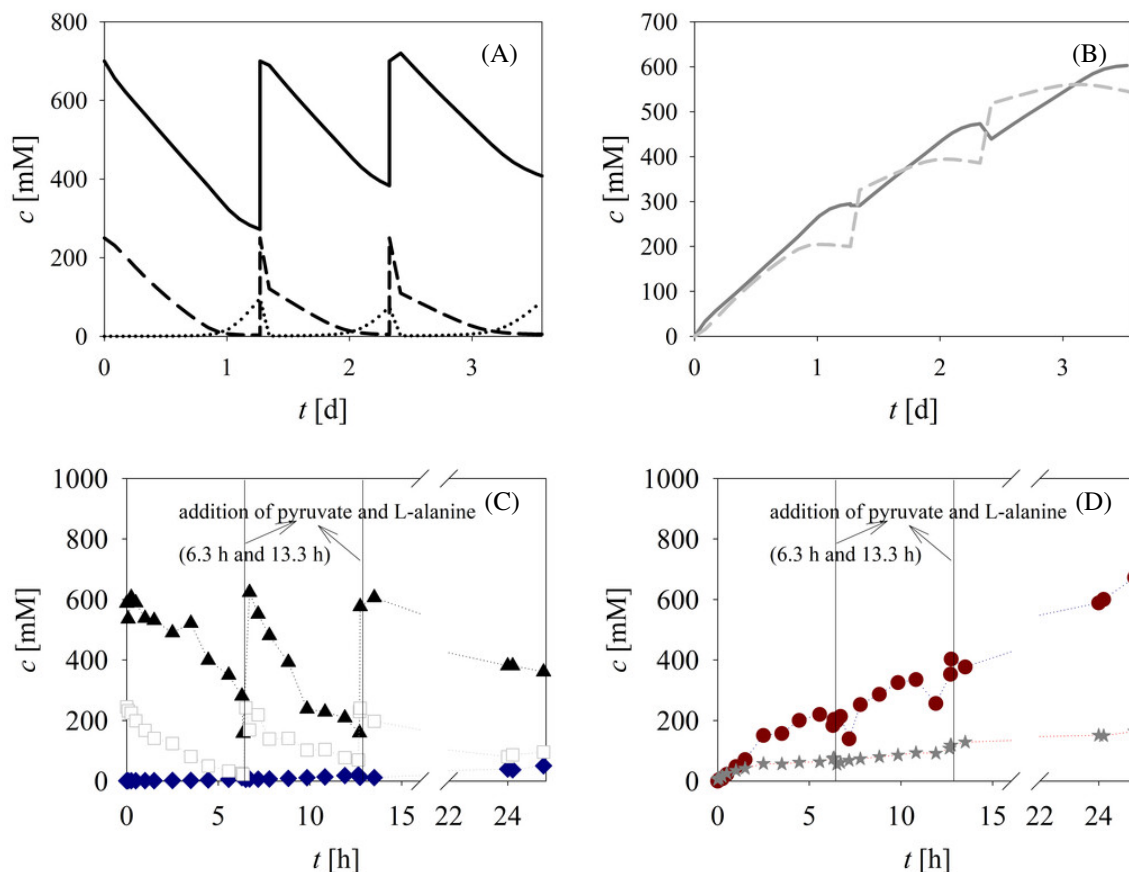
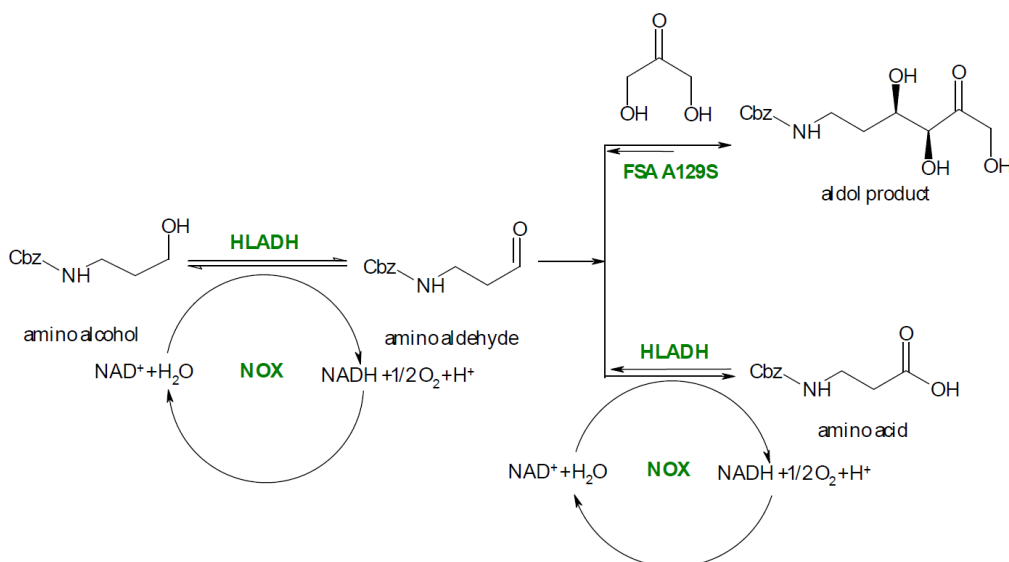


Figure 1: Cascade synthesis of L-homoserine [20] in a fed-batch bioreactor by gradually adding formaldehyde via a pump as well as sequentially adding pyruvate and L-alanine incrementally once the pyruvate had been consumed. (A) (black line – L-alanine, dashed line – pyruvate, dotted line – formaldehyde), (B) (grey line – L-homoserine, grey dashed line – aldol intermediate). In silico experiments, (C) experimental validation (black triangles – L-alanine, white squares – pyruvate, blue diamonds – formaldehyde), and (D) experimental validation (red circles – L-homoserine, grey stars – aldol intermediate).



Scheme 3: Synthesis of the aldol product (3*S*,4*R*)-6-[(benzyloxycarbonyl)amino]-5,6-dideoxyhex-2-ulose in a cascade reaction

caused by the catalytic enzymes due to their low purity or ability to catalyse more than one reaction [8, 23, 24]. Reactions are often carried out with a crude enzyme extract or whole cells in order to reduce the costs of synthesising the protein by avoiding the necessity for purification. Although such systems often offer an additional advantage in terms of enhancing the operational stability of the desired enzyme within the protein mixture or cell compartment, other enzymes in these systems can also catalyse undesirable enzymatic reactions [23].

All of these aforementioned reactions can lower the concentration of the target product as well as decrease the reaction yield, moreover, in some cases, even prevent the formation of the target product. One example of such an event is the oxidation of an alcohol to form an aldehyde catalysed by horse liver alcohol dehydrogenase that reacts further by oxidizing the aldehyde to form the corresponding acid as a side product. In the cascade synthesis of (3*S*,4*R*)-6-[(benzyloxycarbonyl)amino]-5,6-dideoxyhex-2-ulose (Scheme 3), *N*-Cbz-3-aminopropanoic acid was the dominant main product following our first attempt, with only 2% of the target product being formed [25, 26]. Considering the complexity of the system, reaction engineering methodology was applied to determine the reason behind this. A statistical model implied the occurrence of this side reaction [25] which was later confirmed by kinetic studies [26].

Not only did the aforementioned studies reveal the reasons for the poor yield but also determined how to improve it to between 79 and 92%, respectively. In many cases, although commercial compounds that contain small quantities of certain additives are purchased for research purposes, these additives can also frequently act as enzyme inhibitors, such as in the case of 4-methoxyphenol as a stabilizer of acrylonitrile that was used as a substrate in one of the reactions studied by us [27]. In fact, this was one of the crucial reasons why it was not possible to obtain significant amounts of product in any reactor.

3. Investigation of the kinetics of the enzyme-catalysed reaction

To formally identify the system, the effect of all the compounds present in the reaction mixture on the enzyme activity / reaction rate can be evaluated. During these measurements, the effects of all the compounds on the enzyme activity can be measured and, in many cases, substrate, intermediate and product inhibition can be detected, which subsequently help with regard to decision-making and selection of the reactor mode to be used for the reaction. Some examples of reactor designs that can be applied, according to the properties of the studied reaction and desired outcome, are given in Fig. 2. In theory, it is known that the fed-batch bioreactor is a favourable choice for reactions subjected to substrate inhibition to increase the concentration of the obtained product [31].

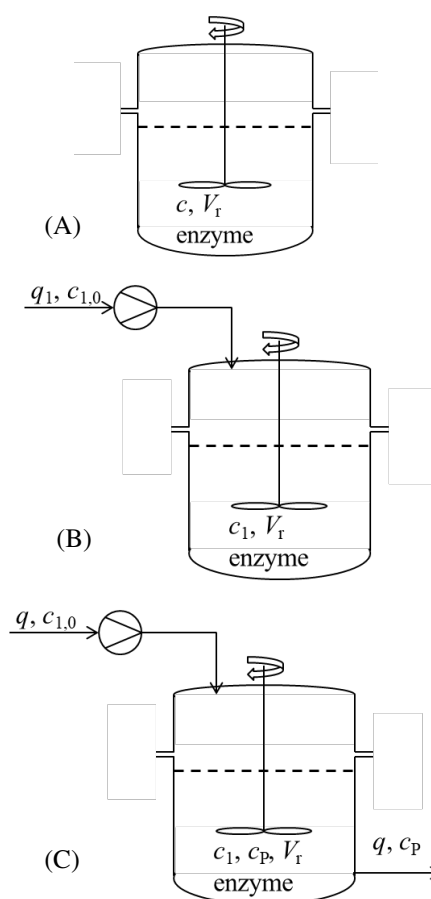


Figure 2: Schemes of different reactors applied in biocatalysis: (A) batch reactor, (B) fed-batch bioreactor, (C) continuous stirred tank reactor

For product-inhibited reactions, a continuous stirred tank reactor operating at the maximum concentration of the product is not recommended and, therefore, the resultant enzyme activity is unsatisfactory [32, 33]. In practice, reactions are rarely inhibited by a single compound, moreover, in many cases, several important inhibitions and/or side reactions take place. Therefore, the reactor mode cannot be easily set by viewing the results of the effect of substrates on the reaction rate. In these cases, kinetic models help simulate different scenarios and enable the best choice for the studied reaction system to be made [13].

The simulations of a relatively simple double-substrate reaction in which the kinetics can be described by double Michaelis-Menten kinetics with both substrate and product inhibition are presented in Fig. 3. The impact of reaction conditions on substrate conversion and volumetric productivity in the batch reactor is presented in Figs. 3A and 3B, while 3C and 3D show the same for the continuous stirred tank reactor (CSTR). Substrate conversion is governed by the enzyme concentration as well as the reaction time and residence time in the batch reactor and CSTR, respectively. The main difference that can be

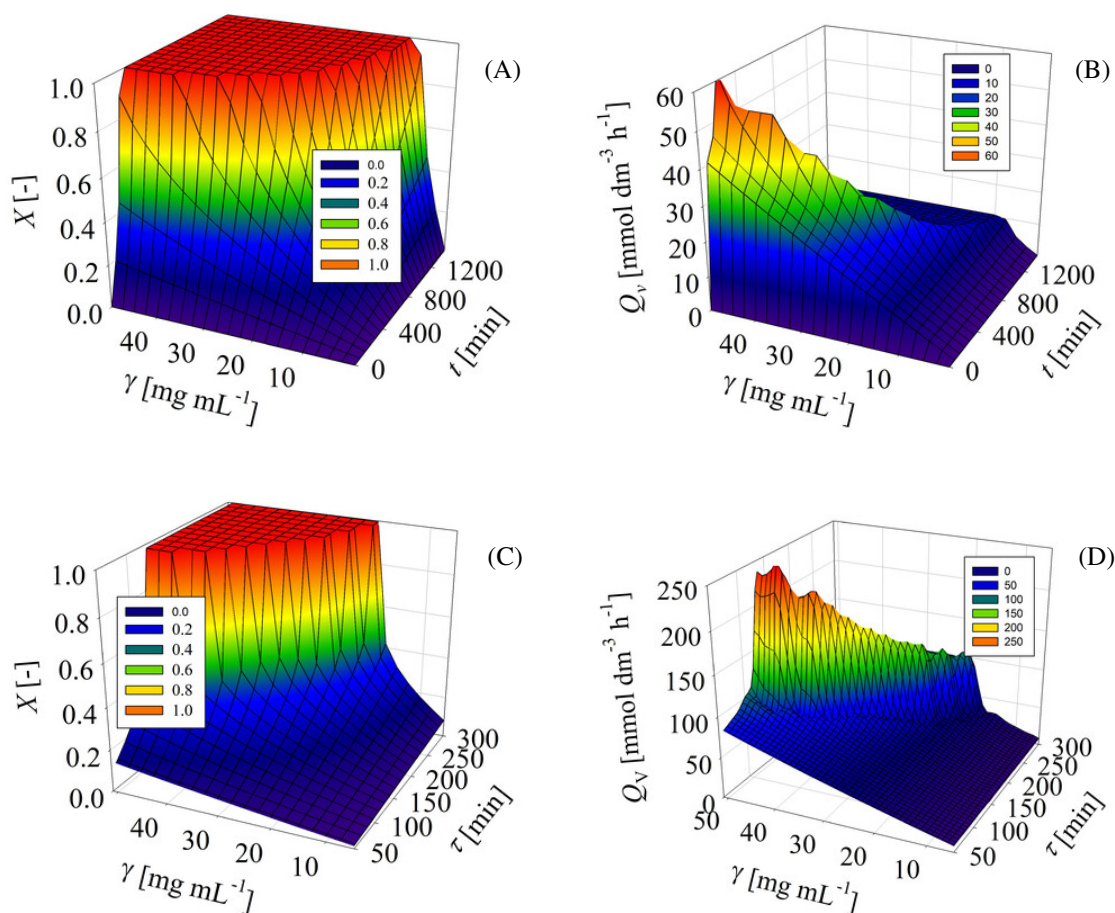


Figure 3: Model simulations demonstrating the impact of the reaction conditions on the conversion and volumetric productivity in the batch and continuous stirred tank reactors

observed is in terms of volumetric productivity, which explains why continuous processes are currently in the spotlight. In this simulation, the maximum volumetric productivity of the CSTR is fourfold greater than that of the batch reactor. Nevertheless, it must be noted that the operational stability of the enzyme is important and that the enzyme activity was assumed to be constant. In practice, since the enzyme activity inevitably drops over time and, therefore, enzymes must be stabilized by a form of immobilization, ensuring the continuous process functions is not a straightforward task.

The first step to investigate enzyme kinetics is to find an appropriate method that will result in the rapid collection of enzyme kinetic data. This can be done by applying a spectrophotometric enzyme assay and microtiter plate reader, however, should these methods be unavailable, this can also be achieved in a traditional manner by determining the initial reaction rates from HPLC or GC data with regard to the concentrations of substrates and products [13]. Given that data collection must be accurate and reliable, analytics is the foundation of the research. Data must be reproducible and trustworthy to be used for modelling. An example of kinetic data is presented in Fig.

4 where the grey line denotes the experiment where the enzyme concentration was too high. Furthermore, even though the linear dependence of absorbance over time is obvious in the initial part of the curve, the error of such measurements can be high and depends on the individual measuring. On the other hand, the black line clearly

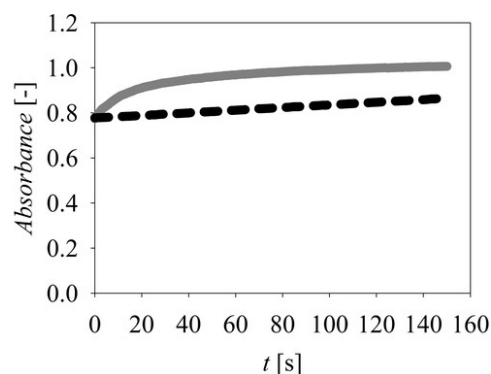


Figure 4: The impact of enzyme concentration on the quality of the experimental data

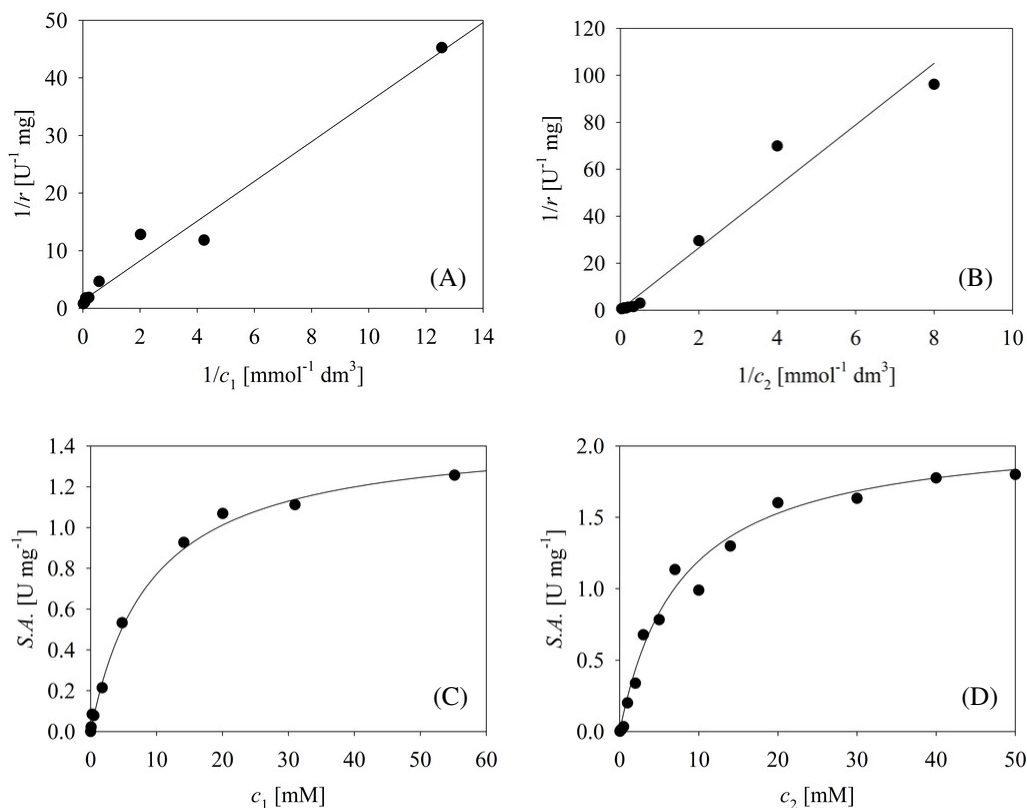


Figure 5: Estimation of kinetic parameters for a two-substrate reaction by applying linear (A and B) and nonlinear regression (C and D) analyses

represents linear data with a relatively small gradient, indicating that the measurements were made properly and the dependence is undoubtedly linear within that range. A series of such experiments performed at different concentrations of substrates, products and intermediates is required to obtain one set of experimental data to be subsequently used for the estimation of kinetic parameters.

Based on the kinetic data, the kinetic parameters can be estimated by using nonlinear regression analysis, which is far better than the still commonly used linear regression analysis [34]. This can be illustrated by the example presented in Fig. 5 whereby a double-substrate reaction was considered and the kinetic data concerning the dependence of the specific enzyme activity on the concentration of the reactants measured. By measuring the initial reaction rate (conversion less than 10%), the effect of product inhibition or enzyme deactivation could be minimized [35]. This example will be used to illustrate the differences between the values of the estimated kinetic parameters when various methods of estimation are applied. In the first case, linear regression analysis was applied by using a Lineweaver-Burk plot (Figs. 5A-5B). The data show discrepancies and, in the case of 5B, two points needed to be removed from the analysis as they were outliers. The estimated kinetic parameters are presented in Table 1. In the second case, the kinetic parameters were estimated by using single-

substrate Michaelis-Menten kinetics, which in all likelihood is frequently used in practice. The estimated kinetic parameters presented in Table 1 are very different from the ones obtained following linear regression analysis. Furthermore, since the maximum reaction rates differ for each substrate, the measurements in all probability were not made in the area of substrate saturation. Michaelis constants estimated by using double-substrate Michaelis-Menten kinetics strongly resemble the values estimated by using single-substrate Michaelis-Menten kinetics. However, when the maximum reaction rates are compared, a significant discrepancy between them can still be observed. Estimating the maximum reaction rate by using double-substrate Michaelis-Menten kinetics is the optimum solution offering a unique value of V_m and taking into consideration the case when the non-varying substrate was not saturated. Therefore, in the case when both substrates are saturated, single-substrate Michaelis-Menten kinetics and nonlinear regression analysis offer a suitable solution to estimate the kinetic parameters.

4. Investigation of the operational stability of the enzyme

Enzyme activity inevitably decreases in the reactor over time, which means that the operational stability reduces as well [28–30]. This also needs to be quantified from the

Parameter	Linear regression analysis $\frac{1}{r} = \frac{1}{V_m} + \frac{K_m}{V_m} \frac{1}{c}$	Nonlinear regression analysis – single-substrate kinetics $r = \frac{V_m c}{K_m + c}$	Nonlinear regression analysis – double-substrate kinetics $r = \frac{V_m c_1 c_2}{(K_{m1} + c_1)(K_{m2} + c_2)}$
V_m [U/mg]	0.743 (3.539)	1.448 (2.119)	4.177
K_{m1} [mmol/dm ³]	2.56	8.2	9.09
K_{m2} [mmol/dm ³]	46.366	7.726	9.191

Table 1: Comparison between different methods to estimate the values of kinetic parameters in an enzymatic reaction

experimental data [29] and incorporated into the kinetic model. In many cases, the enzyme activity can be followed by an independent enzyme assay. In other cases, it can be estimated by using the kinetic model and other experiments. The operational stability of enzymes is an important topic not only in terms of research but also with regard to their applications. Understanding and describing quantitatively as well as qualitatively how enzyme function and structure change during conversion in a bioreactor is of crucial importance [28, 36].

In their work, Börner et al. investigated the mechanistic reasons for the poor operational stability of amine transaminases along with the influence of quaternary structure, cofactors and substrates. Through their kinetic and thermodynamic experiments, they were able to identify the structural domain that appears to confer stability. The study revealed that the enzyme is significantly more stable when at rest than in its operational state, moreover, its operational stability was lower and experiments suggested a mechanism that brought about substrate-induced deactivation [28]. In many reports to date, it has been stated that the presence of substrates and their concentrations can have both positive [37] and negative [30] effects on enzyme stability. In a study by Česnik et al. [30], formaldehyde as a substrate was found to have a negative effect on enzyme activity during experiments (Fig. 6A). Subsequently, it was found that this could be correlated with the operational stability of the enzyme (Fig. 6B). Considering the reactivity of formaldehyde and the size of this molecule, chemical damage to the protein may occur in its presence, as reported in other studies. In a study involving the dehalogenation of 1,3-dichloro-2-propanol (1,3-DCP) catalysed by halohydrin dehalogenases (HHDHs), it was found that the substrate 1,3-DCP causes enzyme deactivation during incubation, moreover, as observed in the previously described case, the substrate concentration has a significant effect on enzyme activity (unpublished data, Fig. 6C). Experiments conducted in batch reactors corroborated that the operational stability decay rate constant can be directly correlated to the substrate concentration (unpublished data, Fig. 6D). These are not the only examples of this behaviour. In a study by Vasić-Rački et al., it was also shown that glycolaldehyde caused operational stability decay in the reactor, the rate of which was dependent on its concentration [38]. In all of these cases, the quantification of the operational

stability decay rate constant and the modelling approach improved the outcome of the reaction and increased process metrics values.

Another example of the effect of a substrate on enzyme activity can be demonstrated by different oxidases. In one study, the operational stability of D-amino acid oxidase was investigated in the presence and absence of aeration [40]. The enzyme operational stability decay rate of D-amino acid oxidase from porcine kidneys was reduced by increasing the oxygen concentration in the reaction solution and the enzyme activity decreased more rapidly. Similar conclusions were drawn in a later study on glucose oxidase [40]. This can be related to the oxidation of protein residues in the presence of oxygen and requires some sort of quantification to enable development of the reaction by focusing on resolving bottlenecks.

If operational stability is considered in a very simple reaction with only a basic Michaelis-Menten model, its effect during dynamic simulations can be observed (Fig. 7A). When the enzyme activity reduces in the batch reactor, the shape of the curve changes slightly. To the untrained eye, this can also resemble the result of reaching equilibrium or product inhibition. Therefore, if the kinetics of the reaction are completely unknown, it is very difficult to draw the right conclusion. The situation is quite different if the continuous stirred tank reactor is used, since this reactor ideally works at a stationary state and, therefore, no changes in enzyme activity nor in stationary concentrations of reactants and products occur. Hence, enzyme operational stability decay in CSTRs results in the stationary state being lost and the clearly visible shape of the curve caused by the reduction in enzyme activity (Fig. 7B). A third type of reactor often applied in biocatalysis due to substrate inhibition are fed-batch bioreactors. Although enzyme operational stability decay can be observed from the shape of the curve (Fig. 7C), here, like in the case of the batch reactor, it is more difficult to clearly define the reason for this trend. The answer that is suggested here concerns quantification of enzyme activity during the reaction.

5. Choosing the best enzyme variant for the reaction

Techniques for genetically modifying enzymes have advanced greatly over recent years and can be applied to produce industrially suitable catalysts more quickly and

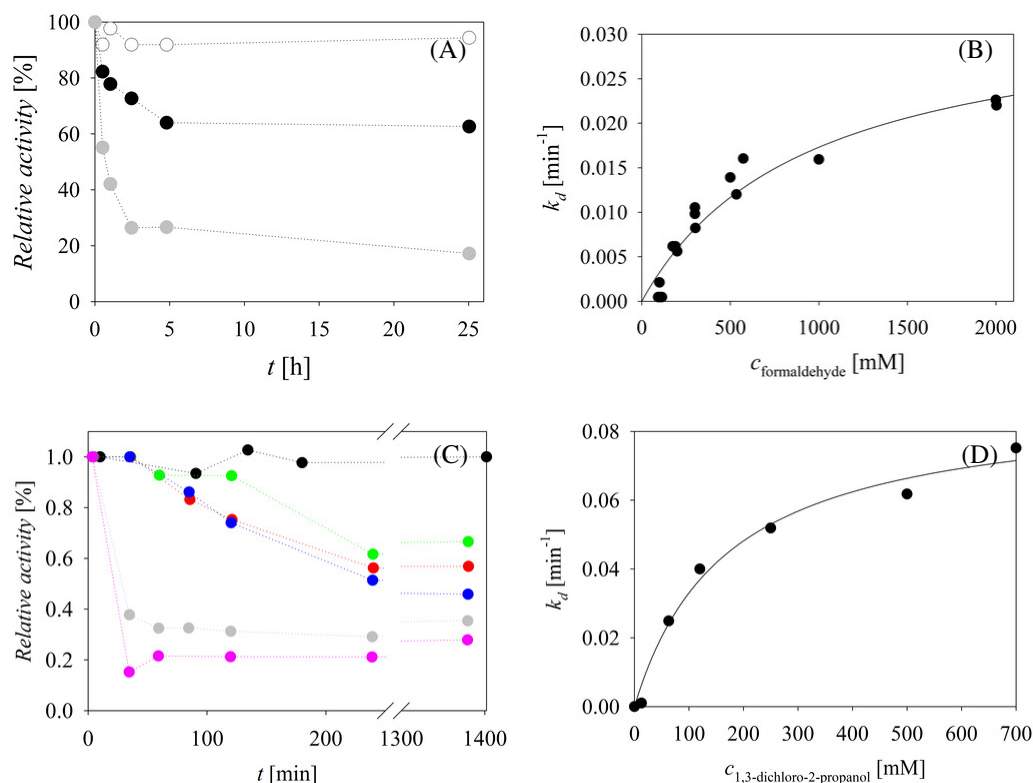


Figure 6: (A) The influence of the initial concentration of formaldehyde on the enzyme activity of FSAD6Q during incubation; (B) Dependence of the operational stability decay rate constants of FSAD6Q on the initial concentration of formaldehyde; (C) The influence of the initial concentration of 1,3-DCP on the enzyme activity of HHDH during incubation; (D) Dependence of the operational stability decay rate constants of HHDH on the initial concentration of 1,3-DCP

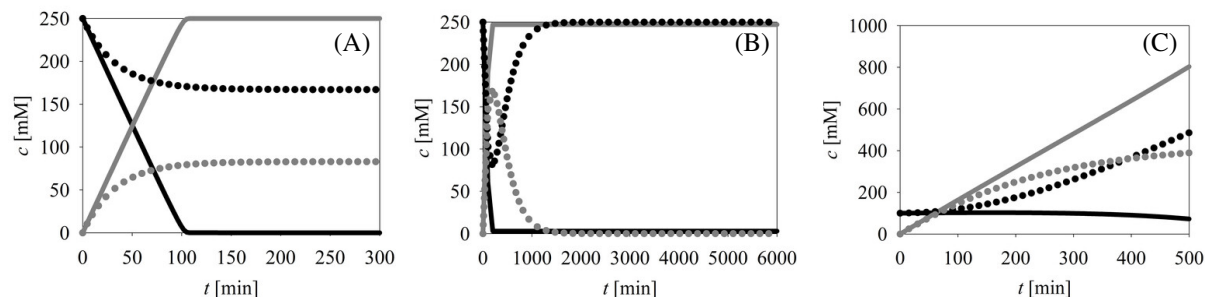


Figure 7: The effect of operational stability decay on model curves in different types of reactors: (A) batch reactor, (B) continuous stirred tank reactor, (C) fed-batch bioreactor

Parameter	Unit	Enzyme 1	Enzyme 2	Enzyme 3
V_m	U/mg	3.42 ± 0.05	1.74 ± 0.11	0.74 ± 0.03
K_m	mM	102.24 ± 4.01	67.52 ± 7.22	36.33 ± 8.82
K_i	mM	679.94 ± 38.81	183.19 ± 29.25	377.28 ± 68.70

Table 2: Estimated kinetic parameters for the three enzyme variants

cost-effectively. However, in order for new biocatalysts to be worthy of industrial large-scale production, reliable and comprehensive methods for the initial kinetic characterization of possible enzyme variants are necessary. In search of an optimal enzyme variant, the en-

zyme with the highest activity (highest V_m value) or highest affinity for the substrate (lowest K_m value) is often sought [41]. This is only valid when Michaelis-Menten kinetics are applied, however, in practice, the situation is rarely that simple. For example, this is not so in the case

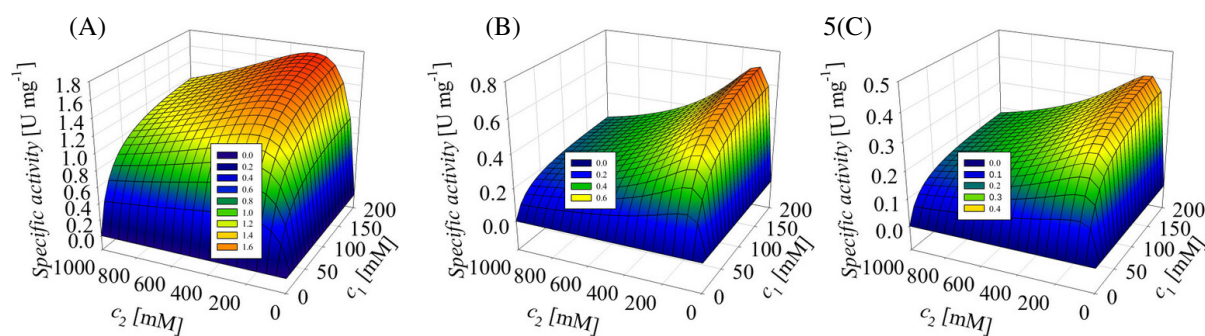


Figure 8: Comparison between the three enzyme variants which exhibit substrate inhibition at different levels

of Michaelis-Menten kinetics with substrate inhibition, when the substrate concentration used during screening is critical. Given that screening seems to only be conducted at one concentration, accurate data of enzyme activity is not provided, considering that the shape of the Michaelis-Menten curve is unknown. Since variants of the same enzyme differ with regard to the estimated values of their kinetic constants, combinations of the relevant kinetic parameters (V_m , K_m , K_i) were obtained for each variant (Table 2). Although it may be assumed that the enzyme with the minimum Michaelis constant and highest activity is most suitable, in practice, this enzyme may exhibit a higher level of substrate inhibition as a result. Three enzyme variants were kinetically characterized and the dependence of their specific enzyme activities on the substrate concentration is presented in Fig. 8, while the kinetic parameters are shown in Table 2. The best applied variant was found to be Enzyme 1, written in bold, in Table 2 because the level of substrate inhibition it is subjected to is by far the least pronounced. In practice, this means a broader substrate concentration area in which the highest enzyme activities can be obtained in the reactor (Fig. 8A) and enhanced stability of the reactor's operating conditions. Simulations presented in Fig. 8 also show that when screening the enzyme variants, it is important to not only evaluate their activities but also estimate all their kinetic parameters.

In further stages of process development, the application of reaction engineering to identify process bottlenecks is required to exploit the full potential of novel enzymes. To develop novel green routes in biocatalysis and scale them up, it is crucial to adopt a multidisciplinary approach by combining the fields of chemistry, biology and chemical engineering.

6. Conclusions

Enzyme reaction engineering can provide explanations for and give answers to different phenomena that occur in bioreactors. This is of particular importance when it comes to multienzyme systems which are very important in terms of sustainable development and green synthesis. Many obstacles to their development must be overcome,

for example, adjusting enzyme activities, choosing suitable enzyme variants, selecting the best reactor and determining the optimal reaction conditions while considering the side reactions that may occur. Therefore, a combined effort and multidisciplinary approach are required to prepare complex enzyme reaction systems for industrial applications.

Acknowledgement

Authors would like to thank the Croatian Science Foundation for the PhD scholarship of N. Milčić. This work was partly supported by the project CAT PHARMA (KK.01.1.1.04.0013) co-financed by the Croatian Government and the European Union through the European Regional Development Fund - the Competitiveness and Cohesion Operational Programme (I. Čevič). We acknowledge the funding from EU H2020-MSCA-ITN-2020 project C-C Top under the grant agreement no. 956631 (M. M. Çakar).

REFERENCES

- [1] Burgess, R.R.; Deutscher, M.P.: Guide to protein purification (Academic Press, Cambridge, UK), 2nd edition, 2009, ISBN: 978-008-092-317-8
- [2] Robinson, P.K.: Enzymes: Principles and biotechnological applications, *Essays Biochem*, 2015, **59**, 1–41. DOI: 10.1042/bse0590001
- [3] Bisswanger, H.: Enzyme kinetics: Principles and methods (Wiley, New York, USA), 3rd edition, 2017 ISBN: 978-352-780-646-1
- [4] Siedentop, R.; Claaßen, C.; Rother, D.; Lütz, S.; Rosenthal, K.: Getting the most out of enzyme cascades: Strategies to optimize in vitro multi-enzymatic reactions, *Catalysts*, 2021, **11**(10), 1183 DOI: 10.3390/catal11101183
- [5] Komáromy, P.; Bélafi-Bakó, K.; Hülber-Beyer, É.; Nemestóthy, N.: Enhancement of oxygen transfer through membranes in bioprocesses, *Hung. J. Ind. Chem.*, 2020, **48**(2), 5–8 DOI: 10.33927/hjic-2020-21

- [6] Schallmeyer, A.; Schallmeyer, M.: Recent advances on halohydrin dehalogenases—from enzyme identification to novel biocatalytic applications, *Appl. Microbiol. Biotechnol.*, 2016, **100**(18), 7827–7839 DOI: [10.1007/s00253-016-7750-y](https://doi.org/10.1007/s00253-016-7750-y)
- [7] González-Pérez, M.; Gómez-Bombarelli, R.; Arenas-Valgañón, J.; Pérez-Prior, M.T.; García-Santos, M.P.; Calle, E.; Casado, J.: Connecting the chemical and biological reactivity of epoxides, *Chem. Res. Toxicol.*, 2012, **25**(12), 2755–2762 DOI: [10.1021/tx300389z](https://doi.org/10.1021/tx300389z)
- [8] Lee, E.Y.: Enantioselective hydrolysis of epichlorohydrin in organic solvents using recombinant epoxide hydrolase, *J. Ind. Eng. Chem.*, 2007, **13**(1), 159–162 <https://www.cheric.org>
- [9] Jin, H.X.; Liu, Z.Q.; Hu, Z.C.; Zheng, Y.G.: Production of (*R*)-epichlorohydrin from 1,3-dichloro-2-propanol by two-step biocatalysis using haloalcohol dehalogenase and epoxide hydrolase in two-phase system, *Biochem. Eng. J.*, 2013, **74**, 1–7 DOI: [10.1016/j.bej.2013.02.005](https://doi.org/10.1016/j.bej.2013.02.005)
- [10] Watanabe, F.; Yu, F.; Ohtaki, A.; Yamanaka, Y.; Noguchi, K.; Odaka, M.; Yohda, M.: Improvement of enantioselectivity of the B-type halohydrin hydrogen-halide-lyase from *Corynebacterium* sp. N-1074, *J. Biosci. Bioeng.*, 2016, **122**(3), 270–275 DOI: [10.1016/j.jbiosc.2016.02.003](https://doi.org/10.1016/j.jbiosc.2016.02.003)
- [11] Yao, P.; Wang, L.; Yuan, J.; Cheng, L.; Jia, R.; Xie, M.; Feng, J.; Wang, M.; Wu, Q.; Zhu, D.: Efficient biosynthesis of ethyl (*R*)-3-Hydroxyglutarate through a one-pot bienzymatic cascade of halohydrin dehalogenase and nitrilase, *ChemCatChem*, 2015, **7**(9), 1438–1444 DOI: [10.1002/cctc.201500061](https://doi.org/10.1002/cctc.201500061)
- [12] Findrik Blažević, Z.; Milčić, N.; Sudar, M.; Majerić Elenkov, M.: Halohydrin dehalogenases and their potential in industrial application – A viewpoint of enzyme reaction engineering, *Adv. Synth. Catal.*, 2021, **363**(2), 388–410 DOI: [10.1002/adsc.202000984](https://doi.org/10.1002/adsc.202000984)
- [13] Ringborg, R.H.; Woodley, J.M.: The application of reaction engineering to biocatalysis, *React. Chem. Eng.*, 2016, **1**(1), 10–22 DOI: [10.1039/C5RE00045A](https://doi.org/10.1039/C5RE00045A)
- [14] Švarc, A.; Fekete, M.; Hernandez, K.; Clapés, P.; Findrik Blažević, Z.; Szekrenyi, A.; Skendrović, D.; Vasić-Rački, Đ.; Charnock, S.J.; Vrsalović Presečki, A.: An innovative route for the production of atorvastatin side-chain precursor by DERA-catalysed double aldol addition, *Chem. Eng. Sci.*, 2021, **231**, 116312 DOI: [10.1016/j.ces.2020.116312](https://doi.org/10.1016/j.ces.2020.116312)
- [15] Matthey, A.P.; Ford, G.J.; Citoler, J.; Baldwin, C.; Marshall, J.R.; Palmer, R.B.; Thompson, M.; Turner, N.J.; Cosgrove, S.; Flitsch, S.L.: Development of continuous flow systems to access secondary amines through previously incompatible biocatalytic cascades, *Angew. Chem. Int. Ed.*, 2021, **60**(34), 18660–18665 DOI: [10.1002/anie.202103805](https://doi.org/10.1002/anie.202103805)
- [16] Britton, J.; Majumdar, S.; Weiss, G.A.: Continuous flow biocatalysis, *Chem. Soc. Rev.*, 2018, **47**(15), 5891–5918 DOI: [10.1039/C7CS00906B](https://doi.org/10.1039/C7CS00906B)
- [17] Klermund, L.; Poschenrieder, S.T.; Castiglione, K.: Biocatalysis in Polymersomes: Improving multienzyme cascades with incompatible reaction steps by compartmentalization, *ACS Catal.*, 2017, **7**(6), 3900–3904 DOI: [10.1021/acscatal.7b00776](https://doi.org/10.1021/acscatal.7b00776)
- [18] Schmidt, S.; Castiglione, K.; Kourist, R.: Overcoming the incompatibility challenge in chemoenzymatic and multi-catalytic cascade reactions, *Chem. Eur. J.*, 2018, **24**(8), 1755–1768 DOI: [10.1002/chem.201703353](https://doi.org/10.1002/chem.201703353)
- [19] Engel, J.; Bornscheuer, U.T.; Kara, S.: Kinetics modeling of a convergent cascade catalyzed by monooxygenase–alcohol dehydrogenase coupled enzymes, *Org. Process Res. Dev.*, 2021, **25**(3), 411–420 DOI: [10.1021/acs.oprd.0c00372](https://doi.org/10.1021/acs.oprd.0c00372)
- [20] Vasić-Rački, Đ.; Kragl, U.; Liese, A.: Benefits of enzyme kinetics modelling, *Chem. Biochem. Eng. Q.*, 2003, **17**(1), 7–18 <http://silverstripe.fkit.hr>
- [21] Česnik, M.; Sudar, M.; Hernández, K.; Charnock, S.; Vasić-Rački, Đ.; Clapés, P.; Findrik Blažević, Z.: Cascade enzymatic synthesis of L-homoserine – mathematical modelling as a tool for process optimisation and design, *React. Chem. Eng.*, 2020, **5**(4), 747–759 DOI: [10.1039/C9RE00453J](https://doi.org/10.1039/C9RE00453J)
- [22] Hernández, K.; Gómez, A.; Joglar, J.; Bujons, J.; Parella, T.; Clapés, P.: 2-Keto-3-Deoxy-l-Rhamnonate Aldolase (YfaU) as catalyst in aldol additions of pyruvate to amino aldehyde derivatives, *Adv. Synth. Catal.*, 2017, **359**(12), 2090–2100 DOI: [10.1002/adsc.201700360](https://doi.org/10.1002/adsc.201700360)
- [23] Dong, J.; Fernández-Fueyo, E.; Hollmann, F.; Paul, C.E.; Pesic, M.; Schmidt, S.; Wang, Y.; Younes, S.; Zhang, W.: Biocatalytic oxidation reactions: A chemist’s perspective, *Angew. Chem. Int. Ed.*, 2018, **57**(30), 9238–9261 DOI: [10.1002/anie.201800343](https://doi.org/10.1002/anie.201800343)
- [24] Toney, M.D.: Reaction specificity in pyridoxal phosphate enzymes, *Arch. Biochem. Biophys.*, 2005, **433**(1), 279–287 DOI: [10.1016/j.abb.2004.09.037](https://doi.org/10.1016/j.abb.2004.09.037)
- [25] Sudar, M.; Findrik, Z.; Vasić-Rački, Đ.; Soler, A.; Clapés, P.: A new concept for production of (3*S*,4*R*)-6-[(benzyloxycarbonyl)amino]-5,6-dideoxyhex-2-ulose, a precursor of D-fagomine, *RSC Adv.*, 2015, **5**(85), 69819–69828 DOI: [10.1039/C5RA14414K](https://doi.org/10.1039/C5RA14414K)
- [26] Sudar, M.; Česnik, M.; Clapés, P.; Pohl, M.; Vasić-Rački, Đ.; Findrik Blažević, Z.: A cascade reaction for the synthesis of D-fagomine precursor revisited: Kinetic insight and understanding of the system, *N. Biotechnol.*, 2021, **63**, 19–28 DOI: [10.1016/j.nbt.2021.02.004](https://doi.org/10.1016/j.nbt.2021.02.004)
- [27] Sudar, M.; Vasić-Rački, Đ.; Müller, M.; Walter, A.; Findrik Blažević, Z.: Mathematical model of the MenD-catalyzed 1,4-addition (Stetter reaction) of α -ketoglutaric acid to acrylonitrile, *J. Biotechnol.*, 2018, **268**, 71–80 DOI: [10.1016/j.jbiotec.2018.01.013](https://doi.org/10.1016/j.jbiotec.2018.01.013)
- [28] Börner, T.; Rämisch, S.; Reddem, E.R.; Bartsch, S.; Vogel, A.; Thunnissen, A.M.W.H.; Adlercreutz, P.; Grey, C.: Explaining operational instability

- of amine transaminases: Substrate-induced inactivation mechanism and influence of quaternary structure on enzyme–cofactor intermediate stability, *ACS Catal.*, 2017, **7**(2), 1259–1269 DOI: [10.1021/acscatal.6b02100](https://doi.org/10.1021/acscatal.6b02100)
- [29] Dias Gomes, M.; Woodley, J.M.: Considerations when measuring biocatalyst performance, *Molecules*, 2019, **24**(19), 3573 DOI: [10.3390/molecules24193573](https://doi.org/10.3390/molecules24193573)
- [30] Česnik, M.; Sudar, M.; Roldan, R.; Hernandez, K.; Parella, T.; Clapés, P.; Charnock, S.; Vasić-Rački, Đ.; Findrik Blažević, Z.: Model-based optimization of the enzymatic aldol addition of propanal to formaldehyde: A first step towards enzymatic synthesis of 3-hydroxybutyric acid, *Chem. Eng. Res. Des.*, 2019, **150**, 140–152 DOI: [10.1016/j.cherd.2019.06.025](https://doi.org/10.1016/j.cherd.2019.06.025)
- [31] Scherkus, C.; Schmidt, S.; Bornscheuer, U.T.; Gröger, H.; Kara, S.; Liese, A.: A fed-batch synthetic strategy for a three-step enzymatic synthesis of poly- ϵ -caprolactone, *ChemCatChem*, 2016, **8**(22), 3446–3452 DOI: [10.1002/cctc.201600806](https://doi.org/10.1002/cctc.201600806)
- [32] Andrić, P.; Meyer, A.S.; Jensen, P.A.; Dam-Johansen, K.: Reactor design for minimizing product inhibition during enzymatic lignocellulose hydrolysis: II. Quantification of inhibition and suitability of membrane reactors, *Biotechnol. Adv.*, 2010, **28**(3), 407–425 DOI: [10.1016/j.biotechadv.2010.02.005](https://doi.org/10.1016/j.biotechadv.2010.02.005)
- [33] Lindeque, R.M.; Woodley, J.M.: Reactor selection for effective continuous biocatalytic production of pharmaceuticals, *Catalysts*, 2019, **9**(3), 262 DOI: [10.3390/catal9030262](https://doi.org/10.3390/catal9030262)
- [34] Cho, Y.S.; Lim, H.S.: Comparison of various estimation methods for the parameters of Michaelis–Menten equation based on in vitro elimination kinetic simulation data, *Transl. Clin. Pharmacol.*, 2018, **26**(1), 39–47 DOI: [10.12793/tcp.2018.26.1.39](https://doi.org/10.12793/tcp.2018.26.1.39)
- [35] Srinivasan, B.: A guide to the Michaelis–Menten equation: steady state and beyond, *FEBS J.*, 2021 DOI: [10.1111/febs.16124](https://doi.org/10.1111/febs.16124)
- [36] Bommarius, A.S.; Riebel, B.R.: Biocatalysis: Fundamentals and applications (Wiley, New York, USA), 1st edition, 2004 ISBN: 978-3-527-30344-1
- [37] Lejeune, A.; Vanhove, M.; Lamotte-Brasseur, J.; Pain, R.H.; Frère, J.M.; Matagne, A.: Quantitative analysis of the stabilization by substrate of *Staphylococcus aureus* PC1 β -lactamase, *Chem. Biol.*, 2001, **8**(8), 831–842 DOI: [10.1016/S1074-5521\(01\)00053-9](https://doi.org/10.1016/S1074-5521(01)00053-9)
- [38] Vasić-Rački, Đ.; Bongs, J.; Schörken, U.; Sprenger, G.; Liese, A.: Modeling of reaction kinetics for reactor selection in the case of L-erythrulose synthesis, *Bioprocess Biosyst. Eng.*, 2003, **25**, 285–290 DOI: [10.1007/s00449-002-0312-y](https://doi.org/10.1007/s00449-002-0312-y)
- [39] Findrik, Z.; Valentović, I.; Vasić-Rački, Đ.: A mathematical model of oxidative deamination of amino acid catalyzed by two D-amino acid oxidases and influence of aeration on enzyme stability, *Appl. Biochem. Biotechnol.*, 2014, **172**(6), 3092–3105 DOI: [10.1007/s12010-014-0735-3](https://doi.org/10.1007/s12010-014-0735-3)
- [40] Lindeque, R.M.; Woodley, J.M.: The effect of dissolved oxygen on kinetics during continuous biocatalytic oxidations, *Org. Process Res. Dev.*, 2020, **24**(10), 2055–2063 DOI: [10.1021/acs.oprd.0c00140](https://doi.org/10.1021/acs.oprd.0c00140)
- [41] McDonald, A.G.; Tipton, K.F.: Parameter reliability and understanding enzyme function, *Molecules*, 2022, **27**(1), 263 DOI: [10.3390/molecules27010263](https://doi.org/10.3390/molecules27010263)

DEVELOPING PLANT MODELS OF REDUCED COMPLEXITY BY CHEMICAL PROCESS ENGINEERING WAY OF THINKING

MÓNIKA VARGA¹

¹Hungarian University of Agriculture and Life Sciences, Kaposvár Campus, Guba Sándor u. 40, Kaposvár, 7400, HUNGARY

Given the increasing complexity of agricultural systems within the broader context of the bio-based circular economy, simplified and unified plant models are needed that represent the primary biomass production by solar-driven carbon-dioxide sequestration. Utilizing experiences from process systems engineering, which was originally inspired by chemical engineering, a suitable plant model is proposed. The structure of the model is generated from the process net of the underlying state and transition elements. Two special-state elements are introduced for the short-term storage of the supplied biomass to be distributed and of the uptake of nutrient-containing water, necessary for evapotranspiration and photosynthesis. The transition-oriented description of functionalities follows the essential causalities and balances of natural self-control. Implementation of the model is illustrated by a simple example.

Keywords: plant model, reduced complexity, stoichiometric processes, process network, supply/demand logistics, natural self-control

1. Introduction

The bio-based circular economy is crucial to secure the supply of food and materials for mankind given the burden of depleting non-renewable resources and finite reservoirs. The replacement of open process systems with circular ones needs conscious engineering planning and operations while systemically over-viewing the underlying processes. Multisectoral process networks require the coupling of sub-models from various disciplines on different scales. In the bio-based circular economy, the photosynthetic biosystems (plants) represent biomass production from solar energy, i.e. from the only external, unlimited energy resource for our planet. Accordingly, the model-based analysis, planning and operation of cultivated and natural plants plays an important role.

Recently, motivated also by the increasingly integrated engineering of natural and man-made systems, intensive bidirectional learning has commenced between the computational modeling of natural and man-made processes whereby:

- the principles of more sustainable and resilient natural ecosystems can be applied in the design and control of man-made systems on the one hand, while

- the experiences of industrial systems designed by engineers can be taken into account with regard to the model-based analysis, planning and operation of agricultural cultivation on the other.

Although systems of chemical process engineering played a unique role in this knowledge transfer because the underlying multidisciplinary processes were complex enough to represent various features, they were not too complex for the application of formerly applied computational tools. The lessons learnt from chemical process systems are still clearly important in terms of the rapidly developing model-supported problem-solving of complex agri-food and agro-environmental process systems. This paper shows how chemical process engineering can be used to develop plant (crop) models of limited complexity.

First, some available plant models will be overviewed in brief. Two different approaches are available, namely (i) empirical (statistical) models to calculate various specific sources of biomass production and (ii) the mechanistic (biophysical) models that describe the underlying physical, chemical and biological processes, representing causalities and balances. This overview focuses on the mechanistic crop models.

Physiological models are important to further our understanding of metabolism, growth and how plants respond to environmental conditions, e.g. climate change [1]. The detailed dynamic modeling of physiological processes is not a novel endeavor, in fact it was

already applied at the end of the previous century [2–5]. However, because of the increasing complexity of Water-Energy-Food-Ecosystems Nexus [6–8], besides detailed biophysical models, the systemic coupling of these biophysical models from various disciplines is also necessary, which also requires flexible models to couple economic considerations [9].

Regarding the level of detail, the improved understanding of physiological characteristics and the expected response to environmental changes require mechanistic models at both the cellular and organ level [10]. However, their practical applicability, considering the available data and knowledge, also requires the development of advanced coupling models.

Various complex crop models are available. In a recent paper, eight kinds of crop models are classified and compared [11], the most important of which are as follows:

Agricultural Production Systems sIMulator (APSIM) is an actively evolving tool for the modeling and simulation of a wide range of agricultural systems, including plants, animals and soil, which also takes into consideration management actions and climatic effects [12]. The crop-related parts contain the detailed biophysical description concerning the phenology, biomass accumulation and distribution of newly synthesized biomass as well as the uptake of water and components by taking into account the related limitations and dependencies on environmental conditions.

STICS is a detailed biophysical modeling tool that considers water, carbon as well as thermal and radiation energy balances for many (ca. 20) different crops ([13, 14]). It also clearly represents the phenological stages and the most important biophysical processes, e.g. light interception, transpiration, uptake of water and nutrients, etc.

Cropping Systems Simulation Model [15] is also a frequently used simulation model that takes into consideration the soil water budget, soil-plant nitrogen budget, crop-canopy and root growth, dry matter production, yield, residue production and decomposition as well as several management options, e.g. cultivar selection, crop rotation, irrigation, fertilization, tillage operations, residue management, etc.

Recently, the rediscovery of advantages regarding the coupling of tree and crop systems by combining their models has also come to the fore. Both APSIM and STICS follow this direction. A few validated tree models are available that are integrated in APSIM to be used in combination with plants [12]. On the other hand, a STICS crop model is embedded in the Hi-sAFe agroforestry tool [16].

2. Challenges and objective

Plant models for well-defined important crops and trees are available. These detailed, specific models require a

considerable set of parameters to be identified, moreover, the increasing design space of the bio-based circular economy needs simplified, approximate, unified, flexible, extensible and connectible plant models.

The objective of this paper is to introduce the conceptual framework and experimental implementation of a unified plant model of reduced complexity. To develop the model, the following chemical process engineering-based principles were applied:

- generalized unit operations;
- specific stoichiometric composition of pseudo-components and other entities;
- stoichiometric conservation processes based on the model-specific conservation laws, e.g. conservation of atoms in chemistry; and
- demand-supply chain-like representation of material flows driven by the underlying push or pull logistics.

3. Materials and methods

3.1 Data and calculation formulae for a typical example of a plant to be modelled

As an illustrative example of a man-made and operational plant ecosystem, a cultivated field of maize was modeled, where 9600 individual plants were cultivated over an area of 1600 m². The maize-related specific data were derived from the literature [17–19].

Within the contours of the outlined system, this cultivated field was associated with the connected layers of soil and the compartment of air. The environmental conditions were taken into consideration in accordance with the data from the respective meteorological database.

The initial data of the plants refer to the stage following the sowing of the seeds when the initial biomass of the plants is contained within the seeds and sprouting has not yet occurred. The initial conditions of the seed biomass (based on estimations by experts) and its components [20, 21] are the following:

$$\text{Biomass} = 0.0003 \text{ kg/plant}$$

$$\text{C} = 0.03747 \text{ kmol/kg}$$

$$\text{H} = 0.06999 \text{ kmol/kg}$$

$$\text{O} = 0.02846 \text{ kmol/kg}$$

$$\text{N} = 0.00154 \text{ kmol/kg}$$

$$\text{P} = 0.00011 \text{ kmol/kg}$$

$$\text{X} = 0 \text{ kmol/kg}$$

$$\text{H}_2\text{O} = 0.118 \text{ kmol/kg}$$

$$\text{O}_2 = 0.00066 \text{ kmol/kg}$$

Germination is an event-driven process that occurs after the time-driven sowing. Sowing, which is a management process, is modelled by putting the seeds into down-flow material storage. Afterwards, in the event of the appropriate environmental (meteorological and hydrological) conditions, the seeds germinate resulting in the release of these stored materials in accordance with the following parameters (based on estimations by experts):

$$\text{Seed biomass} = 0.0001 \text{ kg/pc}$$

Seed rate = 6.579×10^{-7} kg/h
 Proportion of leaves = 0.853
 Proportion of roots = 0.147
 Surface area ratio of leaves = 6.667 m²/kg
 Surface area ratio of roots = 3.003 m²/kg

In our example model, the germination period is from April 20th until May 9th.

After the leaves and roots appear, resulting from the event-driven process of germination, the life processes of plants, that is, photosynthesis, growth, respiration, evapotranspiration and uptake, start.

The rate of *photosynthesis* is calculated by the following simplified equations [19]:

$$\Delta \text{BiomassDry} = \frac{\text{Num Rad } F_t E_t}{\rho} \text{DT} \quad (1)$$

where

$\Delta \text{BiomassDry}$ = biomass produced, kg,

Num = number of plants, pc.

Rad = radiation, W/mJ²

F_t = proportion of radiation absorbed by the plants

E_t = radiation-use efficiency,

ρ = density, number of plants/m², where

$$F_t = 1 - e^{-k_t \text{LAI}_{\text{act}}} \quad (2)$$

$$\text{LAI}_{\text{act}} = \frac{\text{LeavesSurf Num}}{A_{\text{act}}} \quad (3)$$

$$A_{\text{act}} = \text{LAI}_{\text{ratio}} \text{LandSurf} \quad (4)$$

$$\rho = \frac{\text{Num}}{A_{\text{act}}} \quad (5)$$

LandSurf = surface area of land, m²

$\text{LAI}_{\text{ratio}}$ = 1 m² area of leaf / m² area of land

k_t = 0.8 - light extinction coefficient [19]

E_t = 0.01409 kg/MJ, radiation-use efficiency [19]

The process of *evapotranspiration* is calculated from the reference evapotranspiration (ET_0 , mm/day), determined from meteorological data according to the well-known Penman-Monteith combination equation [22]. Based on this equation, the evaporation from the land and plants during a time step are calculated separately based on the following equations:

$$ET_{\text{land}} = K_e ET_M \text{LandSurf} \text{DT} \quad (6)$$

$$ET_{\text{plants}} = K_{\text{cb}} ET_M \text{Surf} \text{Num} \text{DT} \quad (7)$$

where

ET_M = reference evapotranspiration,
 recalculated from ET_0 / kmol/h

ET_{land} = land-related evapotranspiration, kmol

ET_{plant} = plant-related evapotranspiration, kmol

LandSurf = surface area of the land, m²

Surf = surface area of the leaves, m²

Num = number of plants, pc

K_e = 1 m⁻², soil-related part of the dual crop coefficient [22]

K_{cb} = 1 m⁻², basal plant-related part of the dual crop coefficient [22]

DT = the time step in hours, distinguished for the changing actual daylight or night period

Growth is calculated after germination and is interpreted as the distribution of the photosynthetic biomass between the parts of the plants. Before the time- or event-driven appearance of the product, the following ratios are applied in line with estimations by experts:

Proportion of leaves = 0.853,

Proportion of roots = 0.147.

Afterwards:

Proportion of leaves = 0.637,

Proportion of products = 0.253,

Proportion of roots = 0.110.

Respiration is calculated for the individual parts of the plants. For all the parts, two kinds of respiration is simulated: one as a given proportion of the biomass synthesized and the other as a given proportion of the already existing biomass. The applied equations are the following:

$$R_{\text{leaves}} = K \text{DM}_{\text{leaves}} + C \text{M}_{\text{leaves}} \text{Num} \text{DT} \quad (8)$$

$$R_{\text{prod}} = K \text{DM}_{\text{prod}} + C \text{M}_{\text{prod}} \text{Num} \text{DT} \quad (9)$$

$$R_{\text{root}} = K \text{DM}_{\text{roots}} + C \text{M}_{\text{roots}} \text{Num} \text{DT} \quad (10)$$

where

R_{leaves} = respired biomass of leaves, kg

R_{prod} = respired biomass of product, kg

R_{root} = respired biomass of roots, kg

$\text{DM}_{\text{leaves}}$ = synthesized biomass of leaves, kg

DM_{prod} = synthesized biomass of product, kg

DM_{roots} = synthesized biomass of roots, kg

M_{leaves} = existing biomass of leaves, kg

M_{prod} = existing biomass of product, kg

M_{roots} = existing biomass of roots, kg

K = the constant of 0.1 h⁻¹ [22]

C = the constant of 0.0001 h⁻¹ [22]

Num = number of plants, pc.

DT = the time step in hours, distinguished for the changing actual daylight or night period

The *uptake* of water, nitrogen and phosphorus (or of other optional elements) is calculated as the minimum amount:

- required for evapotranspiration and photosynthesis together and
- available in the soil.

3.2 Non-conventional methodology of Programmable Process Structures

Programmable Process Structures (PPS, [23–26]) have developed from its antecedent, that is, Direct Computer Mapping [27]. PPS offers automatic generation of easily extensible, connectible and combined dynamic balance- and rule-based models for the analysis, planning and operation of complex process systems, even beyond industries that apply CIM (Chemical Integrated Manufacturing). These models consist of unified state and transition elements, transition-oriented representations of structures as well as locally programmable functional prototypes.

The main sources of inspiration behind PPS are: 1) the general functional definition of process systems in Kalman's State Space Model [28]; 2) the structural representation of General Net Theory [29]; 3) the concept of communicating autonomous programs in terms of Agent-Based Modeling [30].

Accordingly, PPS models are derived from two general (state and transition) "meta-agents," namely the structure of the generated state and transition elements form a net structure, moreover, the locally programmed state and transition prototypes represent the distributed functionalities in terms of Kalman's model. In addition, PPS can consciously make a distinction between model-specific conservation laws based on additive measures and signals.

In fact, PPS models can be generated from two general meta-prototypes and from the corresponding description of the process net. The local program containing prototype elements (that are responsible for the case-specific calculations), are also derived from the same meta-prototypes. The simulation can be executed according to the connections between the actual state and transition elements, accompanied by the data transfer between the actual elements and their calculated prototypes. This architecture and its AI programming language-based (SWI-Prolog to be exact) implementation strongly support the integration of various field- and task-specific models.

4. Results and discussion

4.1 Chemical process engineering-inspired principles and hypotheses of plant models

Natural and cultivated plants, including crops, vegetables, herbs, grasses and bushes, trees, etc. in a broader context, cover a wide variety of biological species embedded in a naturally occurring and partly human-controlled process system. Since many different species exist, at first glance this resembles the early stages of chemical engineering when individual technologies were interpreted as a system of various case-specific reactors, separators, etc. The essential invariant elements were later generalized according to the concept of unit operations. Similarly, the unified, essential features of agricultural models

can be formulated as "biological engineering unit operations" within the complex system of the connected agro-technological, ecological and environmental systems.

Considering the need for unified and simplified biological, ecological and environmental engineering process units, these systems must be represented by the necessary and sufficient types as well as numbers of state and transition elements calculated by a limited set of generally usable program prototypes.

The coherent and connectible set of the underlying 'first principles'-based mechanistic (physical, chemical and biological) models must be based on causally correct, model-specific conservation laws-based material and energy balances. Considering the numerous biochemical compounds and biological objects, that is, organs, etc., synthesized from these compounds, the various typical biological units can be characterized by their specific stoichiometric composition that facilitates the representation of balances in accordance with the conservation of atoms and in line with chemical principles.

Besides the conservation-based balances, the causally determined (driving force-based) transformations and transportations are the second pillar of process engineering models. In this regard, plant-like biological process units represent a special case because the major driving force is solar radiation originating from beyond the contours of the system. This feature determines the unique position of plants in the bio-based circular carbon economy.

In fact, solar radiation-driven photosynthesis produces a stoichiometric composition of biomass that supplies biomass in the various state elements of plants through downflow transporting short-term storage. Moreover, the forces of solar radiation-driven evapotranspiration result in the uptake of water and dissolved nutrients through upflow transporting short-term storage that supplies the additional resources required for photosynthesis as well as removes the by-products of the energy-producing respiration.

Accordingly, the essential self-control of plant life is organized by the solar radiation-driven push logistics of downflow as well as by the solar radiation-driven pull logistics of upflow. The daily and seasonal changes in plant behavior are determined by the temporally changing environmental functionalities, while human intervention can be taken into consideration by the respective managerial events.

The hypotheses for the simplified and unified plant model can be summarized as follows:

- The state elements are described by the specific biomass (or mass); the stoichiometric amounts of C, H, O, N, P and optional X atoms; as well as those originating from H₂O, O₂ and CO₂.
- The transition elements, e.g. photosynthesis, growth, respiration, evapotranspiration, uptake, etc., determine the functionalities resulting in stoichiometric changes in the aforementioned sources

of biomass, mass, atoms and components in the respective state elements.

- The life processes of plants as self-controlled living systems can be characterized by (i) the supply logistics of the photosynthesis-driven utilization of CO₂ from air and H₂O, N, P, etc. (from top soil) to produce O₂ which is emitted into the atmosphere in addition to stoichiometric pools of C, H, O, N and P that is incorporated into downflow material storage, as well as by (ii) the demand logistics of the solar energy-driven evapotranspiration-controlled uptake of H₂O, N and P from the soil and the emission of CO₂ and H₂O into the air.

4.2 Structure of the investigated process system

The process net structure of the simplified plant model, embedded in its natural environment and extended with human managerial interventions, is illustrated in Fig. 1. In the net model, the dots and bars represent the state and transition elements, respectively. The state and transition elements of the simplified plant model are the following:

Plant-related model elements:

- State elements:
 - roots (responsible for the water uptake, transportation of dissolved nutrients and long-term biomass storage that is also capable of generating useful products);
 - leaves (including stems which are responsible for solar radiation-driven photosynthesis and evapotranspiration);
 - products (which facilitate the storage of biomass for reproduction that also generates useful products);
 - downflow of material (short-term storage of photosynthesized biomass to be distributed amongst the roots, leaves and products);
 - upflow of material (short-term storage of up-taken water and nutrients as well as of respired components to be distributed between evapotranspiration and photosynthesis).
- Transition elements:
 - photosynthesis: utilizes solar radiation to synthesize biomass from atmospheric carbon dioxide, uptaken water and dissolved components, e.g. nitrogen, phosphorus, etc.;
 - growth: distributes the photosynthesized biomass between the parts of the plant according to the phenological phase-specific stoichiometry;
 - respiration: creates energy to synthesize tissues from already synthesized biomass and in part maintain existing plant biomass;
 - evapotranspiration: which is determined by the atmospheric conditions, i.e. level of solar energy, generates the driving force for the uptake

of water and dissolved nutrients from the soil as well as releases the CO₂ and H₂O produced by respiration;

- uptake: supplies the necessary water and dissolved nutrients from the soil.

Soil-related model elements:

- State elements:
 - residue (only in the topsoil): contains organic residues, e.g. from leaf littering or the ploughing of roots;
 - humus (only in the topsoil): transformed organic biomass in the soil;
 - solution containing water and dissolved components;
 - inorganic solid phase.
- Transition elements:
 - transform (only in the topsoil): describes the production of humus and dissolved nutrients from the residues;
 - air_land (only in the topsoil): calculates the levels of precipitation and nitrogen fixation from the atmosphere into the soil as well as those of evaporation and CO₂ emission from the soil into the atmosphere;
 - miner_deminer: determines the degrees of mineralization and demineralization of dissolved components in the soil;
 - seepage: calculates the vertical downflow of water and dissolved components between the layers of soil.

Human interventions in terms of cultivation:

- Typical state elements: manure, seeds, harvested products, etc.
- Typical time- and/or event-driven transition elements: manuring, sowing, harvesting, ploughing, etc.

Other environmental state elements: the atmosphere (air), solar radiation-related meteorology, ground layer below the soil that absorbs water and nutrients.

4.3 Solar radiation-driven “natural supply logistics” of plant biomass generation

The essential functionalities of the investigated process system can be represented as solar energy-driven as well as predominantly self-regulated, natural supply-and-demand logistics. Moreover, the respective supply-and-demand processes are causally connected that establish a natural (basically cooperative) feedback between each other.

Solar radiation facilitates the synthesis of biomass, the latter is calculated according to Eqs. 1-5. The related subprocesses of the plant model are denoted in green lines in Fig. 1.

The synthesis of biomass is driven by solar radiation but limited by the available amounts of water, nitrogen and phosphorus with regard to the upflow material to be

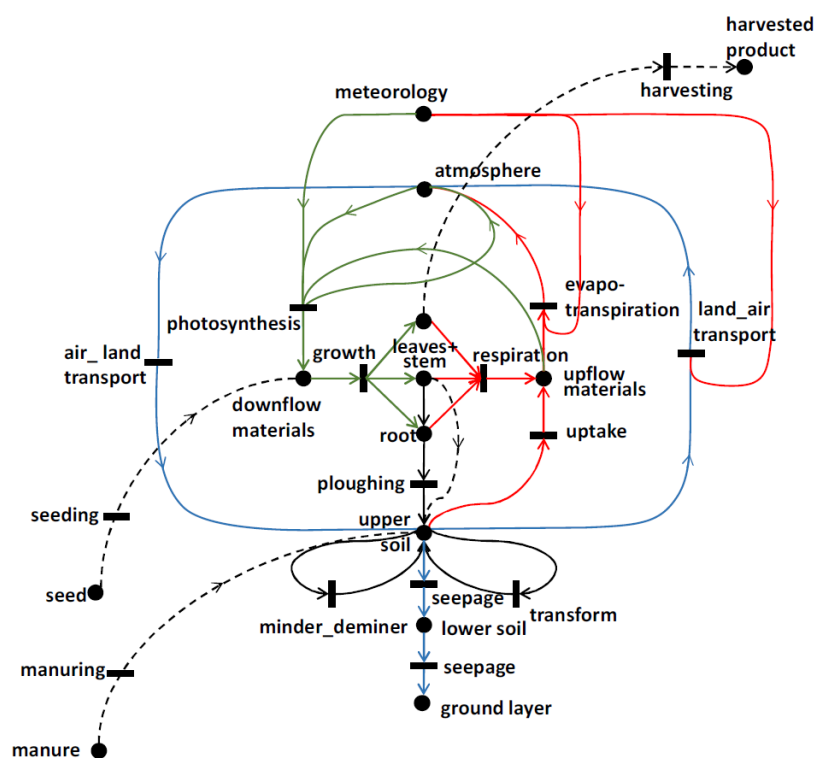


Figure 1: Process network of the simplified plant model

stored. The rate of photosynthesis also depends on the surface area of the leaves and stem. Controlled by these conditions and limitations, the synthesis sequestrates the calculated amount of the practically unlimited supply of atmospheric CO_2 in the biomass. Simultaneously, photosynthesis emits O_2 into the atmosphere as a result of the oxidation of uptaken water, while the associated hydrogen is incorporated into the synthesized biomass. The photosynthesized biomass supplies the downflow of material to be stored according to the plant-specific atomic stoichiometry. In the case of the studied maize, the stoichiometry of the synthesized dry matter was as follows [20,21]:

$$[\text{C}, \text{H}, \text{O}, \text{N}, \text{P}, \text{X}] = [0.037, 0.062, 0.029, 0.00087, 4.8 \times 10^{-5}, 0]$$

The dry matter is supplied by an additional amount of H_2O , according to the average water content of the plant (in our case 0.682).

The synthesized biomass is divided between the leaves, roots and product state elements of the plant, according to the plant-specific ratios that also depend on the phenological condition of the model. Furthermore, different stoichiometries can be used by the various parts of the plant.

In addition to the increase in the amount of synthesized biomass, a given proportion of that which is stored in the short term is utilized to meet the energy demand supplied by respiration for the synthesis of plant biomass according to Eqs. 8-10.

4.4 Solar energy-driven “natural demand logistics” of water and nutrient uptake

Considering the “natural demand logistics,” the solar energy facilitates the uptake of water and dissolved nutrients from the soil as well as of H_2O and CO_2 , the by-products of respiration. The respective evapotranspiration is calculated according to the Penman-Monteith combination equation [22] as well by Eqs. 6-7. The related subprocesses of the plant model are denoted in red lines in Fig. 1.

Depending on the meteorological conditions, the H_2O and CO_2 content of the uptaken material to be stored is emitted into the atmosphere by the process of evapotranspiration. Simultaneously, the by-products of respiration, namely H_2O and CO_2 , accumulate here, moreover, the necessary amounts of H_2O as well as of dissolved nitrogen and phosphorus are utilized for photosynthesis from this store. In the knowledge of the resultant actual conditions with regard to the uptaken material to be stored, the uptake is controlled by demand-determined pull actions according to the concentration bounds and uptake rules as follows:

Lower and upper bounds for H_2O as well as N and P atoms are known. The rule that is applied is the following:
 if $\text{Actual} \leq \text{Lower}$, then
 $\text{Demand} = \min((\text{Upper}-\text{Actual}), \text{Available})$,
 otherwise $\text{Demand} = 0$, where
 Actual = actual amount of uptaken material to be stored,
 Lower = lower bound,

Upper = upper bound,
 Demand = quantity to be uptaken,
 Available = available amount in the topsoil.

4.5 Generation and simulation of the PPS model

The files describing the respective model are found in the “Plant” directory of a Mendeley database [31].

The process network of the example model is defined in the text file named *Plant_N.pl*. The initial conditions (mass, biomass, components, etc.) and parameters (coefficients of equations, bounds, etc.) are described in the text file entitled *Plant_D.pl*, which was derived using an appropriately configured MS Excel spreadsheet. Starting from these case-specific files and the general definition of state and transition meta-prototypes, the general-purpose kernel program generates the editable graphical model *Plant_G.graphml*.

In parallel, by utilizing the meta-prototypes-based templates, modeling experts have to prepare the local programs for the respective elements of the prototypes. The locally executable programs of the prototypes are described in the file entitled *Plant_G_prot.graphml*.

In the knowledge of the prototype elements, the second generating algorithm of the PPS kernel prepares the dynamic databases of the simulation, namely

- *Plant_Exp.pl* containing the declaration of the Prolog clauses describing the local programs; and
- *Plant_Use.pl* containing the declaration of the Prolog facts describing the case-specific elements of the model along with their initial values and parameters.

The actually selected simulation results are saved in the file named *Plant_Out.csv*, while the data can be visualized using a case-specific MS Excel spreadsheet.

Some examples of the simulated results are illustrated in Figs. 2-5.

Fig. 2 shows the change in the total amount of biomass produced over one hectare during consecutive half days in the simulation. Time = 0 indicates when the land was sowed. Biomass begins to be produced following germination and stops at the end of the vegetation period. Fluctuations in biomass production indicate that its rate is higher during the daytime compared to at nighttime.

In Fig. 3, water that evaporated from the plant (blue) and from the land (red) are illustrated. Evaporation from the land follows the weather conditions much more closely and dominates during the early stages of the growing season, particularly when the leaves develop. Similarly to the production of biomass, evaporation rates are also higher in this simulation during the daytime.

In Fig. 4, the biomass of the parts of one plant (leaves, stem, roots, products) can be seen. The leaves, stem and roots begin to develop at the point of germination, while products appear later on. Although the leaves, stem and products are removed at harvest time, the roots are transformed into residues as a result of ploughing. Of course,

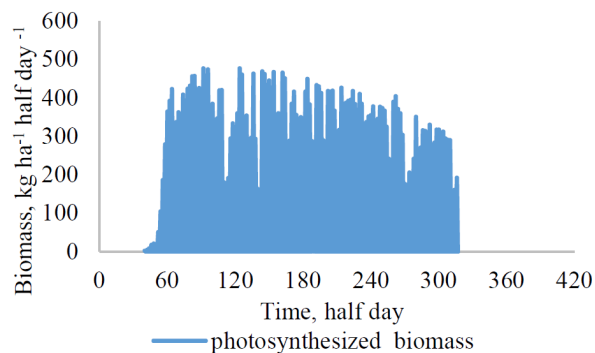


Figure 2: Total amount of photosynthesized biomass per hectare

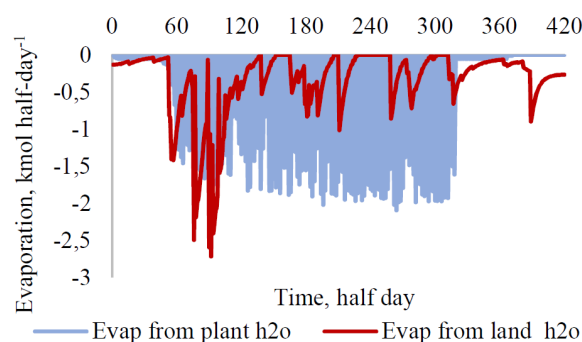


Figure 3: Dynamic changes in the evaporation rate of H₂O from plants and the surface of the land

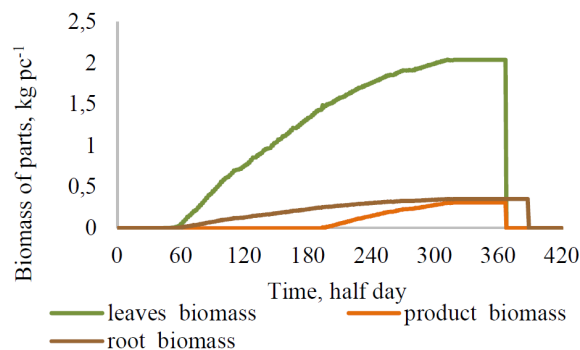


Figure 4: Biomass of plant parts throughout the growing season

the stepwise increase in biomass is insignificant in this integrated illustration.

Fig. 5 shows the sequestered CO₂ over one hectare during consecutive half days of the simulation. The negative values refer to the reduction in its concentration in the surrounding atmosphere.

5. Conclusion

Although detailed plant models for well-defined important crops are available that require hundreds of param-

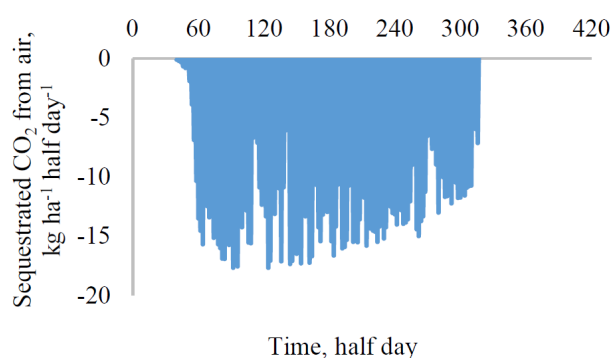


Figure 5: Amount of sequestered CO₂

ters to be identified, the increasing complexity of agricultural systems within the broader context of the bio-based circular carbon economy requires simplified and unified plant models, which can describe the primary production of biomass. The suggested conceptual framework and its experimental implementation show how the chemical process engineering principles of process units, stoichiometric conservational processes, process networks, driving force-controlled functionalities and supply/demand processes can result in a reduced, unified plant model.

The structure of the model can be generated from the process net of the underlying state and transition elements. The model contains two special state elements for the short-term storage of the synthesized biomass to be distributed amongst the state elements of the plant as well as for the short-term storage of the uptaken aqueous nutrients required for evapotranspiration and photosynthesis. These two forms of logistical storage used represent the roles of phloem and xylem in detailed biophysical models.

The transition-related dynamic models follow the essential causalities and balances of natural self-control. Solar radiation-driven photosynthesis produces a stoichiometric composition of biomass that, as a result of the downflow of products to be stored in the short term, increases the biomass in the various plant elements. Moreover, solar radiation-driven evapotranspiration forces water and dissolved nutrients to be uptaken through the upflow of products to be stored in the short term, which increases the amount of water and the additional resources for photosynthesis required, as well as removes the by-products of energy-producing respiration. The natural self-control of plant life is organized by the solar radiation-driven push logistics of downflow as well as by the solar radiation-driven pull logistics of upflow.

The suggested stoichiometric approach underlines the increasing importance of elemental analysis with regard to agriculture-related raw materials and products.

The experimental PPS implementation of a simple example model illustrates the possible application of the reduced plant model prepared according to the suggested principles inspired by process systems engineering.

Acknowledgements

This research was partly supported by the 2019-2.1.11-TÉT-2020-00252 program. The author is especially grateful to Béla Csukás for his valuable advice.

REFERENCES

- [1] Marin, F. R.; Ribeiro, R. V.; Marchiori, P. E. R.: How can crop modeling and plant physiology help to understand the plant responses to climate change? A case study with sugarcane, *Theor. Exp. Plant Physiol.*, 2014, **26**, 49–63 DOI: [10.1007/s40626-014-0006-2](https://doi.org/10.1007/s40626-014-0006-2)
- [2] Whisler, F.; Acock, B.; Baker, D.; et al: Crop simulation models in agronomic systems, *Adv. Agron.*, 1986, **40**, 141–208 DOI: [10.1016/S0065-2113\(08\)60282-5](https://doi.org/10.1016/S0065-2113(08)60282-5)
- [3] Penning de Vries, F.; Jansen, D.; Ten Berge, H.; Bakema, A.: Simulation of ecophysiological processes of growth in several annual crops. Wageningen: Centre for Agricultural Publishing and Documentation (Pudoc); 1989.
- [4] McMaster, G. S.; Morgan, J. A.; Wilhelm, W. W.: Simulating winter wheat spike development and growth. *Agric. For. Meteorol.*, 1992, **60**, 193–220 DOI: [10.1016/0168-1923\(92\)90038-6](https://doi.org/10.1016/0168-1923(92)90038-6)
- [5] Salminen, H.; Saarenmaa, H.; Perttunen, J.; Sievänen, R.; Väkevä, J.; Nikinmaa, E.: Modelling trees using an object-oriented scheme, *Math. Comput. Model.*, 1994, **20**, 49–64 DOI: [10.1016/0895-7177\(94\)90230-5](https://doi.org/10.1016/0895-7177(94)90230-5)
- [6] Garcia, D. J., You, F.: The water-energy-food nexus and process systems engineering: A new focus, *Comput. Chem. Eng.*, 2016, **91**, 49–67 DOI: [10.1016/j.compchemeng.2016.03.003](https://doi.org/10.1016/j.compchemeng.2016.03.003)
- [7] Fouladi, J.; AlNouss, A.; Al-Ansari, T.: Sustainable energy-water-food nexus integration and optimisation in eco-industrial parks, *Comput. Chem. Eng.*, 2021, **146**, 107229 DOI: [10.1016/j.compchemeng.2021.107229](https://doi.org/10.1016/j.compchemeng.2021.107229)
- [8] Yoon, P. R.; Lee, S-H.; Choi, J-Y.; Yoo, S-H.; Hur, S-O.: Analysis of climate change impact on resource intensity and carbon emission in protected farming systems using water-energy-food-carbon nexus, *SSRN Electron. J.*, 2022, **184**, 106394 DOI: [10.2139/ssrn.4054485](https://doi.org/10.2139/ssrn.4054485)
- [9] Henderson, J. D.; Parajuli, R.; Abt, R. C.: Biological and market responses of pine forests in the US Southeast to carbon fertilization, *Ecol. Econ.*, 2020, **169**, 106491 DOI: [10.1016/j.ecolecon.2019.106491](https://doi.org/10.1016/j.ecolecon.2019.106491)
- [10] Poorter, H.; Anten, N. P. R.; Marcelis, L. F. M.: Physiological mechanisms in plant growth models: Do we need a supra-cellular systems biology approach? *Plant, Cell Environ.*, 2013, **36**, 1673–1690 DOI: [10.1111/pce.12123](https://doi.org/10.1111/pce.12123)
- [11] Tao, F.; Palosuo, T.; Rötter, R. P.; et al. Why do crop models diverge substantially in climate impact projections? A comprehensive analysis based on eight barley crop models, *Agric. For. Meteorol.*, 2020, **281**, 107851 DOI: [10.1016/j.agrformet.2019.107851](https://doi.org/10.1016/j.agrformet.2019.107851)

- [12] Holzworth, D. P.; Huth, N. I.; deVoil, P. G.; et al. APSIM – Evolution towards a new generation of agricultural systems simulation, *Environ. Model. Softw.*, 2014, **62**, 327–350 DOI: [10.1016/J.ENVSOFT.2014.07.009](https://doi.org/10.1016/J.ENVSOFT.2014.07.009)
- [13] Brisson, N.; Mary, B.; Ripoche, D.; et al. STICS: A generic model for the simulation of crops and their water and nitrogen balances. I. Theory and parameterization applied to wheat and corn, *Agronomie*, 1998, **18**, 311–346 DOI: [10.1051/agro:19980501](https://doi.org/10.1051/agro:19980501)
- [14] Brisson, N.; Launay, M.; Mary, B.; Beaudoin, N. (Eds.): Conceptual basis, formalisations and parameterization of the STICS crop model (Éditions Quæ, Versailles, France) 2009 ISBN: 978-2-7592-0290-4
- [15] Stöckle, C. O.; Kemanian, A. R.; Nelson, R. L.; Adam, J. C.; Sommer, R.; Carlson, B.: CropSyst model evolution: From field to regional to global scales and from research to decision support systems, *Environ. Model. Softw.*, 2014, **62**, 361–369 DOI: [10.1016/j.envsoft.2014.09.006](https://doi.org/10.1016/j.envsoft.2014.09.006)
- [16] Dupraz, C.; Wolz, K. J.; Lecomte, I.; et al.: HisAFE: A 3D agroforestry model for integrating dynamic tree-crop interactions, *Sustain.*, 2019, **11**(8), 2293, DOI: [10.3390/su11082293](https://doi.org/10.3390/su11082293)
- [17] Bergez, J. E.; Raynal, H.; Launay, M.; et al.: Evolution of the STICS crop model to tackle new environmental issues: New formalisms and integration in the modelling and simulation platform RECORD, *Environ. Model. Softw.*, 2014, **62**, 370–384 DOI: [10.1016/J.ENVSOFT.2014.07.010](https://doi.org/10.1016/J.ENVSOFT.2014.07.010)
- [18] Varga, M.; Gyalog, G.; Raso, J.; Kucska, B.; Csukas, B.: Programmable process structures of unified elements for model-based planning and operation of complex agri-environmental processes. In: Bochtis D. D.; Sørensen, C. G.; Fountas, S.; Moysiadis, V.; Pardalos, P. *Inf. Commun. Technol. Agric. III Decis.*, (Cham.: Springer) 2022, pp. 223–249 DOI: [10.1007/978-3-030-84152-2_11](https://doi.org/10.1007/978-3-030-84152-2_11)
- [19] van der Werf, W.; Keesman, K.; Burgess, P.; et al. Yield-SAFE: A parameter-sparse, process-based dynamic model for predicting resource capture, growth, and production in agroforestry systems, *Ecol. Eng.* 2007, **29** 419–433 DOI: [10.1016/j.ecoleng.2006.09.017](https://doi.org/10.1016/j.ecoleng.2006.09.017)
- [20] TNO Biobased and Circular Technologies, The Netherlands. Database for the physico-chemical composition of (treated) lignocellulosic biomass, micro- and macroalgae, various feedstocks for biogas production and biochar n.d. <https://phyllis.nl/> (accessed January 4, 2022)
- [21] Antal, M.; Allen, S. G.; Dai, X.; Shimizu, B.; Tam, M. S.; Grønli, M.: Attainment of the theoretical yield of carbon from biomass, *Ind. Eng. Chem. Res.*, 2000, **39**, 4024–4031 DOI: [10.1021/ie000511u](https://doi.org/10.1021/ie000511u)
- [22] Allen, R.; Pereira, L.; Raes, D.; Smith, M.: Crop evapotranspiration - Guidelines for computing crop water requirements - FAO Irrigation and drainage paper 56, Chapter 2 - FAO Penman-Monteith equation, Rome: FAO; 1998.
- [23] Varga, M.; Prokop, A.; Csukas, B.: Biosystem models, generated from a complex rule/reaction/influence network and from two functionality prototypes, *BioSystems*, 2017, **152**, 24–43 DOI: [10.1016/j.biosystems.2016.12.005](https://doi.org/10.1016/j.biosystems.2016.12.005)
- [24] Varga, M.; Csukas, B.: Generation of extensible ecosystem models from a network structure and from locally executable programs, *Ecol. Modell.*, 2017, **364**, 25–41 DOI: [10.1016/J.ECOLMODEL.2017.09.014](https://doi.org/10.1016/J.ECOLMODEL.2017.09.014)
- [25] Varga, M.; Csukas, B.; Kucska, B.: Implementation of an easily reconfigurable dynamic simulator for recirculating aquaculture systems, *Aquac. Eng.*, 2020, **90**, 102073 DOI: [10.1016/J.AQUAENG.2020.102073](https://doi.org/10.1016/J.AQUAENG.2020.102073)
- [26] Varga, M.; Berzi-Nagy, L.; Csukas, B.; Gyalog, G.: Long-term dynamic simulation of environmental impacts on ecosystem-based pond aquaculture, *Environ. Model. Softw.*, 2020, **134**, 104755 DOI: [10.1016/j.envsoft.2020.104755](https://doi.org/10.1016/j.envsoft.2020.104755)
- [27] Csukas, B.: Simulation by direct mapping of the structural models onto executable programs, *AIChE Annu. Meet.*, Miami, FL: AIChE, 1998, Paper 239/9.
- [28] Kalman, R.; Falb P.; Arbib, M.: Topics in mathematical system theory (McGraw-Hill, New York, USA) 1969 ISBN: 978-0-0703-3255-3
- [29] Petri, C.: Introduction to general net theory, In: Brauer, W. (Ed.): *Net Theory Appl. Lect. Notes Comput. Sci.* (Heidelberg: Springer, Berlin, Germany), 1980, DOI: [10.1007/3-540-10001-6_21](https://doi.org/10.1007/3-540-10001-6_21)
- [30] Abar, S.; Theodoropoulos, G. K.; Lemarinier, P.; O'Hare, G. M. P.: Agent based modelling and simulation tools: A review of the state-of-art software, *Comput. Sci. Rev.*, 2017, **24**, 13–33 DOI: [10.1016/J.COSREV.2017.03.001](https://doi.org/10.1016/J.COSREV.2017.03.001)
- [31] Varga, M.: Mendeley Data, V1, 2022, linked to this paper DOI: [10.17632/nw3cgv75j5.1](https://doi.org/10.17632/nw3cgv75j5.1)